



ΕΛΛΗΝΙΚΗ ΔΗΜΟΚΡΑΤΙΑ  
Εθνικόν και Καποδιστριακόν  
Πανεπιστήμιον Αθηνών  
— ΙΔΡΥΘΕΝ ΤΟ 1837 —

MSc Programme Earth Sciences and Environment  
Specialization: Mineral Resources- Petrology and Environmental Management

**Long term effectiveness of in-situ trace metal stabilization  
in the “Kavodokanos” waste pile, Lavrion Greece**



MSc Dissertation

**Khaled Ibrahim Elhusseini Mohamed**

RN 21808

Athens  
June 2021



ΕΛΛΗΝΙΚΗ ΔΗΜΟΚΡΑΤΙΑ  
Εθνικόν και Καποδιστριακόν  
Πανεπιστήμιον Αθηνών  
— ΙΔΡΥΘΕΝ ΤΟ 1837 —



Πρόγραμμα  
Μεταπτυχιακών  
Σπουδών  
**Επιστήμες Γης  
και Περιβάλλον**

Τμήμα Γεωλογίας και Γεωπεριβάλλοντος  
Πρόγραμμα Μεταπτυχιακών Σπουδών Επιστήμες Γης και Περιβάλλον:  
Ειδίκευση Ορυκτοί Πόροι - Πετρολογία και Διαχείριση Περιβάλλοντος

**Διαχρονική αποτελεσματικότητα των επιτόπου τεχνικών  
σταθεροποίησης ιχνομετάλλων στον σωρό αποβλήτων  
του Καβδόκανου Λαυρίου**

Διπλωματική Εργασία

**Khaled Ibrahim Elhousseini Mohamed**

AM 21808

**Επιβλέπουσα Αριάδνη Αργυράκη, Καθηγήτρια**

Τριμελής Εξεταστική Επιτροπή:

Αριάδνη Αργυράκη, Καθηγήτρια ΕΚΠΑ

Χριστίνα Στουραϊτή, Επίκουρη Καθηγήτρια ΕΚΠΑ

Ιωάννης Μήτσης, Αναπληρωτής Καθηγητής ΕΚΠΑ

Ιούνιος 2021

## Περίληψη

Στην εργασία παρουσιάζονται τα αποτελέσματα της έρευνας σχετικά με τη διαχρονική αποτελεσματικότητα των επιτόπου τεχνικών σταθεροποίησης ιχνομετάλλων στον σωρό μεταλλευτικών αποβλήτων του Καβοδόκανου Λαυρίου. Τρεις διαφορετικές τεχνικές σταθεροποίησης της ρύπανσης (ανάμιξη με ανθρακικό πρόσθετο, μεμβράνη γεωφραγμού και γεωφραγμός πεπιεσμένης αργίλου) είχαν εφαρμοστεί δοκιμαστικά περίπου 25 χρόνια πριν, για τη σταθεροποίηση της όξινης απορροής στον σωρό αποβλήτων πυριτούχων τελμάτων. Έγινε σύγκριση των αποτελεσμάτων κινητοποίησης δυνητικά τοξικών στοιχείων (ΔΤΣ) στον σωρό σε σχέση με τα αποτελέσματα της αρχικής δοκιμής αποκατάστασης, ενώ μελετήθηκε η κινητοποίηση τριών ΔΤΣ (Pb, Zn, Cd) στην παρούσα κατάσταση κατά την οριζόντια και κατακόρυφη έννοια στον σωρό.

Οι μέθοδοι που χρησιμοποιήθηκαν περιλαμβάνουν χημική ανάλυση μετά από χώνευση με βασιλικό ύδωρ, απλοποιημένη δοκιμή εκχύλισης του βιοπροσβάσιμου κλάσματος των μετάλλων (SBET) και μέθοδο εκχύλισης TCLP. Η ορυκτολογία του σωρού και η αναγνώριση των ξενιστών των μετάλλων ενδιαφέροντος μελετήθηκε με περιθλασιμετρία ακτίνων X (XRD) σε επιλεγμένα δείγματα και ηλεκτρονική μικροσκοπία-μικροανάλυση (SEM-EDS).

Τα αποτελέσματα κατέδειξαν ότι 25 χρόνια μετά την αρχική εφαρμογή των τεχνικών σταθεροποίησης η περιοχή παραμένει ένας ρυπασμένος χώρος υψηλής διακινδύνευσης για την περιβάλλουσα οικιστική περιοχή, λόγω των υψηλών συγκεντρώσεων ΔΤΣ όπως Pb, Cd, As. Τα γεωχημικά δεδομένα της παρούσας έρευνας κατέδειξαν ότι η ανάμιξη με αλκαλικό μέσο (ασβεστόλιθο) δεν απέβη αποτελεσματική για τον περιορισμό των ΔΤΣ στη διηθημένη απορροή πάρα τις ενδείξεις σχηματισμού συμπαγοποιημένου στρώματος (hardpan). Ο γεωφραγμός πεπιεσμένης αργίλου φαίνεται να διατηρεί το pH στο πορικό νερό του υπερκειμένου στρώματος σε ελαφρά αλκαλικές συνθήκες και να συνεχίζει να αποτελεί αποτελεσματικό φραγμό περιορίζοντας το φαινόμενο της διάχυσης των ΔΤΣ προς την επιφάνεια, σε αντίθεση με το control και το πεδίο δοκιμής προσθήκης αλκαλικού μέσου.

Συμπερασματικά, ο φραγμός πεπιεσμένης αργίλου κρίνεται ως η πλέον αποτελεσματική τεχνική για τη σταθεροποίηση των ΔΤΣ στο επιφανειακό κάλυμμα αποδίδοντας χαμηλότερες συγκεντρώσεις μετάλλων κατά τη δοκιμή TCLP. Ένα πρόσθετο πλεονέκτημα της τεχνικής αυτής, σύμφωνα και με την κοστολόγηση της αρχικής μελέτης αποκατάστασης, είναι ότι πρόκειται για την πλέον οικονομική λύση συγκρινόμενη με την συνθετική γεωμεμβράνη. Η αποτελεσματικότητα του αργιλικού γεωφραγμού καθιστά την τεχνική μια επιτυχημένη και βιώσιμη λύση αποκατάστασης με δυνατότητα εφαρμογής σε άλλες περιοχές με παρόμοια χαρακτηριστικά.

## Abstract

This dissertation presents the findings of the study of long-term performance of in-situ mining and metallurgical waste remediation techniques, focusing mainly on the comparison of three different elemental stabilization methods (liming, geomembrane barrier and compacted clay barrier) that have been applied in a waste pile of pyrite tailings almost 25 years ago. Data of potential toxic element (PTE) leachability are compared with data presented in the initial remediation study held in 1998. In this way, the mobility of three PTEs (Pb, Zn and Cd) has been assessed for each treatment technique and the spatial distribution, horizontally and vertically, of the PTEs in the waste pile has been determined.

Chemical analysis after aqua regia dissolution, a simplified bioaccessibility extraction test (SBET), and the Toxicity Characteristic Leaching Procedure (TCLP) have been utilized in this study to gather geochemical data. X-ray diffraction (XRD) with integration of scanning electron microscopy coupled with energy dispersive microanalysis (SEM-EDS) have been hired for mineralogical investigation. The X-ray energy dispersive (EDS) measurements in combination with (XRD) and total chemical analysis helped to identify the corresponding host-speciation of the trace metals and therefore the major factors controlling the environmental mobility of Pb, Zn and Cd.

The results of the present study indicate that almost 25 years after the pilot scale remediation in the Kavodokanos waste pile, the area remains polluted, posing significant risks for the health of nearby inhabitants, being exposed to very high concentrations of PTEs including Pb, Cd and As. From the geochemical data, it is deduced that liming did not reduce the PTEs infiltration to the drainage in spite of the indications for a hardpan layer formation. The compacted clay barrier showed good performance in maintaining neutral to slightly alkaline pH values along the depth profile and sustaining its water content and hence eliminating the effect of evaporation process. The effect of the evaporation process within the pores of the waste material results in high concentrations of PTEs in the surface, especially in the control plot and the lime test plot.

Overall, the long-term performance demonstrates better effectiveness of the compacted clay barrier with the lowest TCLP leachable concentrations of PTEs in surface soil. This means that effective stabilization is better induced by this treatment in the long term. In the original study it is noted that the compacted clay has the additional advantage of low cost compared to the geomembrane barrier. Thus, the compacted clay technique can be considered as an effective sustainable remediation technique that should be considered in other areas with similar characteristics.

## Acknowledgments

I would like to express my sincere appreciation to my supervisor, Professor Ariadne Argyraki, for her guidance, knowledge and persistent help for achieving the goal of this study, and my brother, Mohamed Ibrahim, for his support throughout my studies in the University of Athens.

I want also to acknowledge the efforts done by my colleagues; Petros Tzeferis and Sofia Pietushok. Also, I am thankful to Dr. Zacharenia Kypridou for performing the chemical analysis of solutions in AAS and her help during the interpretation of the mineralogical investigation. Copyright of the Kavodokanos pile photos is preserved to my fellow, Dorin Chiroška. I am thankful also to Dr. Efstathios Kelepertzis and my colleague Evangelos Vourdelis for their participation in the first sampling survey in Lavrion.

I wish also to express my special regards to the examiners; Assoc. Professor Ioannis Mitsis and Assoc. Professor Christina Stouraiti for the thorough reading and their constructive comments on my dissertation.

## Table of Contents

|  |    |
|--|----|
| Περίληψη .....   | 3  |
| Abstract .....   | 4  |
| Acknowledgments.....   | 5  |
| Table of Contents .....  | 6  |
| <b>1. Introduction</b> .....   | 7  |
| 1.1 Research background and rationale of the study .....                                 | 7  |
| 1.2 Aim and Objectives of the study .....  | 8  |
| <b>2. Literature review</b> .....  | 9  |
| 2.1 Soil remediation techniques .....  | 9  |
| 2.2 Waste characterization and risk assessment in Lavrion city .....                     | 12 |
| 2.3 Construction of pilot remediation plot on Kavodokanos waste pile in the 1990’s ..... | 16 |
| <b>3. Materials and methods</b> .....  | 20 |
| 3.1 Field Sampling .....   | 20 |
| 3.2 Sample preparation and analysis .....  | 23 |
| 3.3 Chemical analysis methods .....  | 23 |
| 3.4 Mineralogical investigation methods .....  | 24 |
| <b>4. Results</b> .....  | 25 |
| 4.1 Mineralogy of the waste pile .....   | 25 |
| 4.2 Geochemistry .....   | 33 |
| <b>4.2.1 Surface soil samples</b> .....  | 35 |
| 4.2.2 Vertical profile samples .....   | 39 |
| <b>4.2.3 Drainage samples</b> .....  | 47 |
| <b>5. Discussion</b> .....   | 49 |
| 5.1 Effect of treatment plot composition on the stabilization of PTEs.....               | 49 |
| 5.2 Assessment of PTEs long term mobility in the treated and untreated plots.....        | 49 |
| <b>6. Conclusions</b> .....  | 52 |
| <b>References</b> .....  | 53 |
| <b>Appendix I- XRD patterns of the studied samples</b> .....                             | 56 |
| <b>Appendix II – Chemical analysis results</b> .....                                     | 71 |

## 1. Introduction

### 1.1 Research background and rationale of the study

Soil contamination by potentially toxic elements (PTEs) has become a crucial environmental issue, especially within the last few decades since it poses a direct and indirect risk for human health by affecting the environmental quality. Due to the increasing demand of metal(loid)s after the industrial revolution, the global concerns about soil contamination and the remediation techniques have become an urgent matter. Many studies have reported that PTEs once being introduced to the soil are resistant to chemical and biological degradation for a long time, like Pb which persists for more than 150 years, contradictory to organic contaminants (Khalid, et al. 2016). In order to tackle the problem of contaminated soil, remediation technology has become an imperative demand to minimize the bioavailability and mobility of the heavy metals in soils and innovative techniques for site-specific remediation have been developed. The choice of remediation technique is a function of cost effectiveness, time, applicability and efficiency. Most of the developed techniques show high performance but with high cost of implementation, hence the development of reliable techniques with affordable cost and no technical implications which can demonstrate good performance in long-term is a challenging task.

PTEs in soil can be of natural or anthropogenic origin. They can occur within different chemical phases in rocks and minerals. In metal ore they commonly occur as sulfides of Pb, Co, Fe, As, Pb-Zn, Ag and Ni and oxides of Se, Al, Mn and Sb; while anthropogenic activities are represented in solid wastes disposal, ore mining and refining, pesticides, fertilizers and vehicular exhausts (Khalid et al. 2016). Mine tailings mineralogy has high complexity as most of the ore minerals are sensitive to the environmental conditions i.e. pH and Eh and are capable of getting oxidized or dissolved and hence releasing elements to the groundwater (Boulet et al., 1998). Based on a number of studies, a typical visualization of a sulfide ore waste rock pile consists of: A) a vadose zone at the top which is zone of sulfide oxidation and acid generation B) an underlying capillary zone of acid neutralization and chemical precipitation C) a saturated zone; a zone of attenuation and dissolution D) a zone of transport of the dissolved species to the groundwater underneath the pile (Petruk, 2000).

Lead, Ni, Co, Hg, Cr, Cd, Zn, Cu are toxic metals of environmental concern as they are persistent in the environment causing detrimental impacts on human health and ecosystem. Excessive intake of these metals can cause non-carcinogenic and carcinogenic impacts, and this can happen through three pathways; inhalation of the suspended particulates, the direct oral ingestion and the dermal adsorption (USEPA 1991; Miguel et al., 2007; Na et al., 2010). The process of oxidation of the sulphidic tailings is the main concern as not only is the main reason

for the acidic drainage but also for oxidizing the ferrous iron ( $\text{Fe}^{+2}$ ) to ferric iron ( $\text{Fe}^{+3}$ ). Ferric ions with the aid of bacteria are responsible for the rapid breaking down of the pyrite and hence the produced acidity.

Lavrion is a well-known area of prehistoric-to-recent mining activities which resulted in large amounts of sulphidic and carbonate wastes. A number of environmental characterization studies have been conducted in the area and several remedial actions for the hazardous waste dumps have been tested. The most detailed studies have been performed in the 1990's as part of the EU-LIFE project 93/GR/A/14/GR/4576 entitled "Rehabilitation of contaminated soils in the Municipality of Lavrion" (Demetriades et al., 1999). The Kavodokanos pyrites pilot scale remediation tests were constructed in 1995 and the monitoring of the tests lasted until the year 2002 (Mylona et al, 2003). Since then the site has not been monitored.

The Kavodokanos waste pile is one such example of the crucial spots that needed to be remediated as it posed a health risk through the direct contact with contaminants and dust inhalation and ingestion of small particulates, especially because of the proximity of the waste pile to housing. Also, the runoff water was of concern due to the high concentrations of toxic elements which had been transferred to the adjacent soils. Three remediation options had been applied on the Kavodokanos waste pile in 1996 and included one alkaline additive (limestone) and two covers (a synthetic geomembrane and smectite clay). The applied remediating options were held on a square plot on the top of Kavodokanos waste stockpile on with wide length of 24 m divided into 4 quadrants; one acts as a control plot and in the other 3 different remediating techniques were tested (Paspaliaris et al., 1999).

## 1.2 Aim and Objectives of the study

The main aim of this study is to assess the long-term performance of in-situ pyritic waste remediation techniques in one waste pile (Kavodokanos) at the Lavrion urban area.

The specific objectives of the study are:

- ▶ 1. Comparison between the effectiveness of the three different stabilization agents that have been applied in the waste pile almost 25 years ago.
- ▶ 2. Comparison of obtained data on trace metal leachability with the initial data from 1998 (Life project report).
- ▶ 3. Assess the mobility of two trace metals (Pb and Zn) for each treatment technique and determine their spatial distribution horizontally and vertically in the waste pile.

## 2. Literature review

### 2.1 Soil remediation techniques

There are several soil remediation approaches differing in the regulatory procedures, applicability, implementation, cost and performance; each of which can be applied according to the site conditions including type and number of contaminants, their distribution, climate and the municipality approval. However, in many cases a combination of targeted techniques is applied together for economic cost and efficient performance. It is noted here that the term “soil” in the present dissertation denotes any type of contaminated, loose, overburden material including mining waste. There are many classifications of the soil remediation techniques which can be categorized as traditional, vegetative, immobilization and extractive basis and/or relating to the location where the treatment process occurs; in-situ, on-site or off-site (Meuser *et al.*, 2012). In-situ treatment doesn't require previous excavation or transportation of the contaminated soil, i.e. sealing and subsurface barrier, in contrary to on-site treatment which involves digging and transferring the contaminated soil to a nearby site like soil washing and bioremediation, while off-site measures occur in defined facilities which are mostly located far from the contaminated land for example soil spading.

#### **I. Traditional isolation techniques (*mechanical techniques*):**

1) Soil isolation; mostly used to prevent further contamination of the groundwater and/or the surrounding sites. Soil isolation can be achieved by three ways; sealing or capping, subsurface barrier/liner and lateral barrier. Sometimes, these are performed in combination to bound a contaminated cell. Sealing is a way to minimize the direct contact between the contaminated soil with the meteoric water and the oxygen, while subsurface barrier is to separate the contaminated soil and the effluents from the non-contaminated soils. To ensure high isolation, a low-permeability material, e.g. clay, should be selected for the barrier installation. A conventional composite is usually applied in succession to promote high isolation of the targeted contaminated soil; an impermeable layer or synthetic liner topped by a drainage layer to collect the percolated water and direct it and finally a protective layer ending up with a vegetated soil.

2) Soil replacement; simply replacing the contaminated soil by a non-contaminated soil through two methods; soil spading and importing new soil. This technique is limited to small areas due to the high cost of the bulk excavation and transportation either to short or long distance. However, this technique is suitable for highly contaminated soils, it is not applicable to agricultural sites as it reduces the soil fertility. This technique may be considered as the popular remedial method and this is related to its simplicity “dig and dump”, speed and no need for fu-

ture monitoring, however, its practical and logistic constraints represented in estimating the depth of excavation, side dimensions, engineering challenges when encountering water table and finding a landfill disposal, whereas the logistic drawback by authorities aims to limit disposal of contaminated soils, besides the logistic drawback by authorities which aim to limit disposal of contaminated soils (Hodson 2010).

## II. Immobilization techniques

Can be applied in-situ or ex-situ and use either organic and inorganic amendments which are responsible of proceeding faster in the attenuation of the contaminants' mobility by the reactions of precipitation, adsorption, ion exchange and complexation processes. The most popular amendments can be represented in clay, cement, phosphate, organic compost, minerals, microbes and zeolites.

- 1) Stabilization technique; involves mixing some agents with the contaminated soil for generating new stable compounds unreactive to the external agents. Stabilization/solidification is considered as a conventional technology for contaminated soils remediation and a treatment method of hazardous wastes (Wuana et al. 2011). This technique may not be a good choice for contaminated soils rich in organic forms of contaminants thus incineration before proceeding with mixing agents would be an important pre-treatment step to get rid of volatile organics. The effectiveness of this technique is a function of physical (i.e. moisture content, permeability and grain size) and geochemical characteristics (e.g. metal complexes, leachability and PH value) within the targeted contaminated soil (USEPA 2003). Cement, fly ash, clay and organic matter like bitumen and polyethylene are forms of binders used in stabilization technology. A case study of in-situ pilot scale application of attapulgitic clay as a stabilizer agent for a contaminated soil with metalloids was implemented by Zotiadis et al. (2012) in a pilot scale experiment in Lavrion; dictating that attapulgite is a promising and cost-effective binder as it effectively decreased infiltration, controlled and sustained the pH value at slightly alkaline levels through 7-months monitoring as well as reducing the leachable metal by 17% for Cu, 50% for Pb, 45% for Zn, 41% for Cd, 46% for Ag, 18% for As, 47% for Mn, 45% for Ba, and 29% for Sb. A supplementary version of this study has been released by Zotiadis and Argyraki (2013); incorporating three different applications of the attapulgite as a stabilizer agent i) pilot scale of metal amendment for a polymetallic contaminated soil at Lavrion ii) using an innovative geosynthetic reactive clay in an ordered composite with geotextile for treating toxic soil iii) laboratory scale experiment applying the attapulgite to a sewage sludge in terms of different particle size.
- 2) Vitrification technique; the contaminated soil is subjected to high temperature for reducing the contaminants mobility by turning the materials into solid oxides and vitreous

materials. Treatment process can be either implemented in situ or ex situ although it is preferred to be in situ for low labor. This technique is considered as a non-classical easy method which is applicable to a wide range of soil contaminated with inorganic and organic contaminants (Khalid et al. 2016). Obstacles for this technique are the dry soils where there is no melt to carry the current through the soil medium and soils rich in alkali content may not be a good conductor (Buelt et al. 1992).

### III. Vegetative/ phytoremediation technique:

These are defined as an in-situ remedial technology frequently accompanied with soil amendments or microorganisms working on the degradation and increasing the bioavailability for the metal contaminants in the soil for biota uptake or composing stable precipitates. Phytoremediation can be applied by phytoextraction, phytostabilization or phytofiltration based on the functions of the selected plant. The major concerns about this technique are focused on the longtime required for soil clean-up, applications are limited to subsurface zones "depth of the root", large-scale applications require agricultural knowledge and disposal of crop yields while its advantages revolve around being a friendly-environmental remedial technique as not a destructive to the targeted soil.

1) Phytoextraction; is the uptake of metal contaminants by the plant from the root surroundings to its tissues. Consumption of PTEs depends on the capacity/tolerance of every flora species, thereby the terminology of hyperaccumulator emerged which points out to plants capable of high accumulation of some metal species reaching 100-fold greater concentrations than the typical ones but needs long time for the clean-up because of its slow growing and small biomass. Increasing the mobility of PTEs within the soil by using organic agents like chelate enhance the uptake of the plants (Wuana et al. 2011).

2) Phytostabilization; unlike to phytoextraction, refers to the immobilizing of the PTEs by either adsorption by the plant root or precipitation in complexes. The functionality of phytostabilization may be summed to reducing leaching by the water uptake or transpiration caused by the plant, decreasing contamination of the surroundings caused by soil erosion and minimizing infiltration (Khalid et al. 2016).

### IV. Extractive techniques:

Soil washing; involves either in-situ treatment by soil flushing, on-site or ex-situ. This technology is available based on various methodologies; (i) physical separation which requires soil excavation and moving to off-situ or on-site, frequently applied to sandy soils and granular-fraction soils where clay and silt are in less content, (ii) chemical extraction; involves adding chemical agents to the clayey soils aiming to the significant removal of the contaminants, (iii) an integration of both physical and chemical extraction. Recycled soil may be deposited to its

initial place or deposited in landfills as inert material with low cost. The advantage of this technique is that it doesn't require long-term monitoring and doesn't consume time while cons are the cost of excavation and transportation of the targeted soil, the potential of spreading contaminants dust during those procedures and is destructive to the soil nature.

## 2.2 Waste characterization and risk assessment in Lavrion city

Lavrion city, which located approximately 48 km south-east of Athens (fig. 1), has a long history of intensive mining and metallurgical activities since 3500 BC until 1989 resulting in wide spoils of wastes. Environmental pollution in the city of Lavrion initiates mainly from the mining and metallurgical activities which were held through the industrial and historical heritage of Lavrion. The majority of the city has been developed over the waste spoils and surroundings, these wastes were characterized to be rich in toxic and heavy metals; Pb, Cd, Zn and As (NTUA 1999). By the action of the mechanical weathering represented in the wind and water erosion then transportation, loose sediments covering the spoils had been diffused all around causing soil contamination and chemical alteration which facilitates the mobility of PTEs to the underground water.

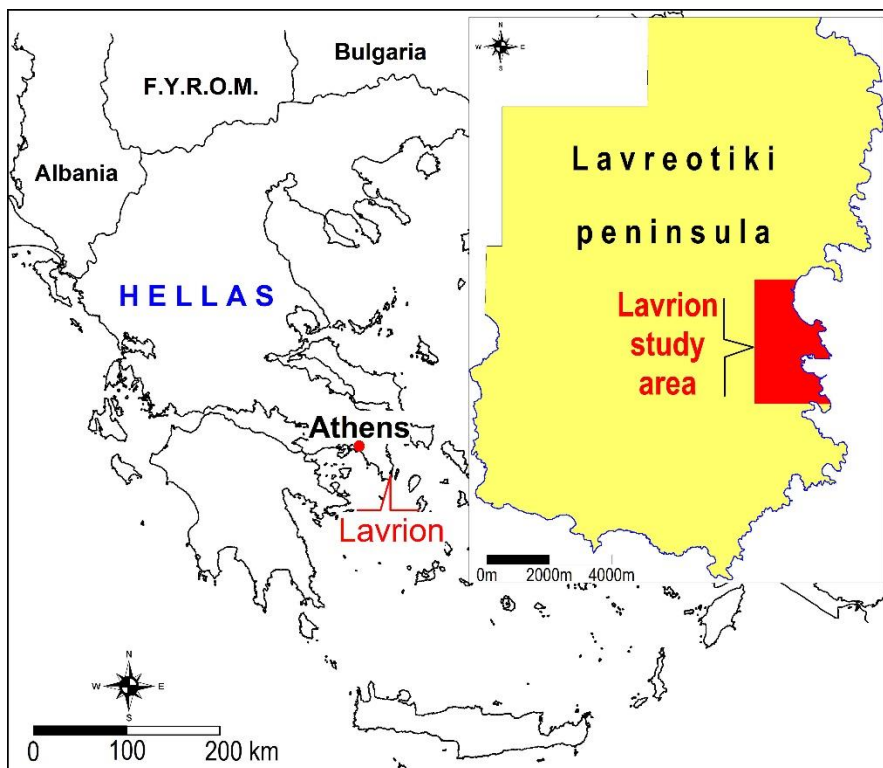


Fig.(1) Location of Lavrion city. (map drawn by A. Demetriades)

The identified spoils can be categorized to three main waste types (NTUA 1999) (Fig. 2):

- Sulfides; are flotation tailings i.e. pyrite and arsenopyrite (Fig 2), easily oxidized by meteoric water and atmospheric oxygen resulting in acidic and contaminated waters transferring PTEs to adjacent soils. The main aspects controlling the oxidation of the pyrite and arsenopyrite in sulfidic spoils are the availability of oxygen and water, temperature, permeability and bacterial activity (Komnitsas et al. 1995).
- Carbonates; beneficiation tailings characterized by high bioavailable metals with high lead leachability.
- Slags; lead smelting residuals with a siliceous matrix, are less hazardous due to the coarse texture and vitreous matrix making it not susceptible to wind erosion or air transfer.

The aspects affecting the oxidation of pyrite and arsenopyrite, the main sources of the acidic solutions and contaminants in the sulfidic wastes of Lavrion, are presented in a study paper by Komnitsas and Xenidis (1995) focusing on the critical factors affecting the oxidation of pyrite and arsenopyrite. Bacterial leaching tests were conducted to pyrite and arsenopyrite samples from a sulfidic stockpile to determine the influence of the bacteria in the oxidation process taking into account the particle size of the grains to simulate the behavior of these minerals in the field. It was noted that arsenopyrite dissolution begins at the same moment of the bacteria existence and proceeds faster than pyrite dissolution which is promoted by the presence of bacterially produced ferric iron, indicating higher oxidation potential of arsenopyrite than pyrite. *T.ferrooxidans* bacteria out of other microorganisms is mostly associated with high concentrations of sulfide minerals and act either directly or indirectly. Direct mechanism proceeds by the physical contact of the bacteria with the sulfide particle surface while indirect mechanisms involve the oxidation of sulfides by the bacterially produced ferric iron. To figure out to what extent the oxidized products exist in Lavrion waste piles, a sum of samples was collected from successive layers and analyzed by XRD and digestion techniques. It was found that the critical factors affecting pyrite and arsenopyrite oxidation in the sulfidic spoils include the availability of oxygen and water, the permeability within the spoils, the temperature and the bacteria activity.

The oxidized products are presented to a depth of 20 cm from the spoil surface where the evaporation process dominates and stop to exist in greater depths. The oxidized products within the upper section are hydrated ferrous sulphate compounds i.e. rozenite  $\text{FeSO}_4 \cdot 4\text{H}_2\text{O}$ , melanterite  $\text{FeSO}_4 \cdot 7\text{H}_2\text{O}$  which are produced by precipitation reactions while in the lower section are hydrous ferric sulphate compounds like kornelite  $\text{Fe}_4(\text{SO}_4)_6 \cdot 15\text{H}_2\text{O}$ . the oxidized layers close to the surface are characterized by little to no detected calcite and arsenopyrite since these phases are converted to gypsum and ferric arsenate respectively, while the lower section of the oxidized layers almost lack any oxidized products due to the low permeability of the waste and are in accordance with the average mineralogical analysis of the spoil mass.

Elements released by oxidation and dissolution of primary minerals may be incorporated into secondary minerals by precipitation, sorption or ion exchange, or transferred by solution thereby contaminating groundwater or causing surface contamination (Boulet and Larocque 1998).

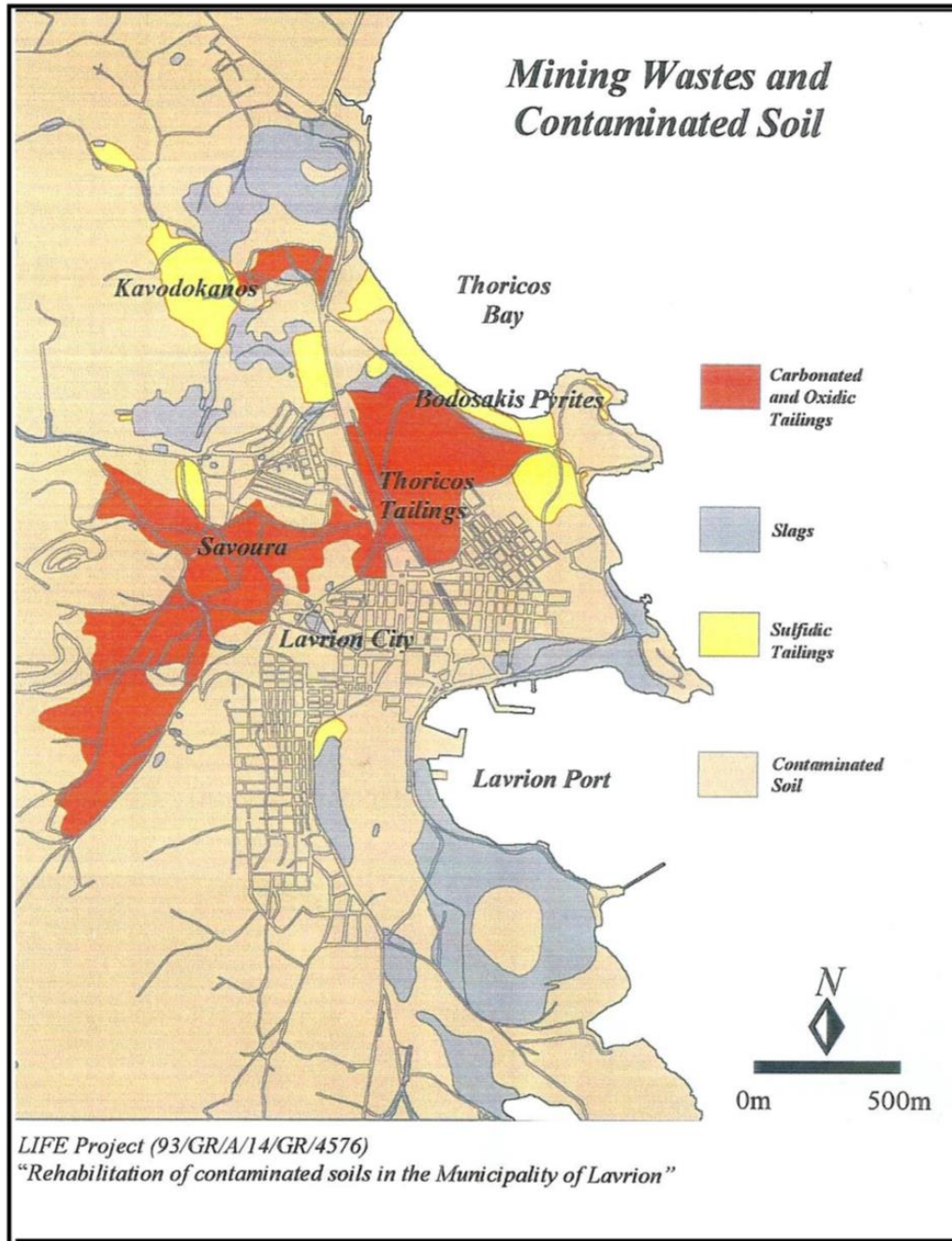


Fig.(2)

Types of mining and metallurgical wastes deposited during different time periods and contaminated soil in Lavrion city as mapped by the Life project in the 1990's (Demetriades et al. 1999)



*Fig.(3) Drone view (looking east) of the Kavodokanos sulfidic flotation tailings pile in Lavrion city, in close proximity to the residential area. The rehabilitated “Bodosakis Pyrites” of Thoricos Bay are also visible in a distance. Photo taken in November 2019.*

Based on the following aspects the risk evaluation of Lavrion waste piles was undertaken by NTUA (1999): capacity for generating acidity, quality of the pore-water, total concentration and bioavailability of the contaminants and toxicity represented in TCLP test.

Sulfidic tailings were characterized as hazardous spoils as they contained a considerable amount of bioavailable and toxic contaminants due to the partial oxidation with the presence of the atmospheric oxygen and the meteoric water.

a) Bodosakis pyrites: pose high potential for generating acidity. The run-off water in this area was found to be very acidic (pH=1.9) with high concentration of toxic metals.

- The spoil is classified as extremely hazardous because of its very high acid generation capacity, high bioavailable fractions of Pb, Cd and As and poor pore water quality; the polluted waters generated within the spoil drain.

It is noted that the Bodosakis pyrites located on the Thoricos Bay are now remediated following a rehabilitation project of the Thoricos Bay (Panagopoulos et al., 2009).

b) Kavodokanos pyrite: considered to be more hazardous with high concerns of its position and volume as well as the development of new properties for residents surrounding and over this stockpile.

- The waste is characterized as toxic according to the TCLP test as the high solubility of Pb.
- The bioavailable (EDTA leachable) fraction of the heavy metals is extremely high.
- Pore-water shows poor quality due to high concentrations of Zn and Cd.
- The observed negativity of NNP of the surface layer indicates the potential of acid generation.

### 2.3 Construction of pilot remediation plot on Kavodokanos waste pile in the 1990's

The detailed design of the pilot remediation plot is described in the EU-Life project report (NTUA, 1999) After leveling off the top surface of the Kavodokanos waste pile, the surface area was subdivided into 4 equal quadrants separated by a 2 mm synthetic liner. Each quadrant has a fixed lysimeter for collecting the percolated water (Fig. 4)



*Fig.(4) Drone view of the Kavodokanos waste pile in November 2019. The borders of the 4 quadrants are still visible due to changing vegetation patterns.*

Based on the US Environmental Protection Agency (EPA) recommendations regarding the isolation techniques, a conventional composite should be placed for achieving an optimal performance. The protective soil used in the two isolation techniques to cover the top and slopes of the pile originated from the area of Keratea, 12 Km NW of Lavrion. The treatments of each one of the quadrants are described below:

A. *Geomembrane cover*: the first installation layer was limestone sand (30cm) acting as a capillary barrier followed by a geotextile sheet for protecting the geomembrane. A high-density polyethylene (HDPE) liner 1mm thick was applied as an impermeable layer then a drainage layer of limestone sand (30cm). A final overlying one-meter layer of protective soil was placed to protect the underneath layers from weathering.

B. *Compacted clay cover*: a fine-texture clayey soil, originating from Markopoulo 20 km NW of Lavrion city, was chemically analyzed and found to meet the Dutch and Canadian guidelines hence it was selected as a low permeability clay layer. Following the same constructional design as in geomembrane plot, about 60 cm-clayey layer were set up above the capillary barrier overlaid by a sand layer to reduce evaporation and cracking then covered by 40 cm of protective soil layer.

C. *Addition of limestone*: limestone sand which has been used as drainage layer in GM and CC plots was also used as alkaline additive containing 90%  $\text{CaCO}_3$  in one of the test plots. Specifically, a mixture containing 20 % w/w limestone and 1000 tons of Bodosakis pyrites (with high acid generation potential) was prepared and placed above Kavodokanos pyrite material. The laboratory studies that preceded the treatment installation determined that the optimal mixing quantity of limestone would be 7 % w/w of Bodosakis pyrites; however, the equivalent amount of limestone that was added in the field plot was 20 % w/w of the excavated Bodosakis pyrites, and this increased amount was due to the coarser grain size utilized in the field compared to the lab test.

D. *Control plot*: The waste was left untreated as a comparative tool between the obtained treatment results; the quantity of the infiltrated water and its acidity. Only a protective top soil of 20 cm was placed on the top of the waste.

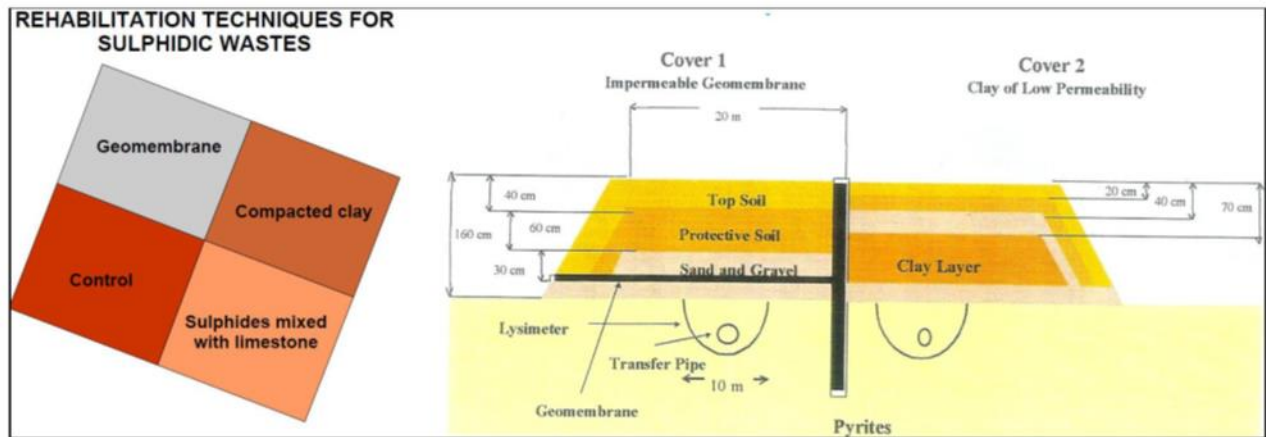


**Fig.(5)** Design of the pilot scale testing of rehabilitation techniques for sulphidic wastes in Kavodokanos waste pile during the Life project in the 1990's.

The short-term assessment of the treatment effectiveness has been based on two years of monitoring of the waste pile and the conclusions are summarized below (NTUA 1999):

- The climatic conditions in Lavrion city are characterized by a dry period with low precipitation parallel to a low permeability of the Kavodokanos pyritic tailings. This led to production of low volume of leachate in CL plot about 5.7 % of the total annual rainfall. This leachate was acidic and rich in contaminants like Fe, Zn, As and Cd.
- The isolation technique of the pyritic wastes with compacted clay showed a good performance with preventing 95% of the total leachate. The produced leachate was related to the desiccation and cracking of the clay layer during the summer period of 1998. Since this time there was no detected leachate which is an indication for coherence of the clay layer which was reestablished after the rainfall of autumn 1998. It has been suggested, based on the field data, that for better performance especially in dry areas like Lavrion the clay layer should retain its moisture and this can be achieved by optimizing a capillary barrier on the top of the clay layer.
- Isolation with the geomembrane synthetic liner effectively prevented any infiltration and thus there was no leachate collected during the two-year monitoring period.
- Adding mixture of the Bodosakis pyrite-limestone over the Kavodokanos pyrite increased the percolated water two folds comparing to the control plot producing a leachate amount of 12% of the total annual precipitation. The alkalinity produced by lime wasn't enough to neutralize the acidity from the underlying pyrite and the leachate posed high levels of contaminants. Despite the high acidity of the leachate, the quality of the infiltration produced was better than the one reported in the control plot of Kavodokanos pyrite. The alleged formation of the hard pan was not observed during the short-term monitoring and was concluded that this plot needs longer time for enhancing the mechanism of hard pan formation.

According to the obtained results in the short-term assessment, the geomembrane cover is considered as the most effective technique for preventing infiltration while the compacted clay is a second alternative which can show better performance based on its establishment.

### 3. Materials and methods

#### 3.1 Field Sampling

In November 2019, five soil samples were collected from each quadrant of the Kavodokanos waste pile, every single sample is a composite of three nearby points. The surface composite samples were collected in a zigzag line (Fig. 6). A sum of twenty surface soil samples have been collected using an auger and packed in resealable plastic bags. The uppermost layer 10-15 cm was collected in order to represent the exposure relevant portion of the soil. The topsoil and/or vegetation layer- was skimmed before sampling and the plastic bags were tightly sealed to prevent any potential reaction with the air after packing the samples.

In May 2020, additional vertical sequence samples were collected from the site by a hand-held auger at depth intervals of 15 to 20 cm per each batch, wherever possible. Up to 105 cm vertical profiles were collected from three of the quadrants, one profile per each plot. The profile samples comprise 5 vertical successive samples for both the control plot (CL) and the sulfidic-lime mixture plot (SL), 3 successive samples from the compacted clay plot (CC) and one from the geomembrane plot (GM). The reason why limited vertical depth profiles are sampled from compacted clay (CC) and geomembrane (GM) plots is that in the CC plot a hardened layer was encountered at a depth of about 35 cm, getting harder with depth, while in the GM plot the synthetic geomembrane was encountered at shallow depth. Four solidified drainage material samples were also collected from the lysimeter tanks situated under each plot. A second drainage sample was collected from the inner part of the pipe of the lysimeter below the CC plot. Finally, 2 hard crust surface samples were collected for mineralogical investigation based on field observation from the SL plot; color and cementation, a thin coating layer and a notable dark green spot on the surface. All samples were put in plastic bags and labeled as following; soil samples are referred to as C, SL, CC, GM, core samples as CCL, CSL, CCCA, CGM, drainage samples as DCL, DSL, DCC, DGM, LYCCI, LYCCO and the SL surface samples as CRUST1 SL, CRUST2 SL. A summary of the sample description is presented in Table 1 and field sampling photos in Fig. 6.

Table (1) List of samples collected during this study with methods applied for analysis and sample description.

| AA | sample ID | XRD | SEM-EDS | Aqua regia | SBET | TCLP | Sample description  |
|----|-----------|-----|---------|------------|------|------|---|
| 1  | CCL1      | ✓   | ✓       | ✓          | ✓    |      | vertical prof. control plot 0-20 cm                           |
| 2  | CCL2      |     |         |            |      |      | vertical prof. control plot 20-40 cm                          |
| 3  | CCL3      |     | ✓       | ✓          |      |      | vertical prof. control plot 40-60 cm                          |
| 4  | CCL4      |     |         |            |      |      | vertical prof. control plot 60-80 cm                          |
| 5  | CCL5      | ✓   | ✓       | ✓          |      |      | vertical prof. control plot 80-100 cm                         |
| 6  | CSL1      | ✓   | ✓       | ✓          | ✓    |      | vertical prof. sulfidic lime                                  |
| 7  | CSL2      |     |         |            |      |      | vertical prof. sulfidic lime                                  |
| 8  | CSL3      |     | ✓       | ✓          |      |      | vertical prof. sulfidic lime                                  |
| 9  | CSL4      |     |         |            |      |      | vertical prof. sulfidic lime                                  |
| 10 | CSL5      | ✓   | ✓       | ✓          |      |      | vertical prof. sulfidic lime                                  |
| 11 | CCC1A     | ✓   |         | ✓          | ✓    |      | vertical prof. compacted clay May drill hole                  |
| 12 | CCC2A     |     |         | ✓          |      |      | vertical prof. compacted clay                                 |
| 13 | CCC3A     | ✓   |         | ✓          |      |      | vertical prof. compacted clay                                 |
| 14 | CGM1      | ✓   | ✓       | ✓          | ✓    |      | vertical prof. compacted clay surface                         |
| 15 | DCL-W     | ✓   | ✓       | ✓          | ✓    |      | drainage from lysimeter under control                         |
| 16 | DCL-Y     |     |         |            |      |      | drainage from lysimeter under control                         |
| 17 | DSL       | ✓   | ✓       | ✓          | ✓    |      | drainage from lysimeter under sulfidic lime                   |
| 18 | DGM       | ✓   | ✓       | ✓          | ✓    |      | drainage from lysimeter under geomembrane                     |
| 19 | DCC       | ✓   | ✓       | ✓          | ✓    |      | drainage from lysimeter under compacted clay                  |
| 20 | LYCCI     | ✓   | ✓       |            |      |      | drainage from lysimeter under compacted clay in pipe          |
| 21 | LYCCO     | ✓   |         |            |      |      | drainage from lysimeter under compacted clay out on container |
| 22 | CRUST1 SL | ✓   |         | ✓          | ✓    |      | from sulfidic lime plot brownish-yellow                       |
| 23 | CRUST2 SL | ✓   |         | ✓          | ✓    |      | from sulfidic lime plot dark green spot                       |
| 24 | C1        |     |         |            | ✓    | ✓    | Surface control plot (Nov 2019)                               |
| 25 | C2        |     |         | ✓          | ✓    | ✓    | Surface control plot (Nov 2019)                               |
| 26 | C3        |     |         | ✓          | ✓    | ✓    | Surface control plot (Nov 2019)                               |
| 27 | C4        |     |         |            | ✓    | ✓    | Surface control plot (Nov 2019)                               |
| 28 | C5        |     |         | ✓          | ✓    | ✓    | Surface control plot (Nov 2019)                               |
| 29 | GM1       |     |         | ✓          | ✓    | ✓    | Surface GEOMEMBRANE plot (Nov 2019)                           |
| 30 | GM2       |     |         |            | ✓    | ✓    | Surface GEOMEMBRANE plot (Nov 2019)                           |
| 31 | GM3       |     |         |            | ✓    | ✓    | Surface GEOMEMBRANE plot (Nov 2019)                           |
| 32 | GM4       |     |         | ✓          | ✓    | ✓    | Surface GEOMEMBRANE plot (Nov 2019)                           |
| 33 | GM5       |     |         | ✓          | ✓    | ✓    | Surface GEOMEMBRANE plot (Nov 2019)                           |
| 34 | SL1       |     |         |            | ✓    | ✓    | Surface sulfidic lime plot (Nov 2019)                         |
| 35 | SL2       |     |         | ✓          | ✓    | ✓    | Surface sulfidic lime plot (Nov 2019)                         |
| 36 | SL3       |     |         |            | ✓    | ✓    | Surface sulfidic lime plot (Nov 2019)                         |
| 37 | SL4       |     |         | ✓          | ✓    | ✓    | Surface sulfidic lime plot (Nov 2019)                         |
| 38 | SL5       |     |         | ✓          | ✓    | ✓    | Surface sulfidic lime plot (Nov 2019)                         |
| 39 | CC1       |     |         |            | ✓    | ✓    | Surface compacted clay plot (Nov 2019)                        |
| 40 | CC2       |     |         | ✓          | ✓    | ✓    | Surface compacted clay plot (Nov 2019)                        |
| 41 | CC3       |     |         |            | ✓    | ✓    | Surface compacted clay plot (Nov 2019)                        |
| 42 | CC4       |     |         | ✓          | ✓    | ✓    | Surface compacted clay plot (Nov 2019)                        |
| 43 | CC5       |     |         | ✓          | ✓    | ✓    | Surface compacted clay plot (Nov 2019)                        |



Fig. (6) Field sampling photos at Kavodokanos waste pile in May 2020.

### 3.2 Sample preparation and analysis

After collection, the samples were transported to the Laboratory of Economic Geology and Geochemistry, NKUA for the pre-analysis procedures. Beginning with drying, samples were unpacked in aluminum containers and put into an oven with a temperature adjustment at 40° C for 2 days then the dried tailings were mixed homogeneously and splatted by the quartering sampling method to achieve representative subsamples which got gently disaggregated using a porcelain mortar and pestle.

The powdered samples were then sieved and subdivided into two proportions; < 2 mm and < 100 µm and the gravels and siliceous particles were excluded. The <2 mm fraction was kept for the physiochemical tests while the finer (<100 µm) fraction was used for chemical analysis and mineralogical investigation. pH measurements were determined by 8:20 soil to water extract ratio while electric conductivity and total dissolved solids (T.D.S) were measured in diluted extract 8:40 ratio using conductivity and T.D.S meter.

### 3.3 Chemical analysis methods

The different analytical methods applied to the samples is presented in Table 1. A selection of 28 samples was sent to *SGS Canada Minerals Burnaby* for total chemical analysis using Aqua Regia Digesting method (HCL/HNO<sub>3</sub>), 0.25g-20mL and a total of 34 elements were analyzed by ICP-AES for every single sample.

Additionally, in the Laboratory of Economic Geology and Geochemistry, the in-vitro metal bioaccessibility assessment method of SBET has been used. This is a simplified version of a Physiologically Based Extraction Test (PBET) and is faster, easier and been validated by US EPA (*Juhasz et al. 2007*) as an extraction test procedure for determining the in vitro lead bioavailability. The SBET test which simulates the gastric solution, was implemented according to the in vitro bioaccessibility assay of U.S. EPA-Method 1340. The extraction solution was of 0.4 mole/ 1 L glycine adjusted to pH 1.5 using concentrated HCl in a 0.5 : 50 solid /solution ratio. A quantity of 0.5 g of each sample was placed in 50 mL Polypropylene Centrifuge Tubes with 50 mL of extraction solution then the mixture tubes got sealed and shook in an incubator at 37 °C for 1 hour, followed by centrifugation and filtration using disposable 0.45µm syringe filters. The filtered solutions were kept in clean tubes in the refrigerator till it got assayed by atomic absorption spectroscopy (AAS). A sum of 40 samples was analyzed including duplicate samples, and blank solutions for quality assurance and quality control. The in vitro Pb bioaccessibility ratio was then calculated following the formula:

$$\text{In vitro Pb bioaccessibility \%} = \left( \frac{\text{SBET Pb}}{\text{total Pb}} \times 100 \right)$$

### 3.4 Mineralogical investigation methods

For mineralogical analysis, a portion of the finer fraction of the samples was top loaded into a circular cavity holder then proceeded for analysis using an X-ray diffractometer Siemens D5000. The obtained recorded patterns were saved on a computer and later mineral phases identification was accomplished by using the “Diffrac Plus XRD ” software. Scanning Electron Microscopy (SEM) (JEOL JSM 5600) coupled with energy dispersive X-ray EDS analysis (Oxford ISIS) has been performed using both bulk and fine specimens, using primary electron beam energy of 20-30 KeV. Specimens’ surfaces have been coated with carbon and vacuumed before proceeding to the SEM-EDS.

## 4. Results

### 4.1 Mineralogy of the waste pile

Both XRD and SEM- EDS results are used in order to characterize the mineralogical composition of the studied samples. Results are presented for each one of the treatment plots in the following paragraphs. The major minerals were identified by XRD and are presented in Table 4. XRD patterns are presented in Appendix I.

#### **Control plot (CL):**

The mineralogical composition from the perspective of EDS measurements consists of Zn-bearing iron oxyhydroxides, silicates, Na-feldspar, limited primary sulfide minerals and abundant gypsum. Secondary gypsum occurs throughout as a cementing mineral, and as massive irregular clumps coated with a thin layer of Fe oxyhydroxides (Fig. 7). Secondary gypsum commonly has traces of Fe and Zn, likely as inclusions contradictory to the tertiary pure gypsum which occurs mainly as microscopic rosettes in fractures and corners of the grains, or as radiating clusters of crystals along grain edges (Boulet et al., 1998).

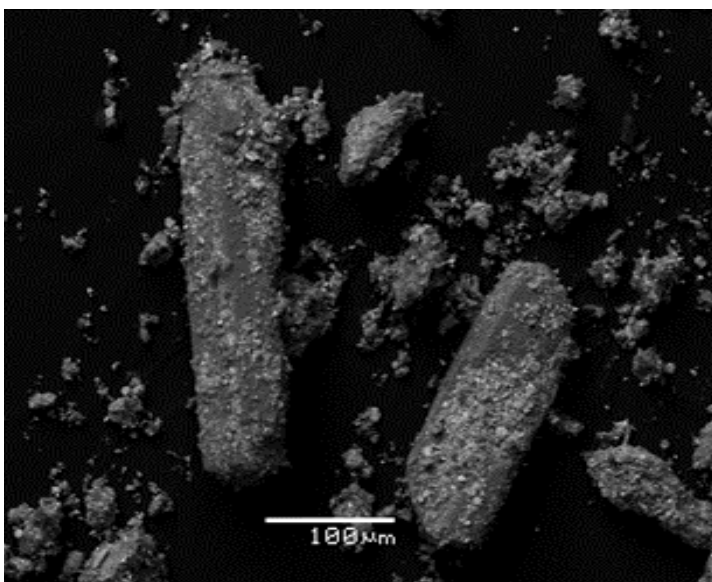


**Fig.(7)** Elongated gypsum crystals

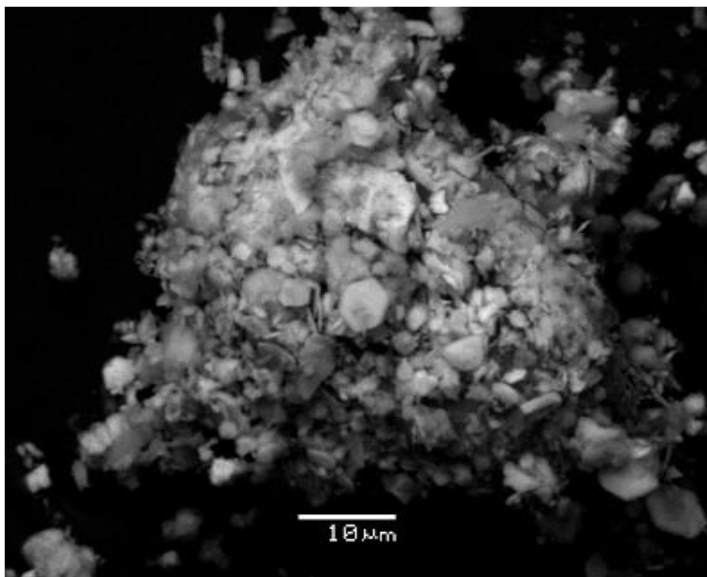
The surface layer of the Control plot contains abundant plumbojarosite crystals (Fig. 8) and is enriched with Zn, Cu and Pb. These efflorescent Fe-hydrosulphate crystals present hexagonal crystal habit overlying equant bodies of aluminosilicates. In greater depths along a depth profile, down to 100 cm, Mg- Al silicates dominate and occurrence of iron oxides and primary phase minerals is increasing.

Table 4. Mineral phases in the studied samples identified by XRD .

| Sample/mineral  | CCL <sub>1</sub> | CCL <sub>5</sub> | DCL-w | CCC <sub>1A</sub> | CCC <sub>3A</sub> | DCC | CSL <sub>1</sub> | CSL <sub>5</sub> | CR <sub>1</sub> SL | CR <sub>2</sub> SL | DSL | CGM <sub>1</sub> | DGM | LYCCI | LYCCO |
|---|------------------|------------------|-------|-------------------|-------------------|-----|------------------|------------------|--------------------|--------------------|-----|------------------|-----|-------|-------|
| <b>Quartz</b><br><i>SiO<sub>2</sub></i>   | ✓                |                  |       | ✓                 | ✓                 |     | ✓                | ✓                | ✓                  |                    | ✓   | ✓                |     |       |       |
| <b>Calcite</b><br><i>CaCO<sub>3</sub></i>   | ✓                |                  |       | ✓                 | ✓                 |     | ✓                |                  | ✓                  | ✓                  |     | ✓                |     | ✓     | ✓     |
| <b>Gypsum</b><br><i>CaSO<sub>4</sub>·2H<sub>2</sub>O</i>  | ✓                |                  |       |                   |                   | ✓   | ✓                | ✓                |                    | ✓                  | ✓   |                  | ✓   |       | ✓     |
| <b>Albite</b><br><i>NaAlSi<sub>3</sub>O<sub>8</sub></i>   |                  |                  |       | ✓                 | ✓                 |     |                  |                  |                    |                    |     | ✓                |     | ✓     |       |
| <b>Kaolinite</b><br><i>Al<sub>2</sub>Si<sub>2</sub>O<sub>5</sub>(OH)<sub>4</sub></i>  |                  |                  |       | ✓                 |                   |     |                  |                  |                    |                    |     |                  |     |       |       |
| <b>Montmorillonite</b><br><i>(Na,Ca)<sub>0,3</sub>(Al,Mg)<sub>2</sub>Si<sub>4</sub>O<sub>10</sub>(OH)<sub>2</sub>·n(H<sub>2</sub>O)</i> |                  |                  |       | ✓                 | ✓                 |     |                  |                  | ✓                  |                    |     | ✓                |     |       |       |
| <b>Anorthite</b><br><i>CaAl<sub>2</sub>Si<sub>2</sub>O<sub>8</sub></i>  |                  |                  |       |                   |                   |     | ✓                |                  |                    |                    |     |                  |     |       |       |
| <b>Illite</b><br><i>(K,H<sub>3</sub>O)(Al,Mg,Fe)<sub>2</sub>(Si,Al)<sub>4</sub>O<sub>10</sub>[(OH)<sub>2</sub>,(H<sub>2</sub>O)]</i>    |                  |                  |       |                   |                   |     | ✓                | ✓                | ✓                  |                    |     |                  |     |       |       |
| <b>Jarosite</b><br><i>KFe<sup>+3</sup><sub>3</sub>(SO<sub>4</sub>)<sub>2</sub>(OH)<sub>6</sub></i>                                      | ✓                |                  |       |                   |                   | ✓   | ✓                | ✓                | ✓                  | ✓                  | ✓   |                  | ✓   | ✓     | ✓     |
| <b>Plumbojarosite</b><br><i>PbFe<sup>+3</sup><sub>6</sub>(SO<sub>4</sub>)<sub>4</sub>(OH)<sub>12</sub></i>                              | ✓                | ✓                |       |                   |                   |     |                  | ✓                | ✓                  |                    |     |                  |     |       |       |
| <b>Rozenite</b><br><i>Fe<sup>+2</sup>SO<sub>4</sub>·4H<sub>2</sub>O</i>   |                  |                  | ✓     |                   |                   | ✓   |                  |                  |                    |                    |     |                  |     |       |       |
| <b>Copiapite</b><br><i>Fe<sub>14</sub>O<sub>3</sub>(SO<sub>4</sub>)<sub>18</sub>·63H<sub>2</sub>O</i>                                   |                  |                  |       |                   |                   |     |                  |                  |                    |                    |     |                  |     | ✓     | ✓     |
| <b>Galena</b><br><i>PbS</i>   |                  |                  | ✓     |                   |                   |     |                  |                  |                    |                    |     |                  |     |       |       |
| <b>Pyrite</b><br><i>FeS<sub>2</sub></i>   |                  |                  |       |                   |                   |     |                  | ✓                |                    |                    |     |                  |     |       |       |
| <b>Szomolnokite</b><br><i>Fe<sup>+2</sup>SO<sub>4</sub>·H<sub>2</sub>O</i>  |                  |                  | ✓     |                   |                   |     |                  |                  |                    |                    |     |                  |     |       |       |
| <b>Gunningite</b><br><i>ZnSO<sub>4</sub>·H<sub>2</sub>O</i>   |                  |                  |       |                   |                   |     |                  |                  |                    |                    |     |                  |     | ✓     | ✓     |

|  |  |   |  |  |  |  |   |  |  |  |   |  |  |  |   |
|--|--|---|--|--|--|--|---|--|--|--|---|--|--|--|---|
| <b>Basaluminite</b><br>$Al_4SO_4(OH)_{10} \cdot 4H_2O$ |  |   |  |  |  |  | ✓ |  |  |  |   |  |  |  |   |
| <b>Boyleite</b><br>$ZnSO_4 \cdot 4H_2O$                |  |   |  |  |  |  |   |  |  |  | ✓ |  |  |  | ✓ |
| <b>Greenockite</b><br>$CdS$                            |  | ✓ |  |  |  |  |   |  |  |  |   |  |  |  |   |
| <b>Clinocllore</b><br>$(Mg_5Al)(Si,Al)_4O_{10}(OH)_8$  |  |   |  |  |  |  | ✓ |  |  |  |   |  |  |  |   |

Aluminosilicate complexes of Fe, Mg and Ca occur as elongated flattened bodies, while metallic greyly precipitates of hematite  $\text{Fe}_2\text{O}_3$  are reported. Zinc ions show high tendency to be sequestered in iron complexes regardless to iron valences hence in the hematite precipitates high content of Zn is noticed possibly due to adsorption. Partially oxidized pyrite was recorded; the pyritic grains show sharp edges denoting retention of the primary phase signature, however, some emerging oxidation is evident on the surface (Fig. 9). The X-ray diffractogram patterns confirm the presence of primary and secondary minerals such as calcite and plumbojarosite, respectively.



**Fig. (8)** Hexagonal plumbojarosite crystals of  $<5\mu\text{m}$  diameter, with Zn and Cu enrichment.

Drainage precipitates collected from the surface of the lysimeter tank of the control plot (DCL) are rich in iron sulphate and specifically rozenite  $\text{Fe}^{+2}\text{SO}_4 \cdot 4\text{H}_2\text{O}$  and szomolnokite  $\text{Fe}^{+2}\text{SO}_4 \cdot \text{H}_2\text{O}$  which were identified by XRD. SEM-EDS results point out to surface precipitation of iron oxyhydrosulphates intersecting with ubiquitous sulphate salt of acicular gypsum. Fine precipitates of szomolnokite  $\text{Fe}^{+2}\text{SO}_4 \cdot \text{H}_2\text{O}$  are abundant and overlapping locally with crystalline plumbojarosite acting as a cementing material.

Arsenic is detected in a number of samples by EDS analysis, denoting possible adsorption on ferric iron oxyhydroxides (Panagiotaras and Nikolopoulos, 2015). An efflorescence mass growth over the lysimeter tank was observed during sampling (Fig 6) with three different rim colors; green in base overlaid by brown and topped with white; the base section contains melanterite with base-metal solid solution of Zn ( $> 1\%$ ), Mn (1262 ppm) and low content of Cu (172 ppm), while the brown rim is established by further oxidation and therefore setting of

new tertiary minerals possibly ferrihydrite, and the top white powder is the dehydrated mineral of rozenite.

### ***Sulphidic-lime mixture plot (SL)***

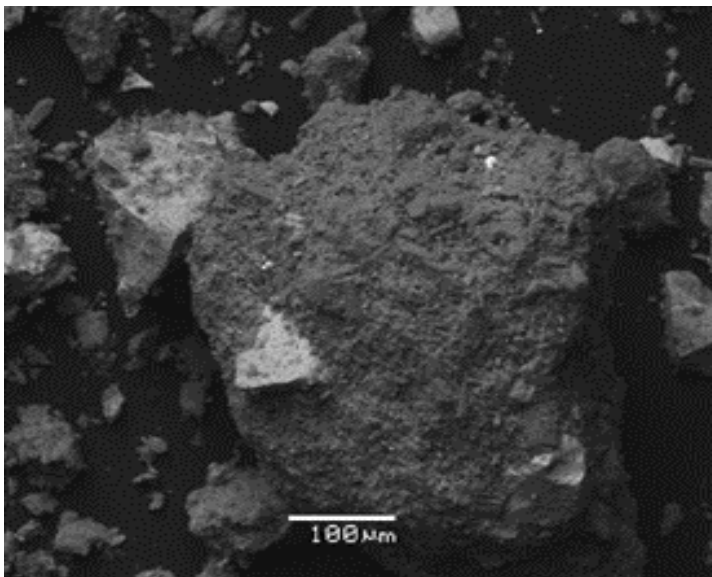


**Fig. (9)** Pyrite crystals (light gray) intersecting with cemented gypsum (grey).

The SL plot is distinguished by its wide variety of identified phases and this can be justified by the fact that this quadrant is a mixture of highly acidic pyrite with  $S > 47\%$  (Bodosakis pyrite), the Kavodokanos tailing waste and the lime as an additive. The mineralogy of collected samples consists mainly of massy flattened aluminosilicate minerals overlaid by common fine precipitates of iron oxides, hydroxides, oxyhydrosulphates, metal sulphate and limited detection of efflorescent crystals.

Al - Si group minerals are dominating the upper layer of SL plot in massive bodies. The following aluminosilicates were identified by XRD: anorthite  $\text{CaAl}_2\text{Si}_2\text{O}_8$ , Illite  $(\text{K},\text{H}_3\text{O})\text{Al}_2\text{Si}_3\text{AlO}_{10}(\text{OH})_2$  and clinocllore  $(\text{Mg}_5\text{Al})(\text{Si},\text{Al})_4\text{O}_{10}(\text{OH})_8$ . Fine cemented precipitates of szomolnokite  $\text{Fe}^{+2}\text{SO}_4 \cdot \text{H}_2\text{O}$  and ferric arsenite compounds are layering the surface of the silicates with infrequent detection of plumbojarosite crystals based on the SEM-EDS study (Fig. 10). Beside silicate minerals, iron compounds have wide occurrence and are present as a coherent bulky mass of goethite typically enriched in the trace metals Zn and Pb.

In subsurface horizons the metal sulphate salt of anglesite ( $\text{PbSO}_4$ ) is present in association with Al - Si matrices, iron hydroxides (possibly goethite  $\alpha\text{-Fe}^{+3}\text{O}(\text{OH})$ ) and hydrosulphates such as jarosite ( $\text{KFe}^{+3}_3(\text{SO}_4)_2(\text{OH})_6$ ).

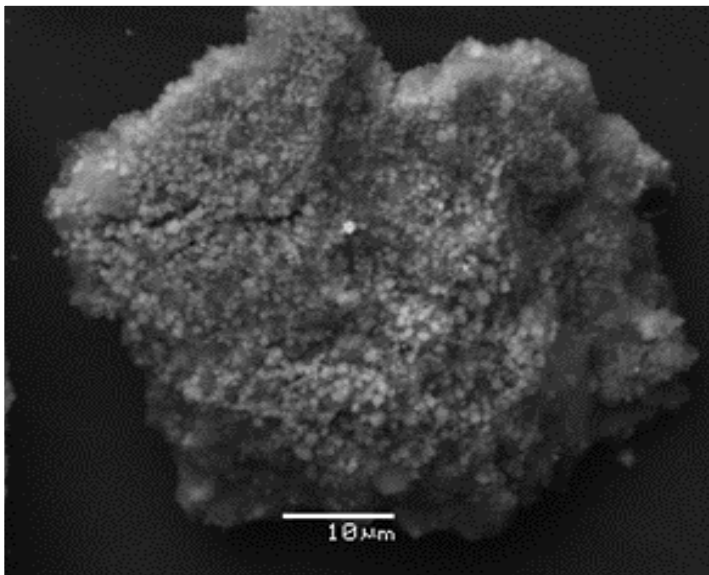


**Fig. (10)** Efflorescent crystals of jarosite group minerals.

Pyrite is dominating as primary phase. Descending further to deeper horizons, there is greater preservation of the pyritic crystals which do occur in sharp edges denoting no oxidation, however, some are partially oxidized or depleted presenting equant bodies with eroded edges. There is also precipitation of gypsum over pyritic minerals shaped in pencil structures. XRD confirmed the pyrite and gypsum presence with two secondary minerals of jarosite and plumbojarosite. Referring to the two "crust" samples of SL plot which were collected based on diversity in coloration, the yellowish coating sample is chiefly composed of the ferrous sulphate salt of rozenite intersecting with anglesite crystals while the greenish one corresponds to pyrite.

Drainage precipitates of sulphidic lime plot (DSL), collected from the surface of the lysimeter tank are characterized by massive crystalline and chiefly efflorescent gypsum in different sizes and lengths; acicular gypsum crystals may extend for more than 0.7 mm length and diameter reaches  $46.5 \mu\text{m}$ . The drainage sample has limited occurrence of iron sulphate salts and iron oxyhydroxides; Coquimbite  $\text{Fe}^{+3}_2(\text{SO}_4)_3 \cdot 9\text{H}_2\text{O}$  and plumbojarosite were identified. The sample surface exhibits two orders in the size of gypsum crystals, bigger ones are superposed to smaller ones depending on the amount and seasonal cycles of the percolated water and its enrichment with calcium. XRD demonstrates gypsum, jarosite, quartz and boyleite  $\text{ZnSO}_4 \cdot 4\text{H}_2\text{O}$ .

### **Geomembrane plot (GM)**

The minerals identified in the samples of GM plot include quartz, gypsum and relatively spherical grains of cemented silicate clusters with minor presence of efflorescent iron hydrosulphates on the surface of the silicates (Fig. 11). Montmorillonite and albite are the representatives of aluminosilicates while goethite and rozenite  $\text{Fe}^{+2}\text{SO}_4 \cdot 4\text{H}_2\text{O}$  are the major iron hydroxides and iron sulphate salts identified.

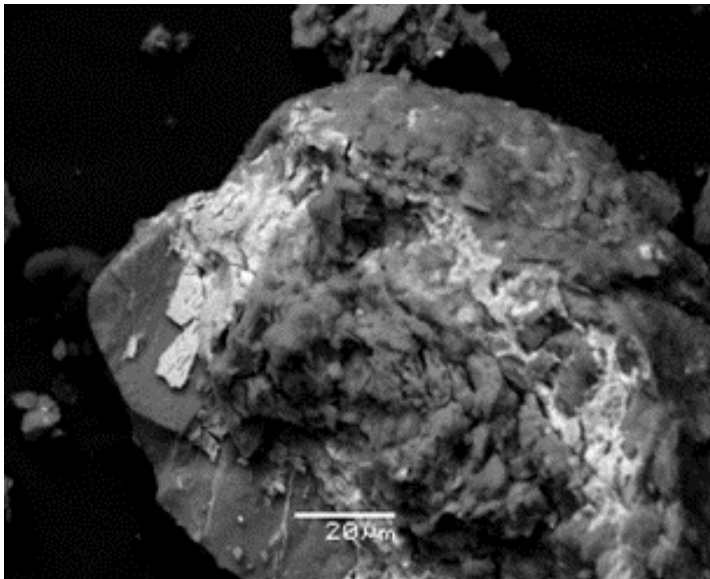


*Fig. (11) Quartz grain overlaid by montmorillonite and goethite encrustations.*

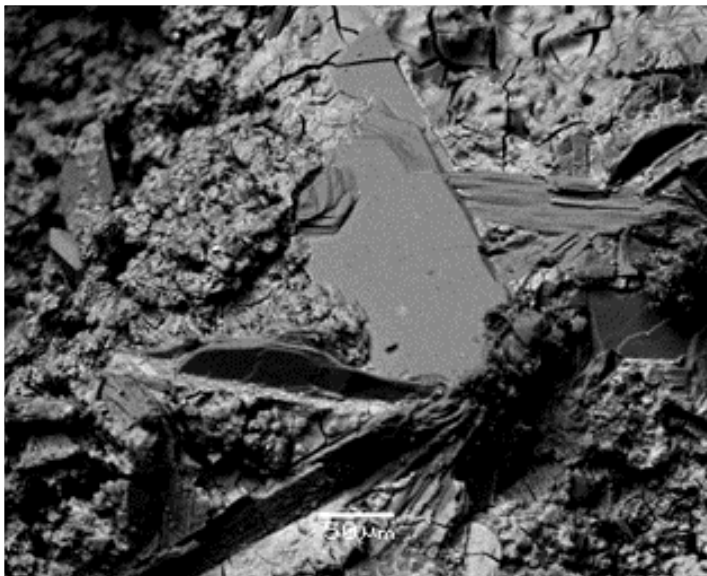


*Fig. (12) Crystalline gypsum intersects with siliceous matrix (DGM sample)*

The frequent contribution of As in the majority of the detected phases possibly denotes substitution of sulphate in jarosite group minerals, forming ferric arsenite compounds or co-precipitation with aluminosilicates complexes.

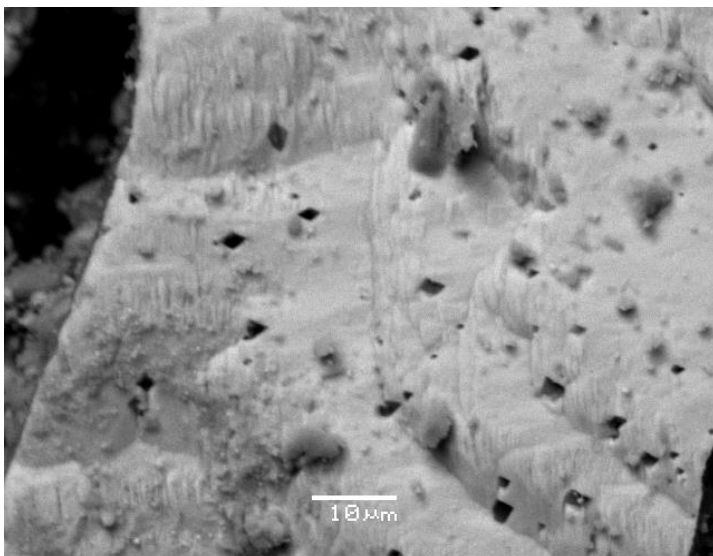


**Fig. (13)** Acid etched pyrite crystal in a GM plot surface sample.

Drainage precipitates of the lysimeter tank below the geomembrane plot (GM) are of iron(III) oxyhydroxides; goethite  $\alpha\text{-Fe}^{+3}\text{O}(\text{OH})$  and secondary gypsum. These minerals are both dominating the sample surface with a diffused occurrence of yellow-mud precipitates of jarosite group minerals intersecting a siliceous matrix identified by SEM-EDS. Jarosite, usually occurs as small clusters of acicular crystals, or as continuous coatings on grains as bands of fine feathery radiating crystals (Boulet et al., 1998). Low proportion of Mn is sequestered by iron oxyhydroxides i.e. goethite. Mud precipitates are attributed to surface cracks referring to desiccation of the sample surface by the action of evapotranspiration, indicating that no percolated water penetrated the applied geomembrane.

### ***Compacted clay plot (CC)***

Quartz, calcite, albite, kaolinite and montmorillonite prevail in the mineralogical composition of the CC plot based on the XRD analysis. Calcite, anglesite and plumbojarosite crystals were detected by SEM-EDS. In the subsurface horizons EDS analysis identified grains rich in  $\text{Cr}_2\text{O}_3$ , FeO,  $\text{TiO}_2$ ,  $\text{As}_2\text{O}_3$ . Brass  $\text{Cu}_3\text{Zn}_2$  and Ca-Mg-Si phases are characterizing the deeper horizons beside persistence of plumbojarosite and anglesite. Some of these metal oxides are dominant and occur as small grains like iron oxide followed by lead oxide.

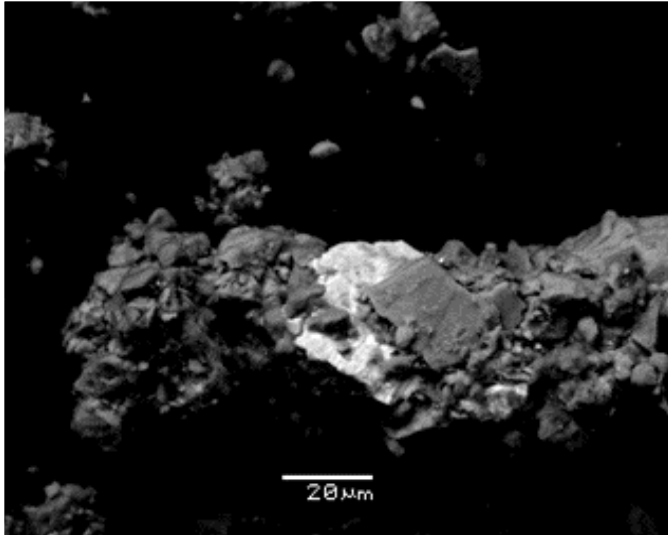


*Fig. (14) Silicate phase rich in Ca, Mg with aluminosilicate clusters and bright areas enriched in Fe, Pb, Zn.*

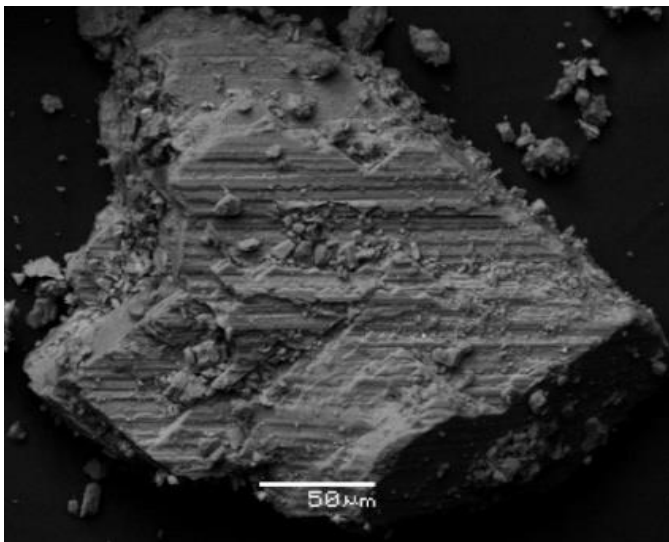


*Fig. (15) Etched calcite crystal, affected by acid drainage.*

Drainage precipitates from the lysimeter tank under the CC plot contains abundant amounts of Zn sulphate salts i.e., goslarite  $ZnSO_4 \cdot 7H_2O$ , Gunningite  $ZnSO_4 \cdot H_2O$  which have been identified by both EDS and XRD, along with the efflorescent jarosite group minerals, especially plumbojarosite.

## 4.2 Geochemistry

The full chemical analysis results are presented in Appendix II. The total results of chemical analysis of all samples by aqua regia are summarized graphically in Figure 16.

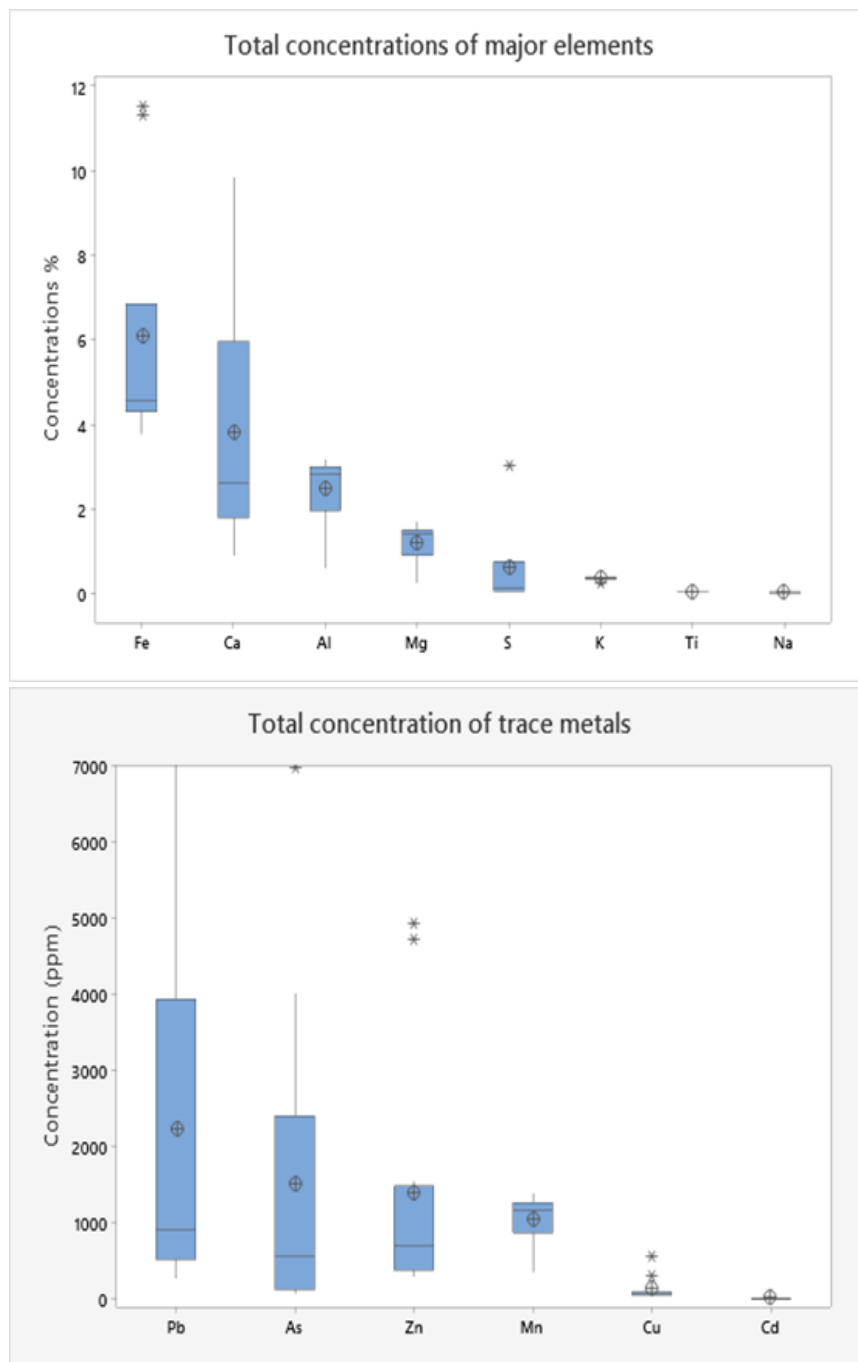


Fig. 16. Boxplots of concentrations of major (upper) and trace elements (lower) in all samples analyzed by aqua regia (n=28).

These results are obtained from different types of samples, i.e. surface samples, vertical profile samples and drainage precipitate samples, and demonstrate the wide range of variability in terms of elemental concentrations in the site, pointing to a highly heterogeneous

waste pile as well as different long term response to the remediation techniques that have been tested. Concerning the concentrations of PTEs it is noted that Pb and As show extremely high concentrations, in the range of thousands of mg/kg, indicating the hazardous nature of the exposed material, since both elements have high toxicity for humans and the environment.

Table 5 summarizes the total chemical analysis results of surface soil, depth profile and lysimeter drainage samples, while Table 6 shows the measurements of the physiochemical parameters and geochemical leaching test results.

#### 4.2.1 Surface soil samples

PTEs concentrations in the surface soils differ from one plot to another and the untreated control plot (CL) demonstrates the highest surface soil concentrations of Pb, Cd, Zn and Cu with mean values of 4864, 9.67, 3730 and 311 mg/kg, respectively. The lowest concentration mean values are observed in the compacted clay (CC) plot with values of 605, 3.33, 454 and 55.4 mg/kg for the same elements. The lime-treated SL plot comes after the CL plot in possessing highest mean values of PTEs with 3085 for Pb, 8.8 for Cd, 882 for Zn and 66.2 for Cu for surface soil samples followed by the geomembrane GM plot. Overall a systematic order in the mean values of PTEs in surface soil is observed as follows: CL>SL>GM>CC.

Surface soil samples of the CL plot have a neutral to slightly alkaline pH; 8.67, 6.22, 7.15, 6.92 except one sample with pH of 4.16 and have high concentrations of Fe ranging from 5.2 to above 15 wt %, S from 0.81 to above 5 wt %, Pb from 1474 to above 10000 mg/kg, Zn from 1554 to 4929 mg/kg, As from 833 to 4008 mg/kg, Cu from 101 to 542 mg/kg and Cd from 5 to 12 mg/kg.

In the SL plot, the surface soil samples show high values of Ca due to mixing with lime (up to 10.53 wt %) comparing to CL plot (up to 6.81 wt %), while Fe and S are up to 11.32 and above 5 wt %, respectively. Also, the PTEs in SL plot show high concentrations as in Pb; 3929, 271, 6437 mg/kg, Zn; 641, 353, 463 mg/kg, As; 6968, 558, >10000 mg/kg and considerable concentrations of Cu; 70.9, 50, 68 mg/kg and Cd; 6, 3, 7 mg/kg. The pH of SL surface soil samples is fluctuating from acidic (1.97, 2.71) to neutral (7.06, 7.22, 6.78) depicting heterogeneity in surface soil composition. The two specific surface-crust samples which were collected based on contrast in color and cementation (CR1 SL, CR2 SL) are acidic 2.11, 2.51 with low water saturation (3.91, 0.14 %) and elevated content of total dissolved solids (T.D.S) of 5.66, 2.1 ppt respectively.

**Table 5 Total chemical analysis results after digestion with aqua-regia.**

| <i>ANALYTE</i> | <i>Al</i> | <i>Ca</i> | <i>Mg</i> | <i>Fe</i> | <i>S</i> | <i>Na</i> | <i>K</i> | <i>Ti</i> | <i>Pb</i> | <i>Cd</i> | <i>Zn</i> | <i>As</i> | <i>Cu</i> | <i>Mn</i> |
|----------------|-----------|-----------|-----------|-----------|----------|-----------|----------|-----------|-----------|-----------|-----------|-----------|-----------|-----------|
| <b>UNITS</b>   | %         | %         | %         | %         | %        | %         | %        | %         | mg/kg     | mg/kg     | mg/kg     | mg/kg     | mg/kg     | mg/kg     |
| <b>LOD</b>     | 0.01      | 0.01      | 0.01      | 0.01      | 0.01     | 0.01      | 0.01     | 0.01      | 2         | 1         | 1         | 3         | 0.5       | 2         |
| <b>C2</b>      | 2.73      | 2.33      | 1.15      | 11.55     | 3.02     | 0.03      | 0.36     | 0.04      | 8254      | 12        | 4708      | 2401      | 289       | 1025      |
| <b>C3</b>      | 1.14      | 6.81      | 0.33      | >15.00    | >5.00    | 0.05      | 0.23     | 0.03      | >10000    | 12        | 4929      | 4008      | 542       | 352       |
| <b>C5</b>      | 3         | 2.45      | 1.43      | 5.2       | 0.81     | 0.03      | 0.37     | 0.04      | 1474      | 5         | 1554      | 833       | 101       | 1277      |
| <b>CCL1</b>    | 0.25      | 5.58      | 0.04      | >15.00    | >5.00    | 0.05      | 0.18     | 0.01      | >10000    | 16        | 6968      | 5285      | 677       | 248       |
| <b>CCL3</b>    | 0.12      | 5.14      | 0.02      | >15.00    | >5.00    | 0.05      | 0.18     | <0.01     | >10000    | 18        | 8286      | 6324      | 696       | 281       |
| <b>CCL5</b>    | 0.21      | 5.78      | 0.03      | >15.00    | >5.00    | 0.05      | 0.22     | <0.01     | >10000    | 18        | 7186      | 4998      | 679       | 282       |
| <b>SL2</b>     | 1.74      | 9.84      | 0.82      | 6.85      | >5.00    | 0.05      | 0.36     | 0.03      | 3929      | 6         | 641       | 6968      | 70.9      | 822       |
| <b>SL4</b>     | 2.89      | 1.84      | 1.47      | 4.54      | 0.7      | 0.02      | 0.39     | 0.04      | 271       | 3         | 353       | 558       | 50        | 1385      |
| <b>SL5</b>     | 0.61      | 9.09      | 0.26      | 11.32     | >5.00    | 0.08      | 0.36     | 0.02      | 6437      | 7         | 463       | >10000    | 68        | 512       |
| <b>CR1SL</b>   | 0.71      | 0.28      | 0.25      | >15.00    | >5.00    | 0.09      | 0.15     | 0.02      | 649       | 12        | 448       | 3327      | 50.8      | 345       |
| <b>CR2SL</b>   | 0.23      | 10.53     | 0.16      | >15.00    | >5.00    | 0.1       | 0.11     | <0.01     | 4140      | 16        | 2506      | 7889      | 91.2      | 5181      |
| <b>CSL1</b>    | 2.39      | 6.07      | 1.39      | 7.55      | 2.57     | 0.04      | 0.28     | 0.04      | 711       | 4         | 242       | 1726      | 47.8      | 906       |
| <b>CSL3</b>    | 0.25      | 7.16      | 0.09      | >15.00    | >5.00    | 0.03      | 0.24     | <0.01     | >10000    | 11        | 448       | >10000    | 105       | 242       |
| <b>CSL5</b>    | 0.08      | 7.85      | 0.02      | >15.00    | >5.00    | 0.03      | 0.15     | <0.01     | 7002      | 11        | 350       | >10000    | 76.3      | 118       |
| <b>GM1</b>     | 3.02      | 1.66      | 1.51      | 4.35      | 0.12     | 0.02      | 0.41     | 0.04      | 801       | 4         | 910       | 180       | 69.6      | 1248      |
| <b>GM4</b>     | 2.99      | 2.76      | 1.63      | 4.3       | 0.13     | 0.03      | 0.39     | 0.05      | 1096      | 4         | 1257      | 213       | 80.9      | 1251      |
| <b>GM5</b>     | 2.91      | 3.42      | 1.71      | 4.14      | 0.08     | 0.02      | 0.35     | 0.05      | 518       | 3         | 470       | 123       | 51.9      | 1168      |
| <b>CGM1</b>    | 2.99      | 2.85      | 1.62      | 4.16      | 0.06     | 0.02      | 0.39     | 0.04      | 439       | 3         | 403       | 100       | 48.7      | 1117      |
| <b>CC2</b>     | 2.74      | 1.79      | 1.4       | 6.53      | 0.71     | 0.03      | 0.37     | 0.04      | 909       | 5         | 777       | 1151      | 69.9      | 1141      |
| <b>CC4</b>     | 2.68      | 2.96      | 1.48      | 3.76      | 0.05     | 0.02      | 0.35     | 0.04      | 296       | 2         | 302       | 69        | 44        | 1128      |
| <b>CC5</b>     | 3.19      | 0.9       | 1.38      | 4.57      | 0.05     | 0.02      | 0.44     | 0.05      | 609       | 3         | 284       | 108       | 52.4      | 1269      |
| <b>CCC1A</b>   | 2.63      | 0.76      | 1.25      | 4.22      | 0.1      | 0.02      | 0.36     | 0.03      | 948       | 3         | 456       | 183       | 53.9      | 1094      |
| <b>CCC2A</b>   | 0.98      | >15.00    | 2.79      | 1.47      | 0.09     | 0.02      | 0.16     | 0.02      | 248       | 1         | 184       | 127       | 17.5      | 447       |
| <b>CCC3A</b>   | 1.87      | 13.73     | 1.77      | 2.66      | 0.08     | 0.02      | 0.28     | 0.02      | 153       | 2         | 111       | 108       | 21.1      | 530       |
| <b>DCL</b>     | 0.05      | 0.19      | 0.12      | >15.00    | >5.00    | <0.01     | <0.01    | <0.01     | 17        | 28        | >10000    | 9         | 172       | 1262      |
| <b>DSL</b>     | 0.08      | 0.49      | 0.23      | >15.00    | >5.00    | 0.03      | <0.01    | <0.01     | 479       | 21        | 4589      | 683       | 294       | 2314      |
| <b>DCC</b>     | 0.09      | 9.45      | 0.08      | >15.00    | >5.00    | 0.3       | 0.02     | <0.01     | 245       | 22        | 9146      | 100       | 72.5      | 800       |
| <b>DGM</b>     | 0.14      | 12.31     | 0.06      | 12.29     | >5.00    | 0.14      | 0.04     | <0.01     | 459       | 16        | 5299      | 308       | 409       | 521       |

**Table 6. Results of physiochemical and leaching tests.**

| AA | sample ID | humidity | PH   | conductivity | T.D.S     | Pb bioacc. % | Zn bioacc. % | Cd bioacc. % | Pb TCLP | Zn TCLP |
|----|-----------|----------|------|--------------|-----------|--------------|--------------|--------------|---------|---------|
| 1  | CCL1      | 18.28%   | 3.07 | 1.56 mS      | 828.7 ppm | 0.83         | 1.56         | 21.88        |         |         |
| 2  | CCL2      | 18.24%   | 2.94 | 1.35 mS      | 707.1 ppm |              |              |              |         |         |
| 3  | CCL3      | 19.98%   | 2.8  | 1.47 mS      | 770.7 ppm |              |              |              |         |         |
| 4  | CCL4      | 19.97%   | 2.73 | 2.69 mS      | 1400 ppm  |              |              |              |         |         |
| 5  | CCL5      | 21.51%   | 2.63 | 2.84 mS      | 1460 ppm  |              |              |              |         |         |
| 6  | CSL1      | 6.59%    | 6.32 | 1.48 mS      | 760.6 ppm | 4.84         | 30.38        | 41.25        |         |         |
| 7  | CSL2      | 19.00%   | 5.23 | 2.3 mS       | 2500 ppm  |              |              |              |         |         |
| 8  | CSL3      | 12.30%   | 3.16 | 2.34 mS      | 1200 ppm  |              |              |              |         |         |
| 9  | CSL4      | 11.71%   | 2.99 | 2.51 mS      | 1290 ppm  |              |              |              |         |         |
| 10 | CSL5      | 10.87%   | 2.64 | 3.16 mS      | 1620 ppm  |              |              |              |         |         |
| 11 | CCC1A     | 2.58%    | 6.96 | 0.146 mS     | 76.18 ppm | 23.45        | 48.37        | 39.22        |         |         |
| 12 | CCC2A     | 8.63%    | 7.76 | 0.192 mS     | 99.14 ppm |              |              |              |         |         |
| 13 | CCC3A     | 11.93%   | 7.8  | 0.156 mS     | 80.37 ppm |              |              |              |         |         |
| 14 | CGM1      | 2.82%    | 7.79 | 0.985 mS     | 506.5 ppm | 39.95        | 68.42        | 48.67        |         |         |
| 15 | DCL-W     | 23.49%   | 2.73 | 40.1 mS      | 20.61 ppt | 100          | 100.00       | 70.96        |         |         |
| 16 | DCL-Y     |          | 2.99 | 12.21 mS     | 6.21 ppt  |              |              |              |         |         |
| 17 | DSL       | 20.63%   | 2.71 | 32.18 mS     | 16.54 ppt | 4.03         | 100.00       | 57.14        |         |         |
| 18 | DGM       | 9.72%    | 2.32 | 7.67 mS      | 3.94 ppt  | 9.15         | 100.00       | 82.50        |         |         |
| 19 | DCC       | 25.25%   | 2.5  | 9.36 mS      | 4.81 ppt  | 11           | 93.85        | 82.49        |         |         |
| 20 | LYCCI     | 10.94%   | 1.82 | 27.87 mS     | 14.35 ppt |              |              |              |         |         |
| 21 | LYCCO     | 26.17%   | 2.03 | 40.04 mS     | 20.55 ppt |              |              |              |         |         |
| 22 | CR1 SL    | 3.91%    | 2.11 | 11.02 mS     | 5.66 ppt  | 3.11         | 100.00       | 24.37        |         |         |
| 23 | CR2 SL    | 0.14%    | 2.51 | 4.12 mS      | 2.1 ppt   | 5.17         | 100.00       | 61.06        |         |         |
| 24 | C1        |          | 8.67 |              |           |              |              |              | <dl     | <dl     |
| 25 | C2        |          | 6.22 |              |           | 0.64         | 69.64        | 59.29        | 3.0     | 1240    |
| 26 | C3        |          | 4.16 |              |           | 0.38         | 13.40        | 34.23        | 2.6     | 426     |
| 27 | C4        |          | 7.15 |              |           |              |              |              | 2.3     | <dl     |
| 28 | C5        |          | 6.92 |              |           | 14.53        | 54.70        | 68.63        | 2.7     | 16.9    |
| 29 | GM1       |          | 8.68 |              |           | 40           | 64.94        | 56.82        | 23      | 265     |
| 30 | GM2       |          | 8.63 |              |           |              |              |              | 38      | 680     |
| 31 | GM3       |          | 8.55 |              |           |              |              |              | 6.4     | 42.6    |
| 32 | GM4       |          | 8.16 |              |           | 33.34        | 59.29        | 68.40        | 31      | 402     |
| 33 | GM5       |          | 8.71 |              |           | 26.54        | 58.51        | 54.49        | 6.6     | 68      |
| 34 | SL1       |          | 7.06 |              |           |              |              |              | 4.4     | 36.6    |
| 35 | SL2       |          | 6.78 |              |           | 4.36         | 31.95        | 48.08        | 3.4     | 78      |
| 36 | SL3       |          | 1.97 |              |           |              |              |              | 2.8     | 216     |
| 37 | SL4       |          | 7.22 |              |           | 31.29        | 29.96        | 48.08        | 5.8     | 25.6    |
| 38 | SL5       |          | 2.71 |              |           | 1.13         | 23.50        | 29.41        | 2.8     | 62      |
| 39 | CC1       |          | 8.03 |              |           |              |              |              | 2.8     | <dl     |
| 40 | CC2       |          | 7.26 |              |           | 21.19        | 35.45        | 45.28        | 2.2     | 3.2     |
| 41 | CC3       |          | 7.35 |              |           |              |              |              | 2.2     | 372     |
| 42 | CC4       |          | 6.84 |              |           | 42.42        | 66.23        | 62.50        | 2.2     | <dl     |
| 43 | CC5       |          | 7.86 |              |           | 27.23        | 33.55        | 37.74        | <dl     | <dl     |

The geochemical data of the surface soil in addition to field observations depict high heterogeneity of the SL plot with remarkable spots of dark green and dark orange colors and a hardened surface coating. The SL plot demonstrates intensive action of evaporation process, hence migration of contaminants to the surface and formation of the cemented coating layer.

In the GM plot, surface soil results do not differ substantially in terms of elemental concentrations denoting homogeneity in the processes controlling the dispersion of the elements in contrast to the SL plot. The GM surface soil samples, show more alkaline pH conditions compared to the three other plots, ranging from 8.16 to 8.71 with Al and Fe content around 3 and 4 wt %, respectively. Finally, in the CC plot, surface soil samples display pH values indicating neutral to slightly alkaline conditions and relatively lower total elemental concentrations compared to the other plots.

Linear regression graphs are plotted to depict the relationship between the 3 heavy metals; Pb, Zn and Cd in the surface soil samples (Fig. 17). Pb and Zn total concentrations show a strong positive correlation indicating common sources of the two such as sulfide phases in the pyritic waste, however, chemical leaching tests revealed poor correlation between the two metals. Plumbojarosite is the most ubiquitous Pb mineral detected in all 4 plots according to the mineralogical analysis. Zn was also found to be associated with this mineral. Pb and Zn occurred also as trace metals linked to iron oxyhydroxides minerals i.e., goethite as in GM plot or being adsorbed by iron sulphate salts like rozenite in SL plot. It is notable that Zn mobility is related mainly to the mineralogy and phases sequestering Zn, whereas the samples with the highest Zn extractability consist mainly of plumbojarosite and anglesite. In contrast to Zn, Pb is more stable in plumbojarosite which contributes to the lowest leachable Pb. Cd correlates positively to Zn and Pb, however, has a better correlation to Zn ( $r=0.78$ ) and shares almost the same hosting phases with Pb and Zn. Cd bioaccessibility (SBET results) in the surface soil samples corresponds adequately to the Zn pattern ( $r=0.94$ ) indicating more mobility in Pb secondary phases and more stability in Fe oxides.

Pb-Zn and Pb-Cd linear regression plots of the SBET data show discrete distributions deducing no correlation contradictory to Zn-Cd plot. The leachability of Pb in CL plot surface soil is negligible; 0.83, 0.38, 0.64 % excluding one sample of high percentage of leachable Pb (40 %). Contrarily there are significant bioaccessible concentrations of 40%, 33%, 40% and 27 % for GM surface soil samples. Zn bioaccessibility for CL plot surface soil contributes to 69.6, 54.7, 13.4 and 1.6 % while for SL plot; 30.38, 31.95, 29.96 and 23.50%, then for CC plot 48.37, 35.45, 66.23 and 33.55% and 64.94, 59.29, 58.51 and 68.42% for the GM plot.

The application of TCLP to the surface samples indicated significant differences in the leachability of Pb and Zn between the different treatments. The results of this test are presented graphically in Fig. 18. In the GM plot, although the pH values of the surface samples

are alkaline, Pb concentrations in the leachate exceed the EPA regulatory limit of 5mg/L (US EPA 1311 method) in all samples. For the other three plots Pb leachable concentrations are below the limit of 5 ppm, indicating sufficient degree of stabilization of the metal probably through co-precipitation or absorption by secondary phases that are steady at the pH of the TCLP solution. The best results were achieved by the compacted clay treatment technique. Thus, it is possible that significant amounts of Pb are "trapped" by clay minerals and do not get released to the TCLP leachate. It is noted that low TCLP extractability is recorded for the control site, indicating sequestration of Pb in rather stable phases. Zinc TCLP leachable concentrations are well below the EPA regulatory limit of 500 mg/L for all samples of CC and SL plots. Exceedance is noted for some samples of the GM and the control (CL) plots. Zinc is rather sensitive in pH changes but also the mineralogical study indicated that it is sequestered in significant amounts within secondary Fe-oxyhydroxide phases that might be responsible for its stability in the pilot remediation plots.

#### 4.2.2 Vertical profile samples

The vertical profile data are presented graphically in Fig. 19. The pH values of vertical profile in the CL plot show a slight increase with depth initiating from 3.07 on the surface to 2.63 in deeper horizons and so do total dissolved solids and electric conductivity; 828.7 to 1460 ppm and 1.65 to 2.84 mS respectively. Total chemical analysis in the CL plot indicates homogeneity in PTEs distributions within the three studied horizons. Specifically, As concentrations from surface and subsurface to deep horizons are 5285, 6324, 4998 mg/kg, Zn has concentrations of 6968, 8286, 7186 mg/kg, Cu of 677, 696, 679 mg/kg and Cd of 16, 18, 18 mg/kg. The homogeneity concentration values vertically indicate that no cemented layers or sealing exists to minimize metal mobility. It is notable here that the vertical profile of CL plot contributes to the highest concentrations of Zn and Cu hence deducing the intensive dissolution of the pyritic minerals such as pyrite and chalcopyrite which share the same oxidation products but with different impurities of Zn and Cu (*table 3*). Water content of the samples increased downward in the May 2020 sampling, starting from 18.28% at surface to 21.51% at 90 cm depth indicating high permeability and accordingly high concentrations percolating to the drainage.

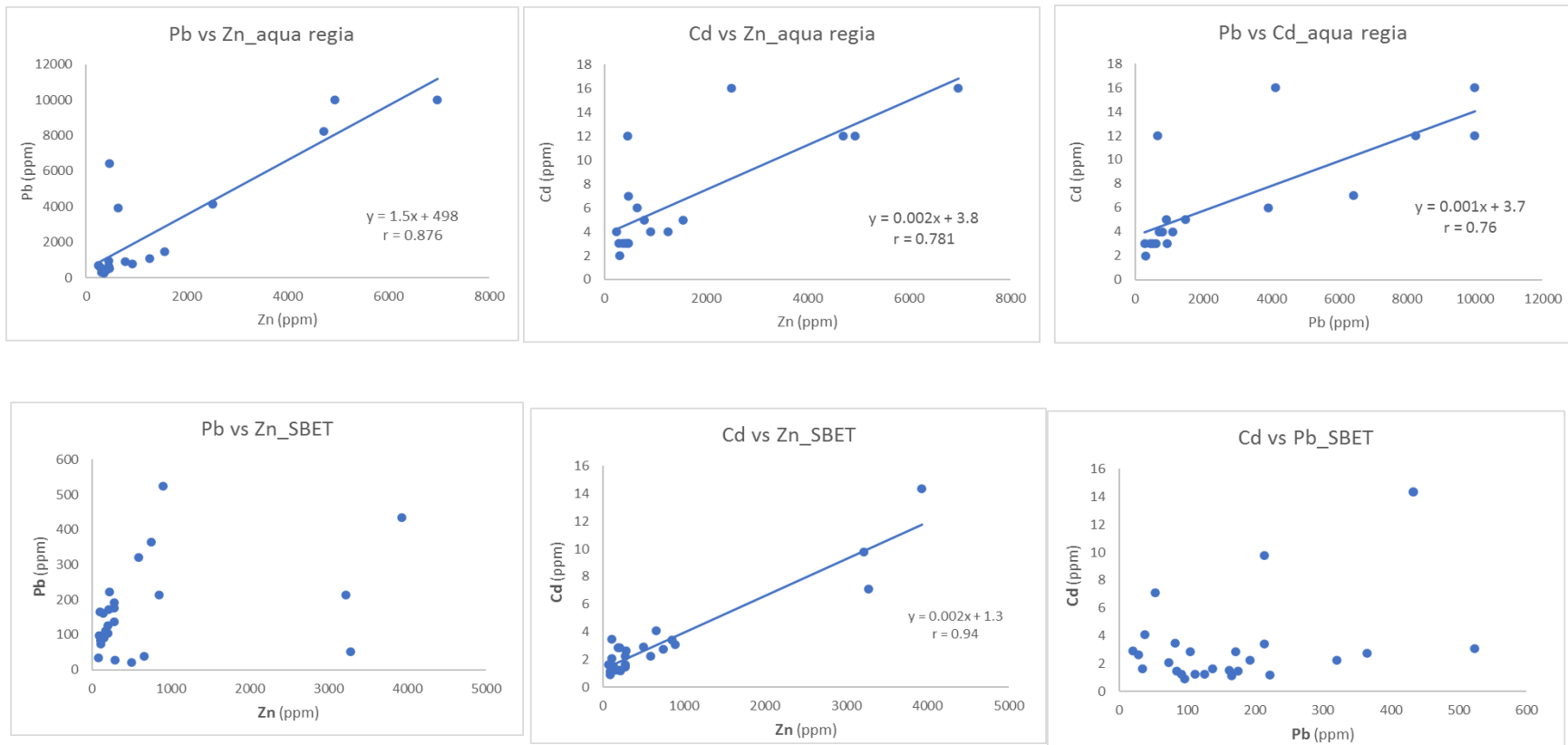


Fig. 17. Linear regression plots between Pb, Zn and Cd total and SBET leachable concentrations in the surface soil samples.

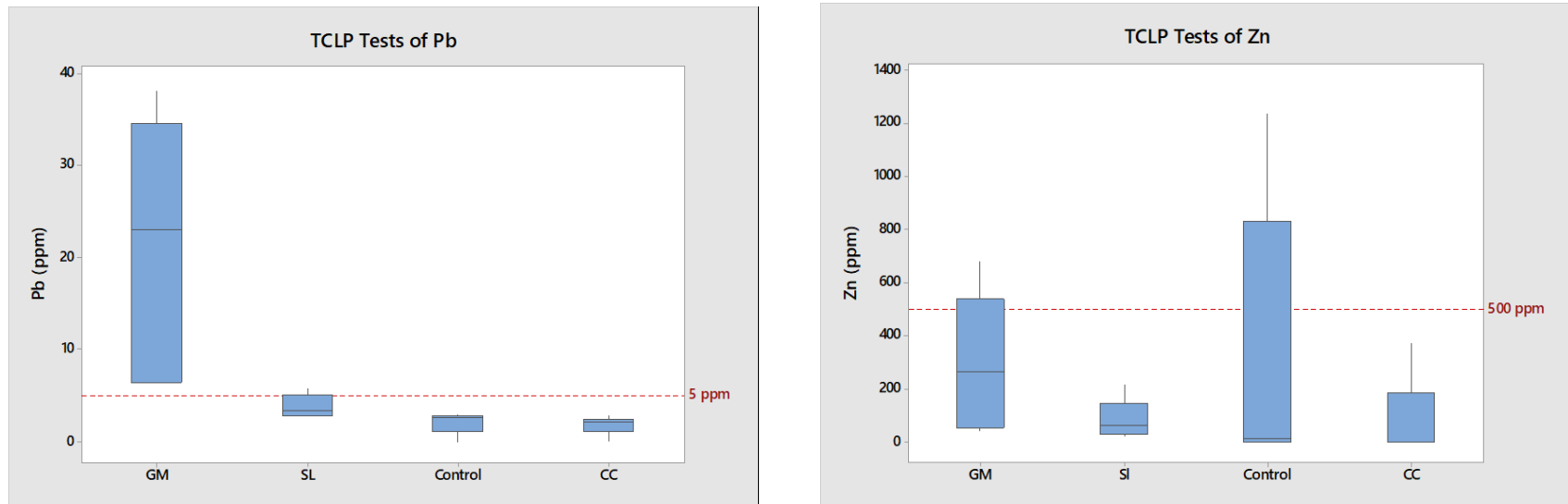


Fig.18 TCLP extractable concentrations of Pb and Zn from the surface samples of the Kavodokanos plots.

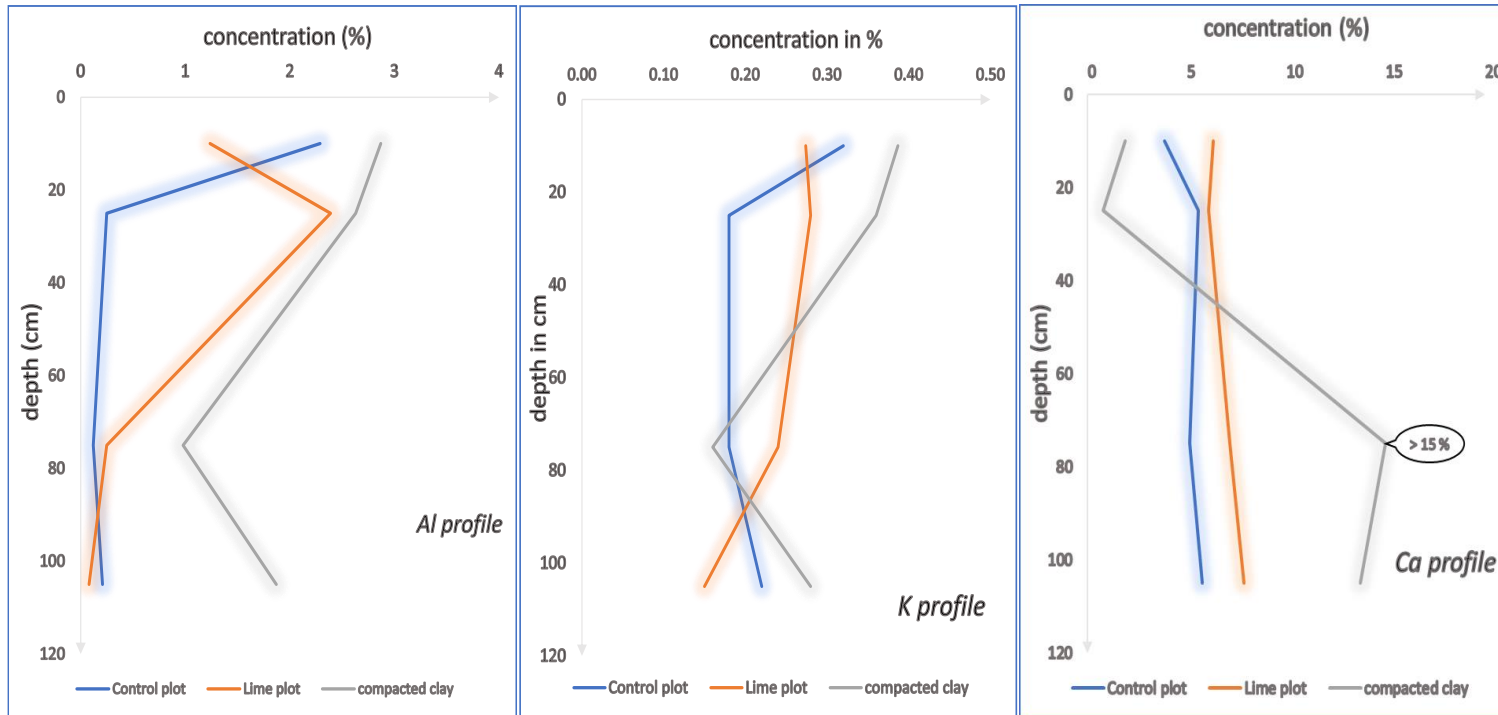


Fig. 19. Elemental concentrations along the vertical profiles in the three different treatment plots. No vertical profile samples were collected from the GM plot because of the shallow depth of the synthetic membrane applied.

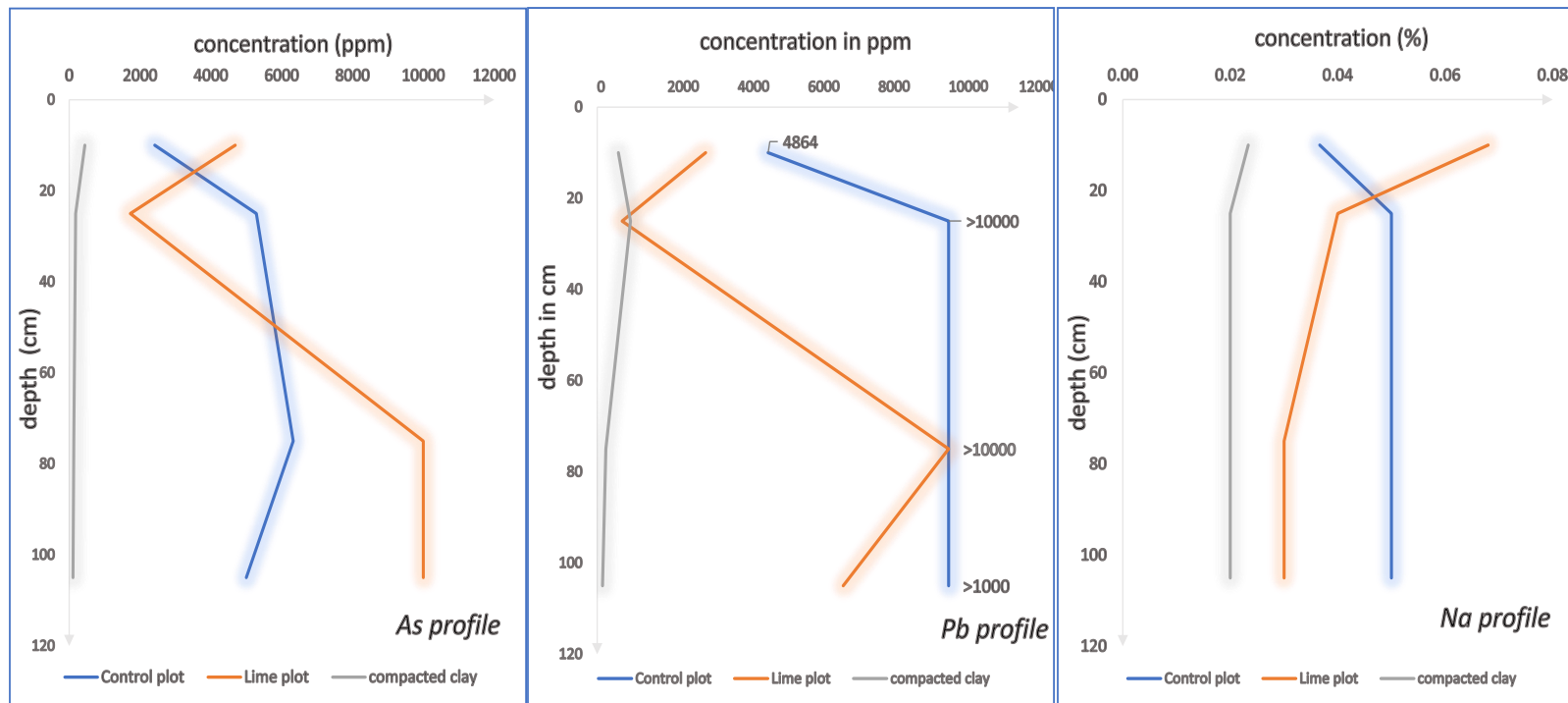


Fig. 19 continued

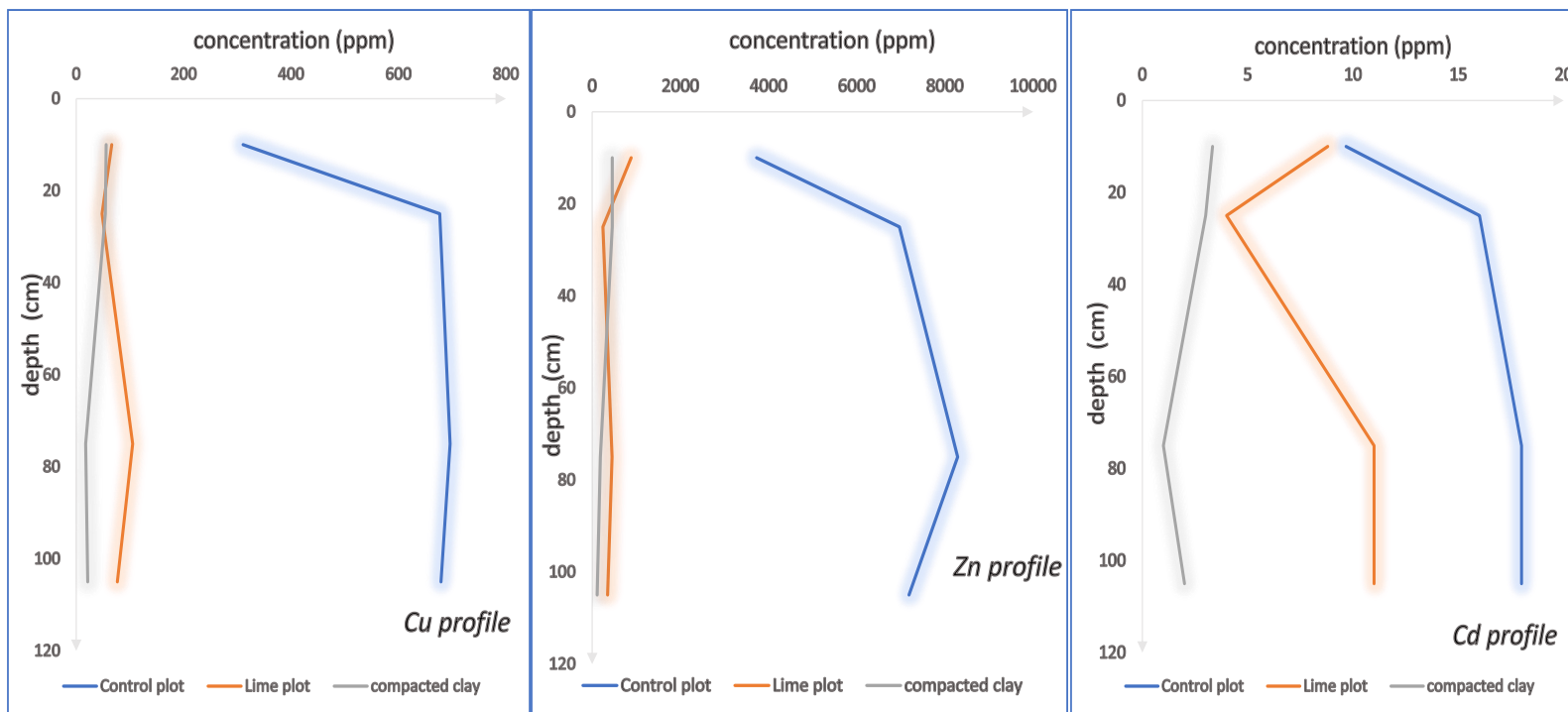


Fig 19 continued

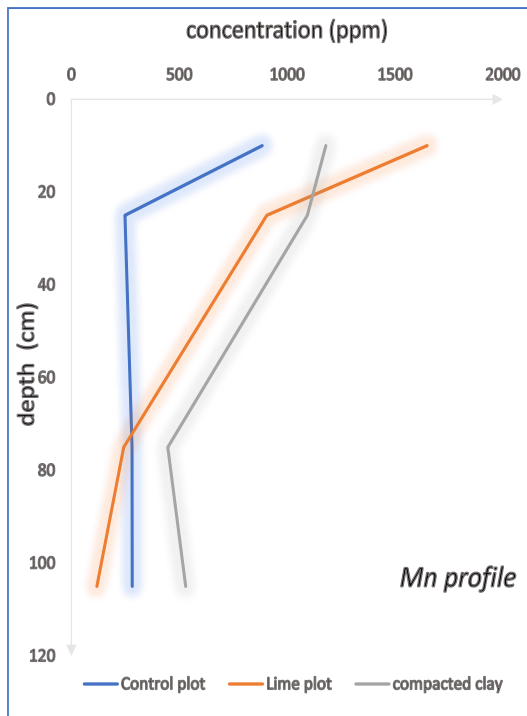


Fig 19 continued

The physiochemical measurements of the SL vertical profile samples have elevated values in the subsurface horizon (20-40 cm down the surface), showing T.D.S of 2500 ppm (the highest among the four studied plots) and humidity 19% with high electric conductivity 2.3 mS and high concentrations of Zn, As, Cu and Cd. This fact, in addition to the EDS results, could point to a complex subsurface layer rich in trace metals. The acidity of SL quadrant increases downwards starting from a pH of 6.32 then 5.23, 3.16, 2.99 ending up with 2.64 in the deepest sampled horizon. Iron and sulfur minerals and their complexes are dominating downwards with excess of Pb and As exceeding 10000 ppm.

PTE concentrations within GM plot subsurface soil are considerable, corresponding to 439, 403, 100, 48.7 and 3 ppm for Pb, Zn, As, Cu and Cd respectively. Comparing these values to the CL plot subsurface values, we will find Pb content in CL plot more than 22 times as in GM, more than 17 times for Zn, more than 52 times for As, 13.9 times for Cu and 5.3 times for Cd. Furthermore, if we compare GM surface soil measurements to the initially selected and utilized protective layer used for the construction of the upper surface (NTUA 1999), we will see Pb concentration in GM equals to a 2.7 fold increase from the utilized layer, 6.9 fold for Zn, 6 fold for As and 3.9 for Cd and this might be attributed to physical weathering and action of air, transporting PTEs from neighboring areas during the last 25 years.

This comparison indicates that evapotranspiration process within GM quadrant was lower than the ones in CL and SL plots and that the synthetic membrane successfully separated the underground wastes from the upper developed composite layers into two different geochemical systems.

The CC plot is characterized by the lowest conductivity and T.D.S out of the 4 assigned remediation techniques with a neutral to slightly alkaline acidity values ranging from 6.96 to 7.8. Some PTEs tend to decrease downwards such as Pb initiating from 948 mg/kg at subsurface to 153 mg/kg at deep horizons, Zn from 456 to 111 mg/kg, As from 183 to 108 mg/kg and S from 0.1 to 0.08 %. There is a notable increase in Ca concentration in two samples; one equals 13.7 and the other exceeds 15 wt % and a comparable content of Mn, otherwise CC plot shows low contributions of Na, As, Pb, Cd, Zn and Cu. Vertical profiles illustrate that PTEs play a minor role in CC profile as it shows almost a steady line for Pb, As, Cd, Cu and Zn excluding Mn (Fig. 18). It is reasonable that CC plot has highest concentration of Al and varying percentages of K due to the clayey phase used as a barrier between the waste and the surface cover. There is a clear evidence that CC plot corresponds to the lowest PTEs contributions within the vertical profiles whereas Pb, As, Cd, Zn and Cu concentrations are negligible comparing to CL plot (Fig. 18). Al, K, Ca and Mn show different behavior, since Al has the highest values in the CC plot out of the 3 quadrants and K has comparable values because of the involved clay minerals in the CC plot. Ca concentrations show significant increase in the subsurface horizons contradictory to CL and SL profiles which show steady lines. The sharp rise in Ca concentrations in the subsurface horizons is

related to the initially developed drainage layer which acts as capillary barrier of sandy limestone according to the composite design by NTUA 1998.

The dendrogram of Fig. 20 is the graphical display of cluster analysis of the vertical profile data. It shows 3 linkage clusters denoting elemental assemblages within the vertical profiles based on the total concentrations; the first cluster contains Al, K and Mg with similarity of 92.64 referring to the clay minerals, while Mn correlates to these clayey assemblages with similarity equal to 82.88. The second cluster consists only of Ca showing low correlation to other assemblages, the third cluster exhibits Fe-S assemblages with correlation to Pb and Cd of 93.74 and also As associates to this assemblage with similarity of 85.71 whilst the fourth cluster shows perfect correlation between Zn and Cu with value of 99.68. The first cluster points to clay minerals such as montmorillonite and kaolinite which dominate in CC technique plot. The high correlation of Mn to the aluminosilicate minerals can be an indicator of Mn adsorption by the clay mineral surface. The second cluster of Ca is denoting to the lime addition in SL plot and its poor correlation to the other assemblages. The Fe-S complexes which are referred to by the third cluster has good linkage to Pb, Cd and As and are predominating in CL plot assuring the important role of Fe complexes in trace metals mobility. Zn-Cu cluster refers to the products originating from dissolution of the pyritic minerals and participating in the same mineralogical phases.

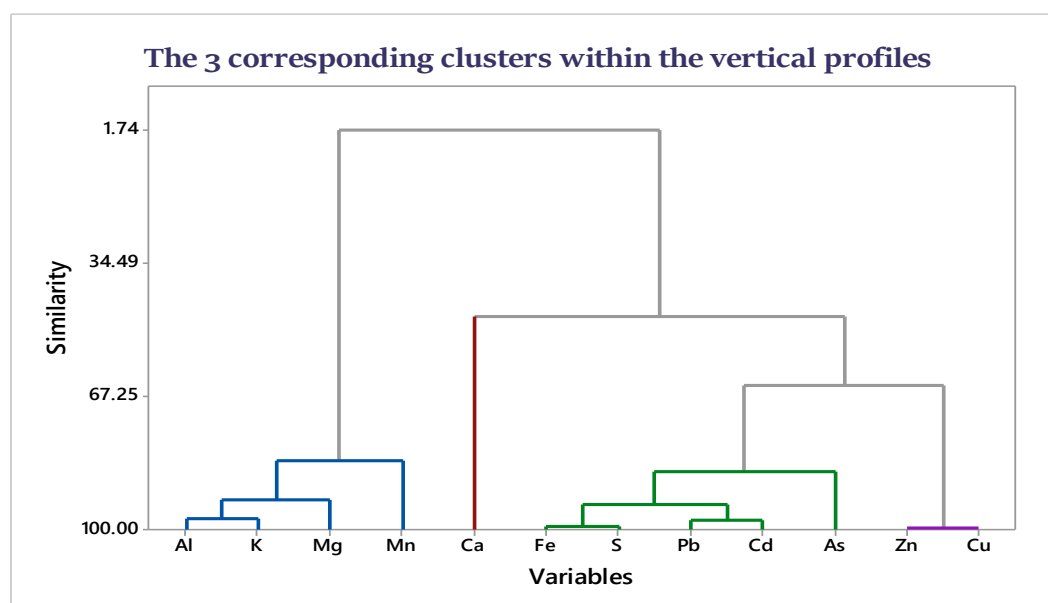


Fig. 20. Dendrogram showing the linkage clusters of elements within the vertical profiles.

#### 4.2.3 Drainage samples

Lysimeter drainage precipitate samples of the 4 quadrants are sharing a common aspect, as they are all Fe-SO<sub>4</sub> efflorescent minerals with elevated concentrations of Zn. Also, all samples contain gypsum. Lead concentration in the CC drainage precipitate sample is

lower compared to SL and GM drainage samples and this can be related to the alkalinity recorded along the CC depth profile hence the tendency of Pb to form secondary phases like anglesite which has been detected by EDS measurements or being adsorbed by the clay mineral surface. Contrasting to CC drainage precipitate sample, SL plot shows the highest Pb concentration percolated to the drainage with 479 mg/kg followed by GM plot with a value of 459 mg/kg while CL plot contributes to the lowest Pb content in the drainage sample with 17 mg/kg.

Although the DCL sample has experienced the lowest Pb infiltration, 100% of the Pb concentration is leachable while DSL, DCC and DGM contributes to 4.03, 11, 9.15% of leachable Pb, respectively (Fig. 21). As previously pronounced that SL plot shows acidic values on the surface soil with increasing acidity downward reaching a pH of 2.64 at the deeper horizon and a subsurface horizon with high T.D.S and competing cations, this can motivate Pb mobility and hence percolation to the drainage. Several studies have demonstrated decreased sorption of Pb in the presence of complexing ligands and competing cations and at pH values above 6 Pb is either adsorbed on clay surfaces or forms lead carbonate (EPA 1992).

Samples from all 4 plots show that significant amounts of Zn infiltrates to the drainage lysimeters resulting in significant concentrations in the efflorescent precipitates, containing more than 10000 mg/kg in DCL, 9146 mg/kg in DCC, 5299 mg/kg in DGM and 4589 mg/kg in DSL. Cd concentrations within the drainage precipitate samples are of similar values in all plots; DCL contains 28 mg/kg while DSL, DCC and DGM contain 21, 22 and 16 mg/kg respectively.

Bar chart of Pb, Zn and Cd total concentrations in the drainage samples VS their corresponding SBET bioavailability

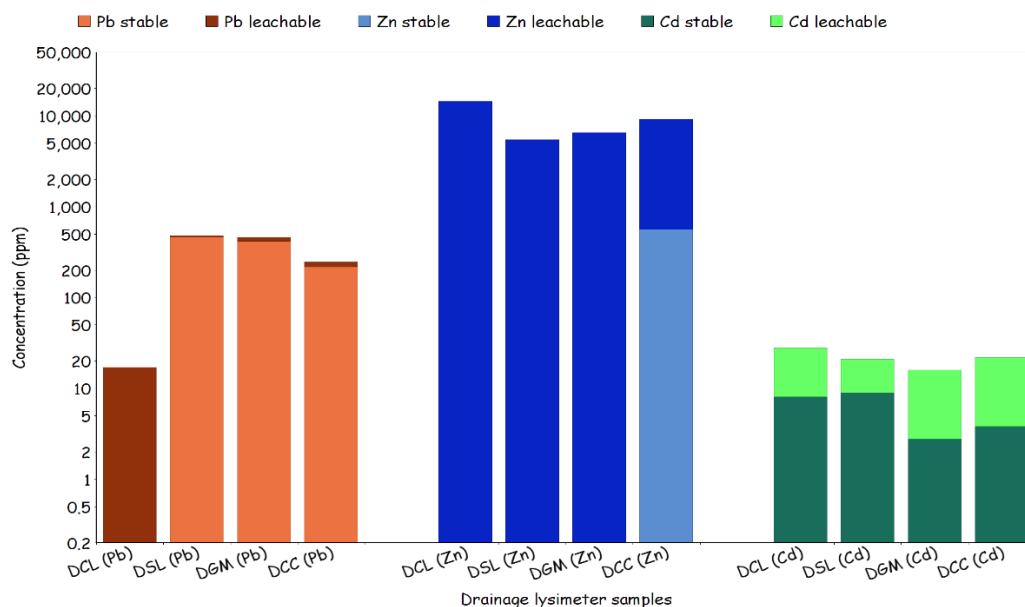


Fig. 21. Cummulative bar chart of Pb, Zn and Cd comparing the total concentrations in the drainage precipitate samples from each plot with the corresponding SBET leachable concentration.

## 5. Discussion

### 5.1 Effect of treatment plot composition on the stabilization of PTEs

Major elements contribution to the remediation plots composition are ordered as follows: Fe; ranging from 4.3 to 6.85 wt %, Ca; 1.8 to 5.9 wt %, Al; 1.97 to 2.99 wt %, Mg; 0.9 to 1.5 wt % and then S, K, Na and Ti with concentrations less than 1 wt % while Pb, As, Zn, Mn, Cu and Cd are the prevailing PTEs and are of more concern. Iron is one of the main components involved in the composition of the solid phases identified in the remediation plots. Consequently, Fe is considered as a major factor controlling PTEs mobility by the action of iron oxides surface charge in metal adsorption in all plots. Many studies have referred to the role of Fe oxides and its surface charge, Mn oxides and sulphate phases in Pb and As mobility and solubility (Courtin *et al.*, 2016; Juhasz *et al.*, 2007). The abundance of Ca is due to the applied lime-mix technique in SL plot and the initially constructed capillary barrier component in GM and CC plots according to the composite design of the remediating process (NTUA 1998). Al and Mg are the third and fourth most important contributors to the pilot scale plots chemistry, following Fe and Ca and representing the clay layer in the CC plot while S originates from the pyritic wastes and the secondary sulfur products.

Out of the studied PTEs, Pb exists in a wide range of concentrations from 518 to 3929 mg/kg with an average value of 2236 mg/kg; this significant rise in the concentration range is linked to the intense metallurgical works on Pb ore, especially the argentiferous galena, and is also a matter of the ore grade. Arsenic is of high concern as well due to the high concentrations displayed in SL plot, even higher than in the CL plot, emphasizing the dissolution of large amounts of the Bodosakis arsenopyrite, while Zn concentrations reach their maximum in CL plot. The contributions of PTEs on the surface soil are significant in CL plot followed by SL and GM plots and are lower in CC plot indicating the transition of these elements upward by the action of the evapotranspiration process which prevails in CL and SL plots.

### 5.2 Assessment of PTEs long term mobility in the treated and untreated plots

The surface soil of the applied remediation techniques in GM and CC plots shows neutral to slightly alkaline acidity sharing almost the same mineralogical phases while the SL surface soil ranges between acidic and neutral values. A positive correlation between the PTEs was noted, as Pb, Zn and Cd are participating in Fe oxyhydrosulphates, hydroxides and Fe sulphate salts as well as Pb secondary minerals i.e., anglesite. Jarosite group minerals and specifically jarosite precipitates and plumbojarosite hexagonal crystals are the common hosts sequestering these metals and limiting their mobility. Plumbojarosite and gypsum are the predominating secondary phases while the only recognized tertiary mineral is gypsum.

The formation of the alleged hardpan layer in the SL quadrant is confirmed at a depth of 20 cm with the highest T.D.S concentration among the 4 quadrants, high contributions of Zn, As and Cd and diverse mineralogical phases of ferric iron hydroxides, primary minerals signature and emerging metal sulphate salts resulting in complex layer of secondary products. However, the formation of the hardpan layer in the SL plot neither guarantees the attenuation of metals infiltration to the drainage since comparable concentrations of Zn and Cd and highest concentration of Pb are obtained by DSL lysimeter, nor limit the effect of evaporation process to the surface soil.

The acidity measured along the SL depth profile facilitates the mobility of the PTEs, hence either percolating to deeper horizons in the rainy season or moving towards the surface in the summer. It has been mentioned that the corresponding amount of the alkaline additive of limestone to the Bodosakis pyrite is considerably lower than the stoichiometric need and the acidity produced by Bodosakis pyrite would not be sufficiently neutralized in the long term (*NTUA 1999*). It was predictable that the alkaline additive will not be able to efficiently neutralize the acidity in the long term and the aim of sulphidic-lime mix technique plot was the formation of a cemented layer to prevent further oxidation of sulphidic minerals.

The CL quadrant is characterized by 4 main geochemical horizons: the surface horizon represents the initially constructed protective soil where silicates and plumbojarosite in sub-microscopic hexagonal crystals with Zn and Cu inclusions dominate and the subsurface horizon or the vadose zone characterized by a layer of oxidized sulfide minerals presenting partially oxidized pyrite weathered to Fe oxides and hydroxides. Below that, a zone of chemical precipitation is formed with assemblages of plumbojarosite crystals then a saturated zone of mostly dissolved minerals with domination of secondary minerals. The identified mineralogical phases correlate significantly to the initial study findings since the upper section consisted of hydrated ferrous sulphates of rozenite and melanterite while the subsurface horizons were of ferric iron hydrosulphates. Thus, in the long term the simple soil protective layer is not effective in contamination containment.

Overall, CL plot and SL plot surface soils are affected by intense evapotranspiration process that mobilizes the PTEs within the acid environment of the waste pile material, leading to significant concentrations of PTE on the surface, hence exposing potential risk to inhabitants. It can be hypothesized that the remediation composite column in SL plot is not effective for the following reason: the amended column length is shorter than the length needed to prevent evaporation during the hot periods.

In the other two plots (GM and CC) the constructed barriers – either in the form of the synthetic geomembrane or the compacted clay layer- seem to be still effective in constraining the mobility of PTEs. Among the two the CC performs better when using the criterion of TCLP PTEs extractability for the surface samples.

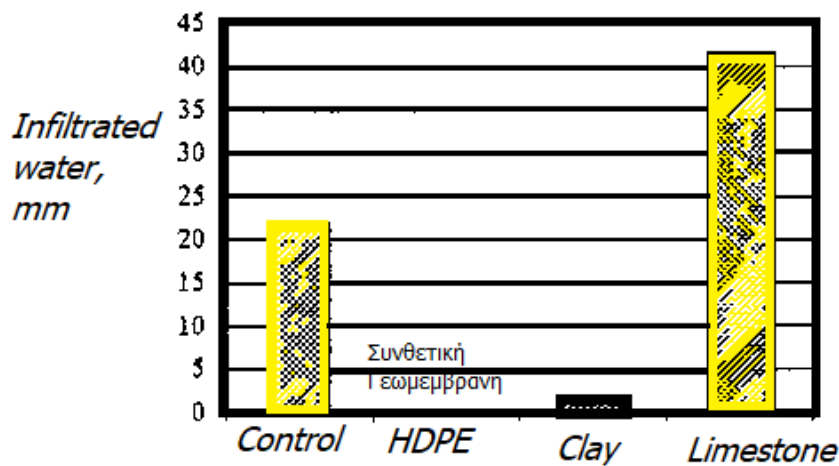


Fig. 22. Comparison of infiltrated water through the Kavodokanos test plots, based on data from the EU-LIFE study in 1996.

The comparison of infiltration through the different treated plots in the EU-LIFE study of the 1990's indicates that the geomembrane and the compacted clay barriers effectively prohibited the infiltration during the first two years of plot monitoring (Fig. 22). Of course, today there is infiltration through the GM and CC plots as evidenced by the full lysimeter tanks underneath the respective plots. However, differences in the composition of the drainage efflorescence precipitates indicate that both treatments have the potential of remaining at least partially effective after almost 25 years with respect to PTEs mobilization.

## 6. Conclusions

The long-term performance of the applied stabilization techniques has been assessed based on mineralogical and chemical analysis of solid samples from the Kavodokanos waste pile. The following conclusions are deduced from the present study:

- Almost 25 years after the pilot scale remediation in the Kavodokanos waste pile, the area remains polluted, posing significant risks for the health of nearby inhabitants, being exposed to very high concentrations of PTEs including Pb, Cd and As. Exposure is related to the airborne transfer of polluted grains from the surface of Kavodokanos pile within the dry and windy conditions prevailing in Lavrion.
- The effect of evaporation process within the pores of the waste material results in high concentrations of PTEs in the surface, especially in the control plot and the lime test plot. In the compacted clay and geomembrane test plots this effect is limited resulting in lower concentrations of PTEs in the surface. The compacted clay barrier technique shows superiority in maintaining neutral to slight alkaline pH values laterally and vertically in the long term.
- In the original LIFE-project study in the 1990s was concluded that within the 2-years (short-term) monitoring period after the pilot scale remediation, the geomembrane technique was the most effective for preventing infiltration followed by the compacted clay technique. However, the present study evidenced full lysimeter tanks underneath all test plots meaning that continuous infiltration occurs. However, the differences in the composition of drainage precipitates indicate that the two treatment utilizing barriers (CC, GM) have the potential of remaining at least partially effective after almost 25 years with respect to PTEs mobilization.
- The highest concentrations of PTEs; Pb, Zn and Cd were recorded in drainage precipitates underneath the liming technique plot. Therefore, in the long term, the alkalinity produced by liming in the sulfide- lime mix technique failed to neutralize the high acidity generated by the Bodosakis pyritic minerals resulting in highest infiltration of Pb, Zn and Cd into the drainage. The limited long-term performance of the applied liming technique may be attributed to failure of formation of a homogenous hard-pan horizon as anticipated.
- Overall, the long-term performance from the perspective of the present study demonstrates better effectiveness of the compacted clay barrier with the lowest TCLP leachable concentrations of PTEs in surface soil. This means that effective stabilization is better induced by this treatment. In the original study it is noted that the compacted clay has the additional advantage of low cost compared to the geomembrane barrier. Thus, the compacted clay technique can be considered as an effective sustainable

remediation technique that should seriously be considered in other areas with similar characteristics.

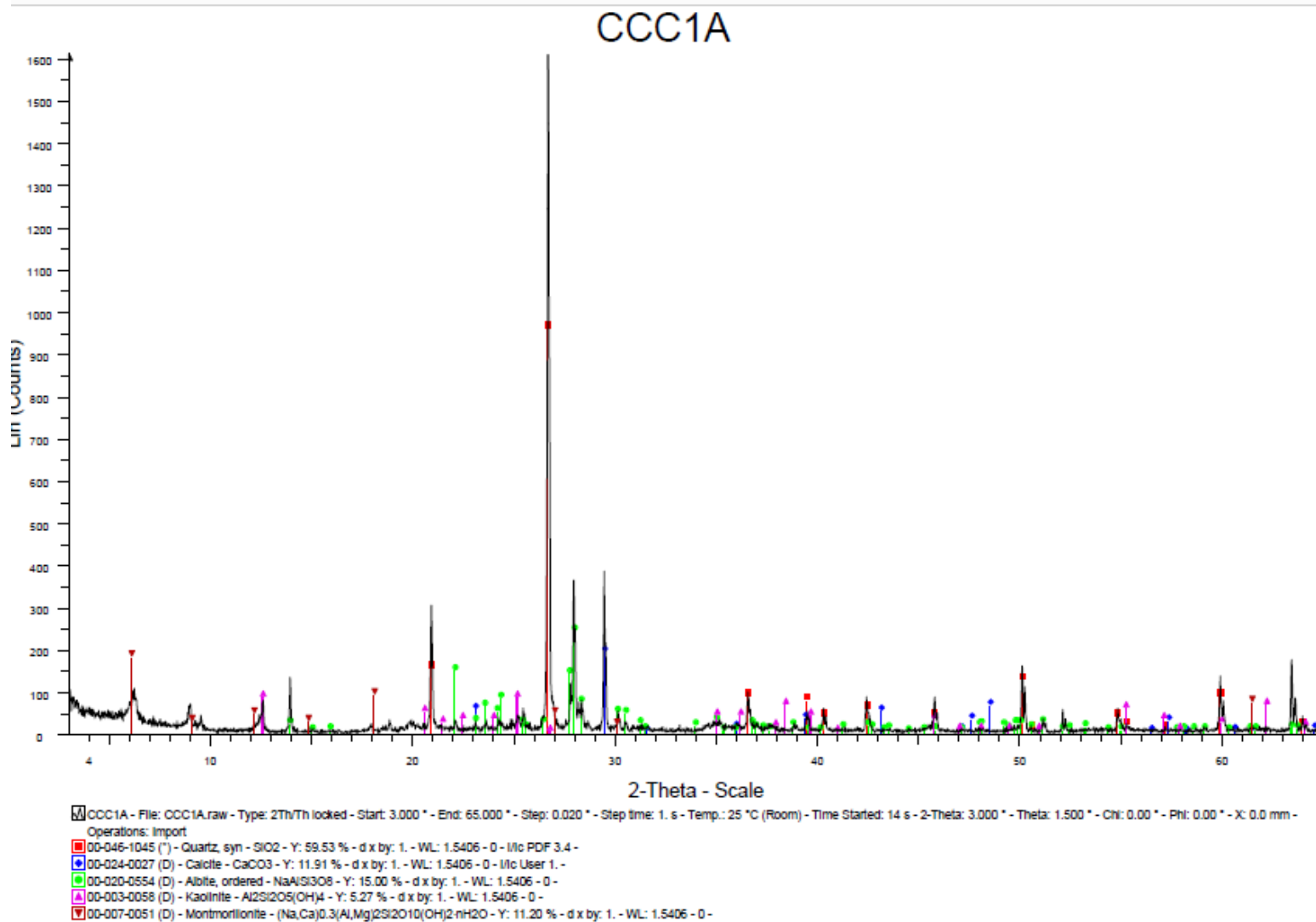
## References

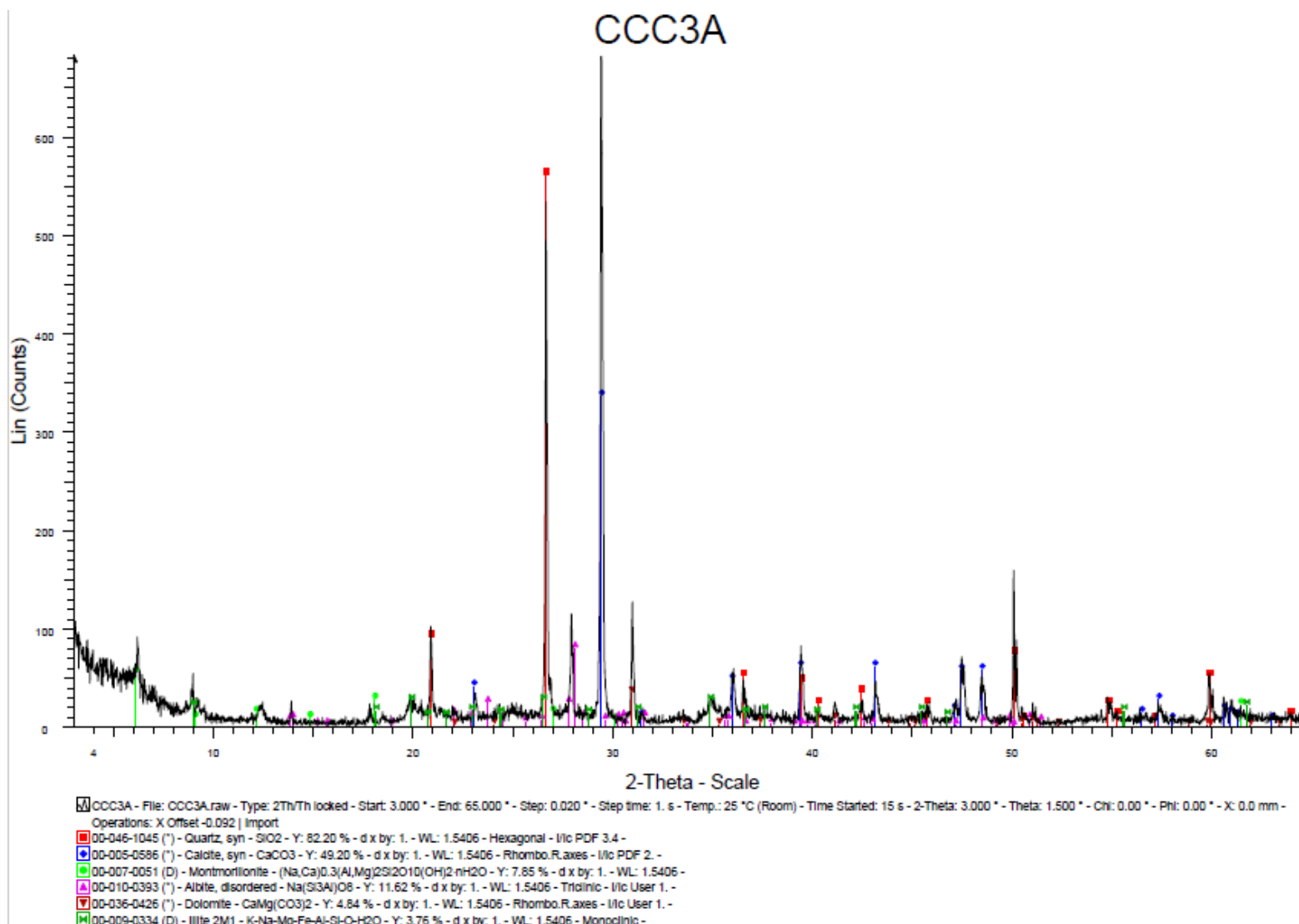
- Argyraki, A., Boutsis, Z., & Zotiadis, V. (2017). Towards sustainable remediation of contaminated soil by using diasporic bauxite: Laboratory experiments on soil from the sulfide mining village of Stratoni, Greece. *Journal of Geochemical Exploration*, 183, 214–222. <https://doi.org/10.1016/j.gexplo.2017.03.007>
- Beesley, L., Moreno-Jiménez, E., & Gomez-Eyles, J. L. (2010). Effects of biochar and green-waste compost amendments on mobility, bioavailability and toxicity of inorganic and organic contaminants in a multi-element polluted soil. *Environmental Pollution*, 158(6), 2282–2287. <https://doi.org/10.1016/j.envpol.2010.02.003>
- Benardos, A. (2017). *Rehabilitation of old mine waste sites : The case of Lavrion Technological & Cultural Park Contaminated sites ...*
- Boulet, M. P., & Larocque, A. C. L. (1998). A comparative mineralogical and geochemical study of sulfide mine tailings at two sites in New Mexico, USA. *Environmental Geology*, 33(2–3), 130–142. <https://doi.org/10.1007/s002540050233>
- Buelt, J. L., & Thompson, L. E. (1992). *The In Situ Vitriification Integrated Program: Focusing an innovative solution on environmental restoration needs*.
- Courtin-Nomade, A., Waltzing, T., Evrard, C., Soubrand, M., Lenain, J. F., Ducloux, E., ... & Bril, H. (2016). Arsenic and lead mobility: From tailing materials to the aqueous compartment. *Applied Geochemistry*, 64, 10-21.
- Demetriades, A. (Editor), 1999: LIFE Program Contract No: 93/GR/A14/GR/4576, Soil rehabilitation in the Municipality of Lavrion. Geochemical atlas of the Lavrion urban area for environmental protection and planning. Institute of Geology and Mineral Exploration, Athens.
- E.P.A. (1997). Recent Developments for In Situ Treatment of Metal Contaminated Soils. *U.S. Environmental Protection Agency*, 703, 64.
- Kontopoulos, A., Komnitsas, K., Xenidis, A. and Papassiopi, N. (1995) Environmental characterization of the sulphidic tailings in Lavrion. *Minerals Engineering*, 8(10), 1209–1219.
- Guo, G., Zhou, Q., & Ma, L. Q. (2006). Availability and assessment of fixing additives for the in situ remediation of heavy metal contaminated soils: A review. *Environmental Monitoring and Assessment*, 116(1–3), 513–528. <https://doi.org/10.1007/s10661-006-7668-4>
- Hammarstrom, J. M., Seal, R. R., Meier, A. L., & Kornfeld, J. M. (2005). Secondary sulfate minerals associated with acid drainage in the eastern US: recycling of metals and acidity in surficial environments. *Chemical Geology*, 215(1-4), 407-431.
- Hansen, J., Reed, C., Scudese, M., Lazarus, L., & Park, F. (1994). Technical assistance document for complying with the TC rule and implementing the toxicity characteristic leaching procedure (TCLP). United States Environmental Protection Agency.
- Hering, J. G., Zhu, C., & Oelkers, E. H. (2011). Global Water Sustainability. In *Elements* (Vol. 7, Issue 3).

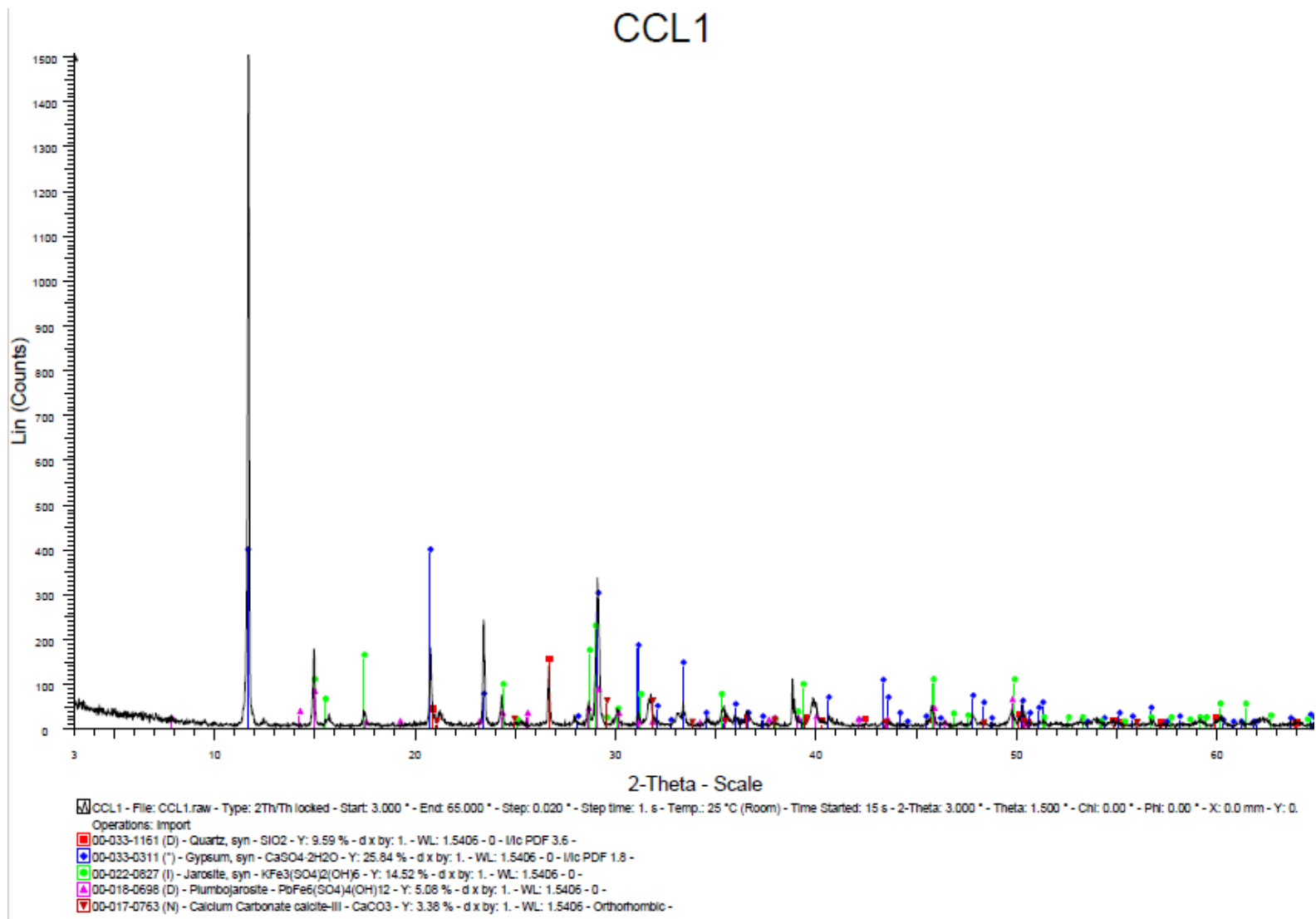
- Hodson, M. E. (2010). The need for sustainable soil remediation. *Elements*, 6(6), 363–368. <https://doi.org/10.2113/gselements.6.6.363>
- Hu, X., Zhang, Y., Luo, J., Wang, T., Lian, H., & Ding, Z. (2011). Bioaccessibility and health risk of arsenic, mercury and other metals in urban street dusts from a mega-city, Nanjing, China. *Environmental Pollution*. <https://doi.org/10.1016/j.envpol.2011.01.037>
- Juhasz, A. L., Smith, E., Weber, J., Rees, M., Rofe, A., Kuchel, T., ... & Naidu, R. (2007). In vitro assessment of arsenic bioaccessibility in contaminated (anthropogenic and geogenic) soils. *Chemosphere*, 69(1), 69-78.
- Kalaitzidis, S. (2018). Symposium on Environmental Pollution from Abandoned Mines Abstracts Book & Lavreotiki-Lavrion Excursion Guide. *Symposium on Environmental Pollution from Abandoned Mines, June*, 180.
- Katsaros, H. (n.d.). *A trip to the Geological and Ancient Mining Lavrion By Dimitris Bitzios, Dr. Geologist*. 1–41.
- Khalid, S., Shahid, M., Niazi, N. K., Murtaza, B., Bibi, I., & Dumat, C. (2017). A comparison of technologies for remediation of heavy metal contaminated soils. *Journal of Geochemical Exploration*, 182, 247–268. <https://doi.org/10.1016/j.gexplo.2016.11.021>
- Komnitsas, K., Xenidis, A., & Adam, K. (1995). Oxidation of pyrite and arsenopyrite in sulphidic spoils in Lavrion. *Minerals Engineering*, 8(12), 1443–1454. [https://doi.org/10.1016/0892-6875\(95\)00109-3](https://doi.org/10.1016/0892-6875(95)00109-3)
- Larocque, A. C. L., & Rasmussen, P. E. (1998). An overview of trace metals in the environment, from mobilization to remediation. *Environmental Geology*, 33(2–3), 85–91. <https://doi.org/10.1007/s002540050227>
- Lavazzo, P., Adamo, P., Boni, M., Hillier, S., & Zampella, M. (2012). Mineralogy and chemical forms of lead and zinc in abandoned mine wastes and soils: An example from Morocco. *Journal of Geochemical Exploration*. <https://doi.org/10.1016/j.gexplo.2011.06.001>
- McLean, J. E., & Bledsoe, B. E. (1992). Behavior of Metals in Soils. Office of Research and Development, EPA/540/S-, 1–25.
- Meuser, H. (2012). Soil remediation and rehabilitation: treatment of contaminated and disturbed land (Vol. 23). Springer Science & Business Media.
- Mylona, E., Papassiopi, N., Xenidis A. & Paspaliaris I., “Field performance of dry covers and limestone addition for acid generation control of Lavrion sulphidic tailings, Greece” in Proc. of 6th Int. Conf. on Acid Rock Drainage, ICARD 2003, (Australia, 2003), 319-326.
- NTUA. (1999). Soil Rehabilitation in The Municipality of Lavion. LIFE Program Contract No: 93/GR/A14/GR/4576. Vol. 3., Athens.
- Olyphant, G. A., Bayless, E. R., & Harper, D. (1991). Seasonal and weather-related controls on solute concentrations and acid drainage from a pyritic coal-refuse deposit in southwestern Indiana, USA. *Journal of contaminant hydrology*, 7(3), 219-236.
- Panagiotaras, D., & Nikolopoulos, D. (2015). Arsenic occurrence and fate in the environment; a geochemical perspective. *Journal of Earth Science & Climatic Change*, 6(4), 1.

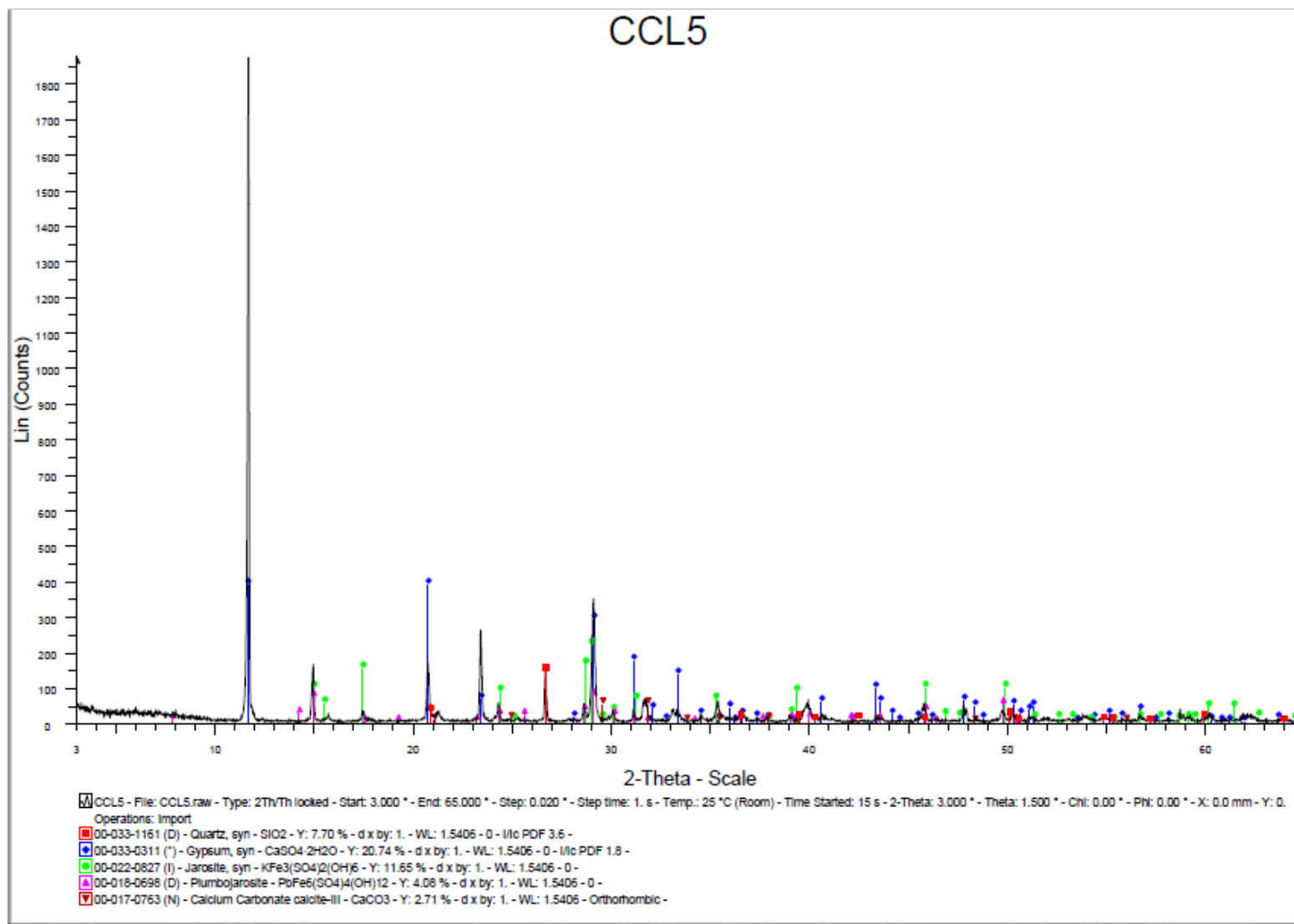
- Panagopoulos, I., Karayannis, A., Adam, K. Aravossis, K. (2009) Application of risk management techniques for the remediation of an old mining site in Greece. *Waste Management*, 29(5), 1739-1746.
- Paspaliaris, I., PAPANASSIOU, N., XENIDES, A., & KOMNITSAS, K. (1999). Remediation of land contaminated by mining and metallurgical activities in Lavrion area. *Mining and Metallurgical Ann* 1999, 9: 31, 54.
- Søndergaard, J., Hansen, V., Bach, L., Jørgensen, C. J., Jia, Y., & Asmund, G. (2018). *Geochemical test work in Environmental Impact Assessments for mining projects in Greenland - Recommendations by DCE and GINR* (Issue 132). <http://dce2.au.dk/pub/TR132.pdf>
- Interstate Technology & Regulatory Council (ITRC). (2011). Green and sustainable remediation: A practical framework. GSR-2.
- van der Sloot, H. A., & van Zomeren, A. (2012). Characterisation Leaching Tests and Associated Geochemical Speciation Modelling to Assess Long Term Release Behaviour from Extractive Wastes. *Mine Water and the Environment*, 31(2), 92–103. <https://doi.org/10.1007/s10230-012-0182-8>
- U.S. EPA, 1986. Toxicity characteristic leaching procedure, Appendix 1, Federal Register 51:216
- Wuana, R. A., & Okieimen, F. E. (2011). Heavy Metals in Contaminated Soils: A Review of Sources, Chemistry, Risks and Best Available Strategies for Remediation. *ISRN Ecology*, 2011, 1–20. <https://doi.org/10.5402/2011/402647>
- Yanful, E. K., Simms, P. H., & Payant, S. C. (1999). Soil covers for controlling acid generation in mine tailings: a laboratory evaluation of the physics and geochemistry. *Water, Air, and Soil Pollution*, 114(3), 347-375.
- Zotiadis, V., & Argyraki, A. (2017). Development of innovative environmental applications of attapulgite clay. *Bulletin of the Geological Society of Greece*, 47(2), 992. <https://doi.org/10.12681/bgsg.11139>
- Zotiadis, V., Argyraki, A., & Theologou, E. (2012). Pilot-Scale Application of Attapulgitic Clay for Stabilization of Toxic Elements in Contaminated Soil. *Journal of Geotechnical and Geoenvironmental Engineering*, 138(5), 633–637. [https://doi.org/10.1061/\(asce\)gt.1943-5606.0000620](https://doi.org/10.1061/(asce)gt.1943-5606.0000620)

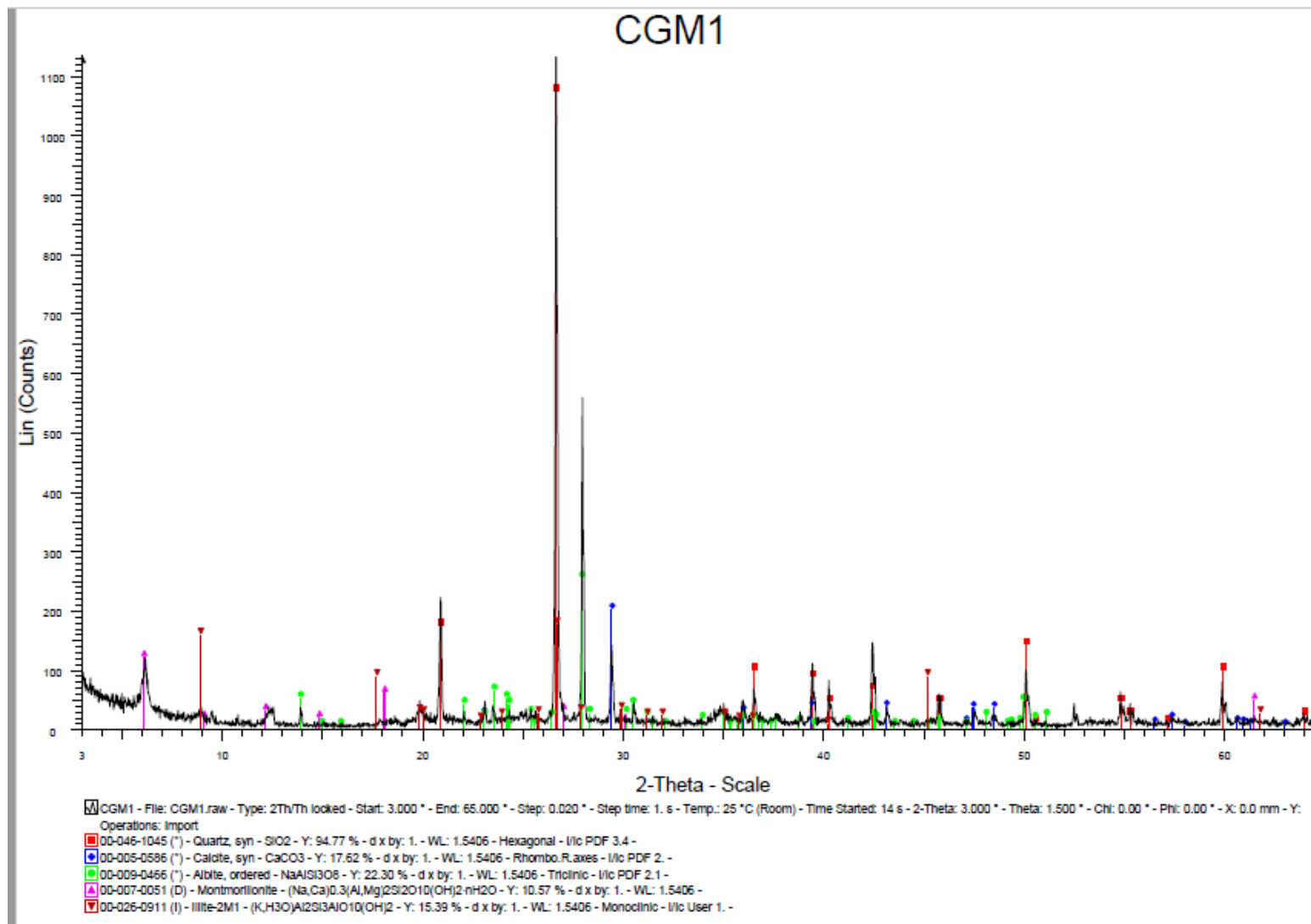
## Appendix I- XRD patterns of the studied samples

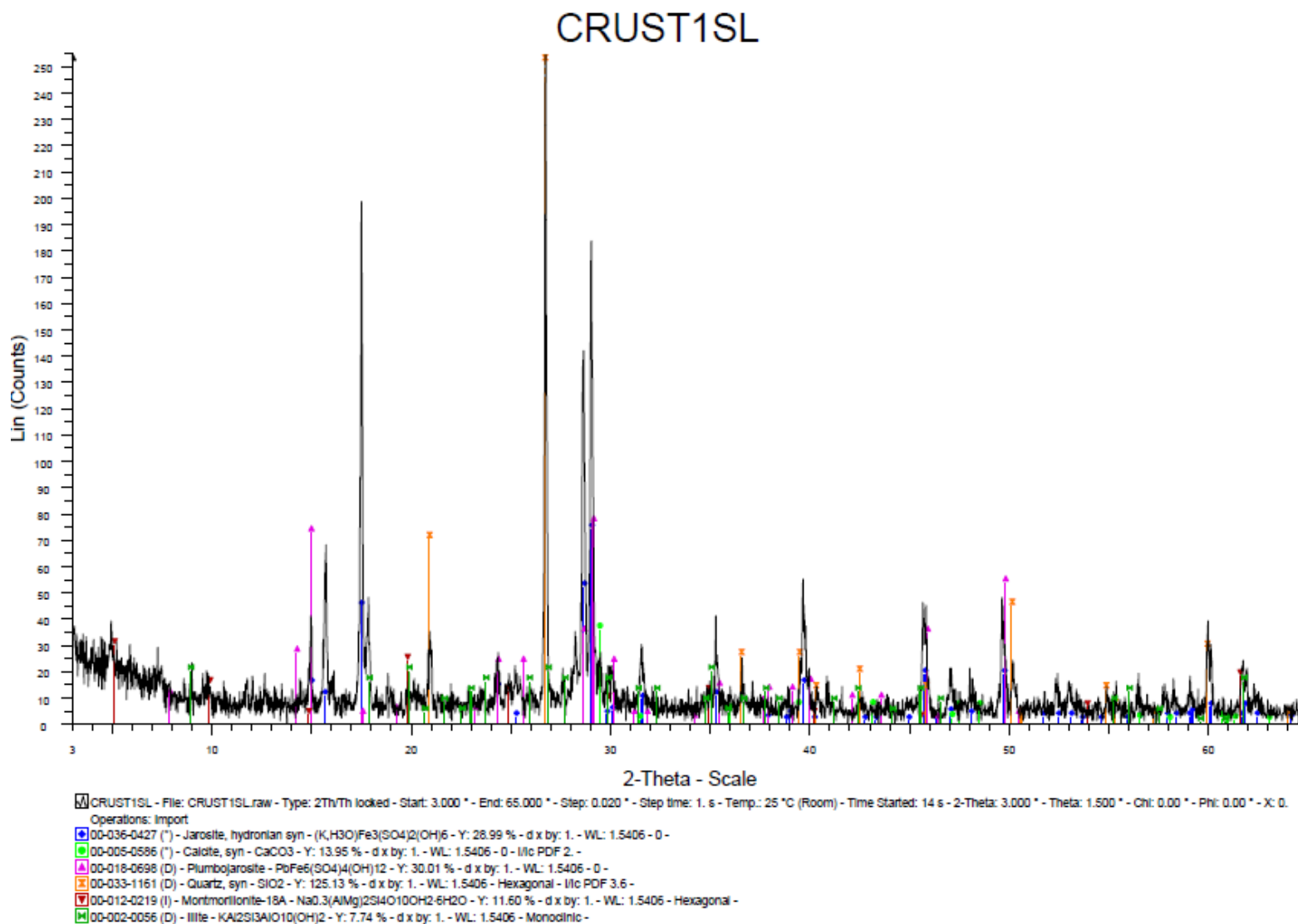




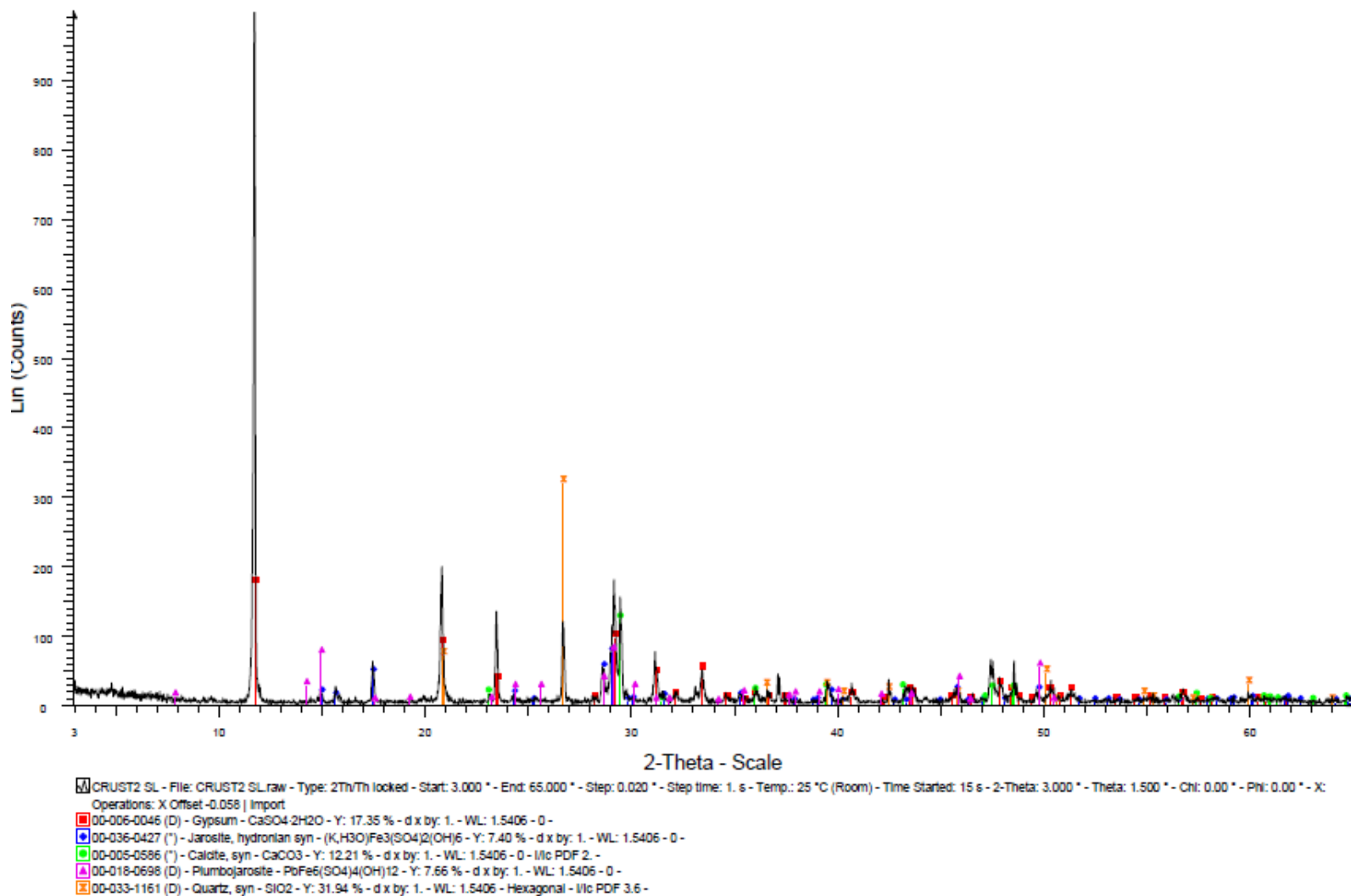


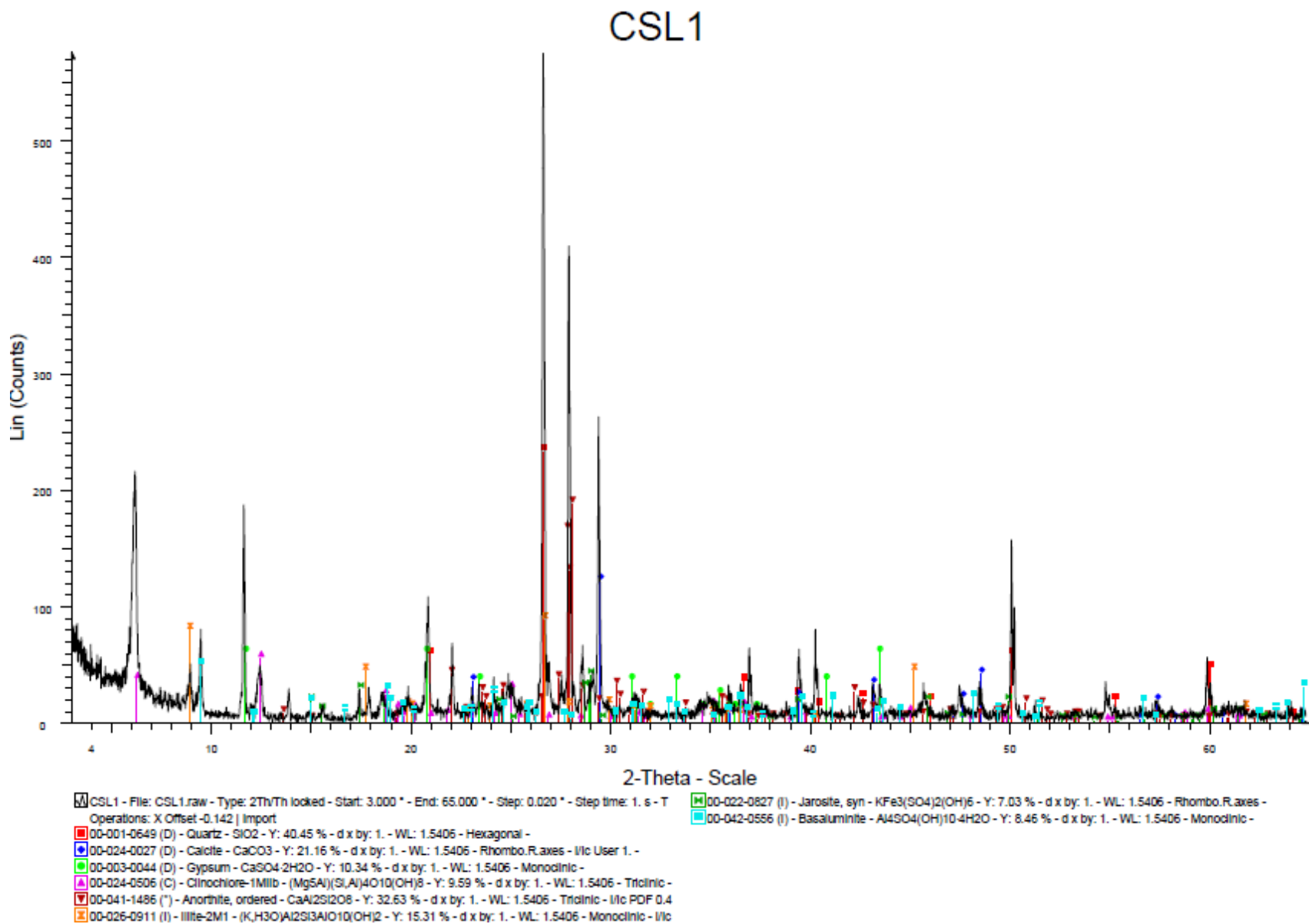




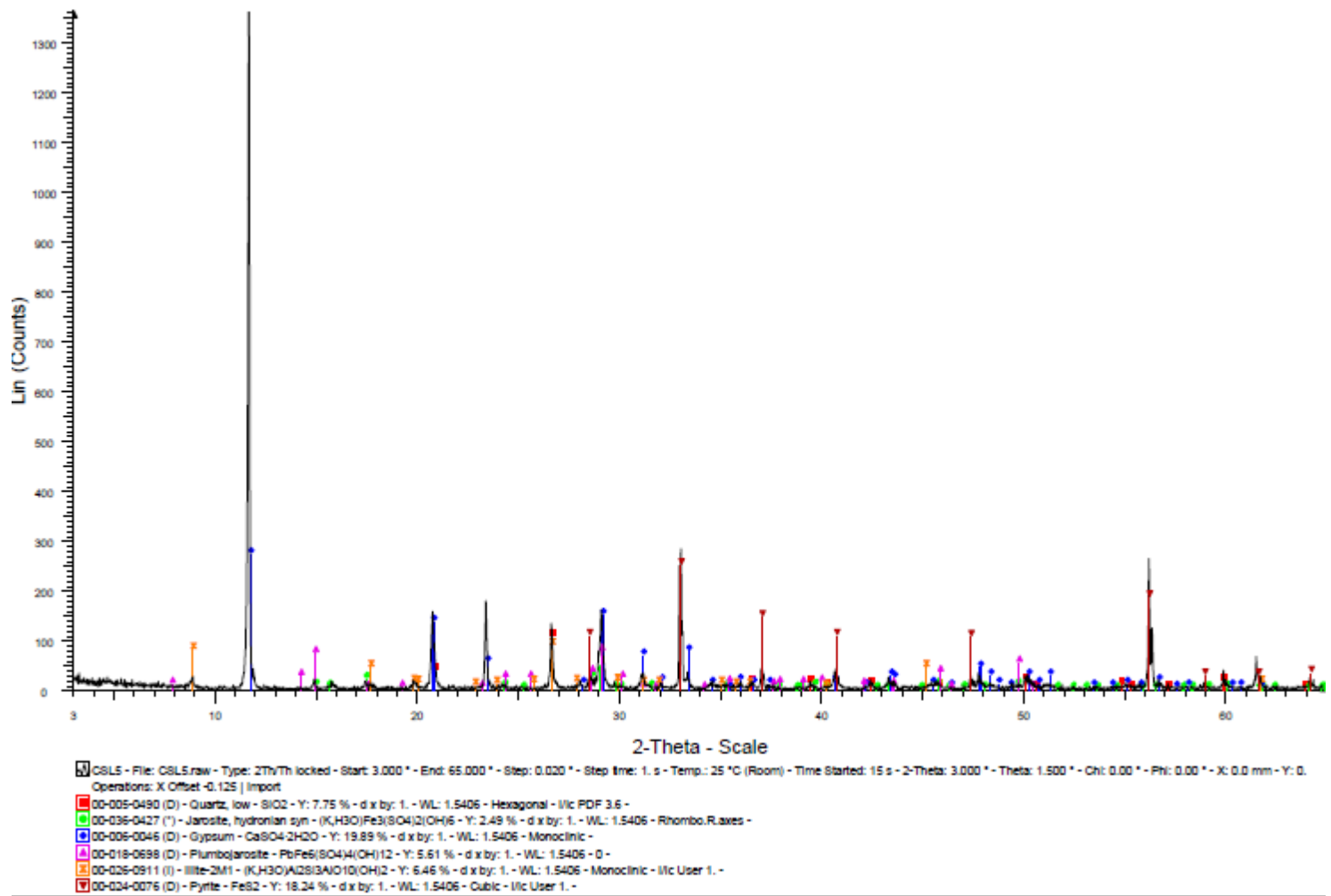


## CRUST2 SL

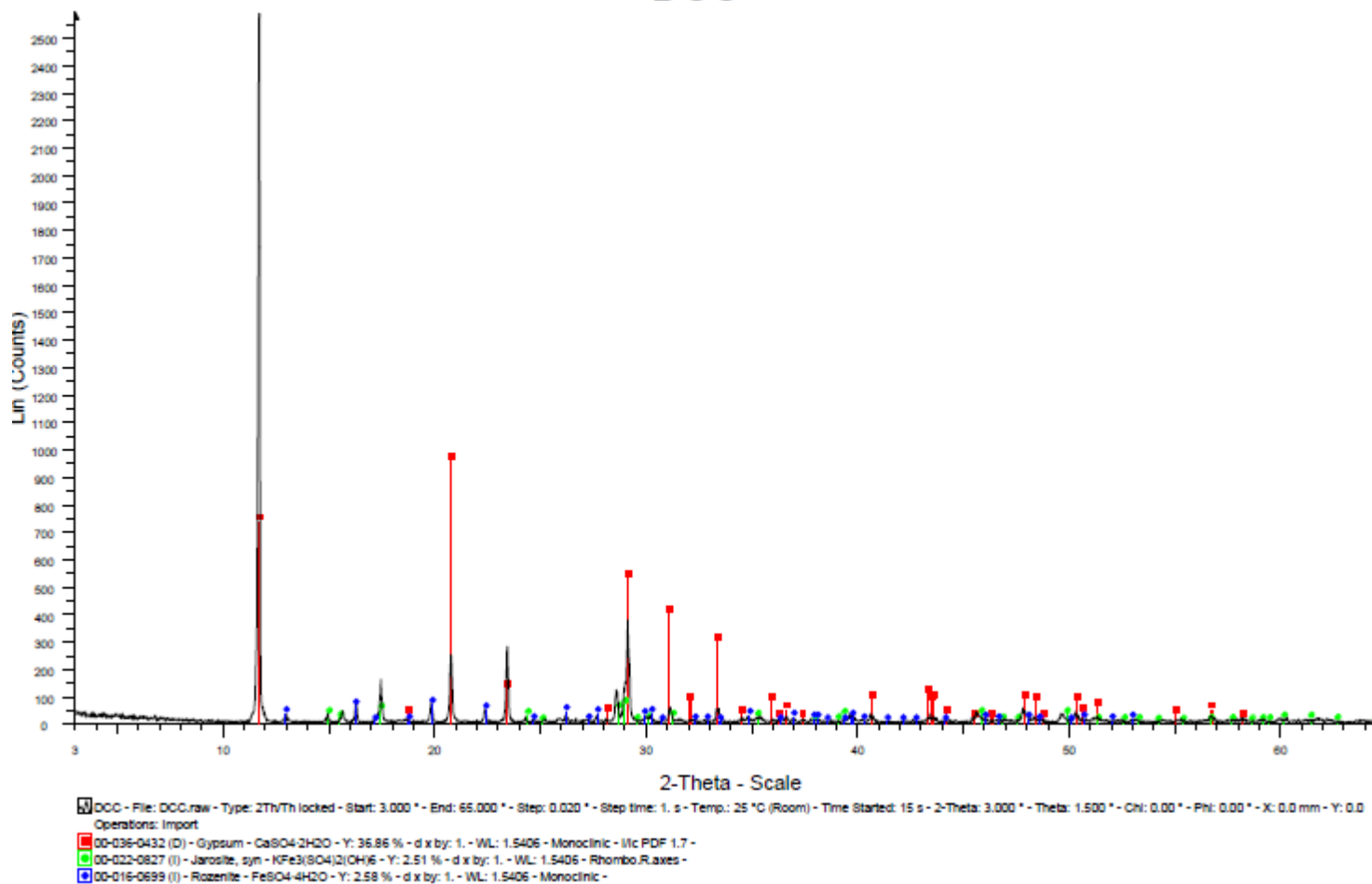


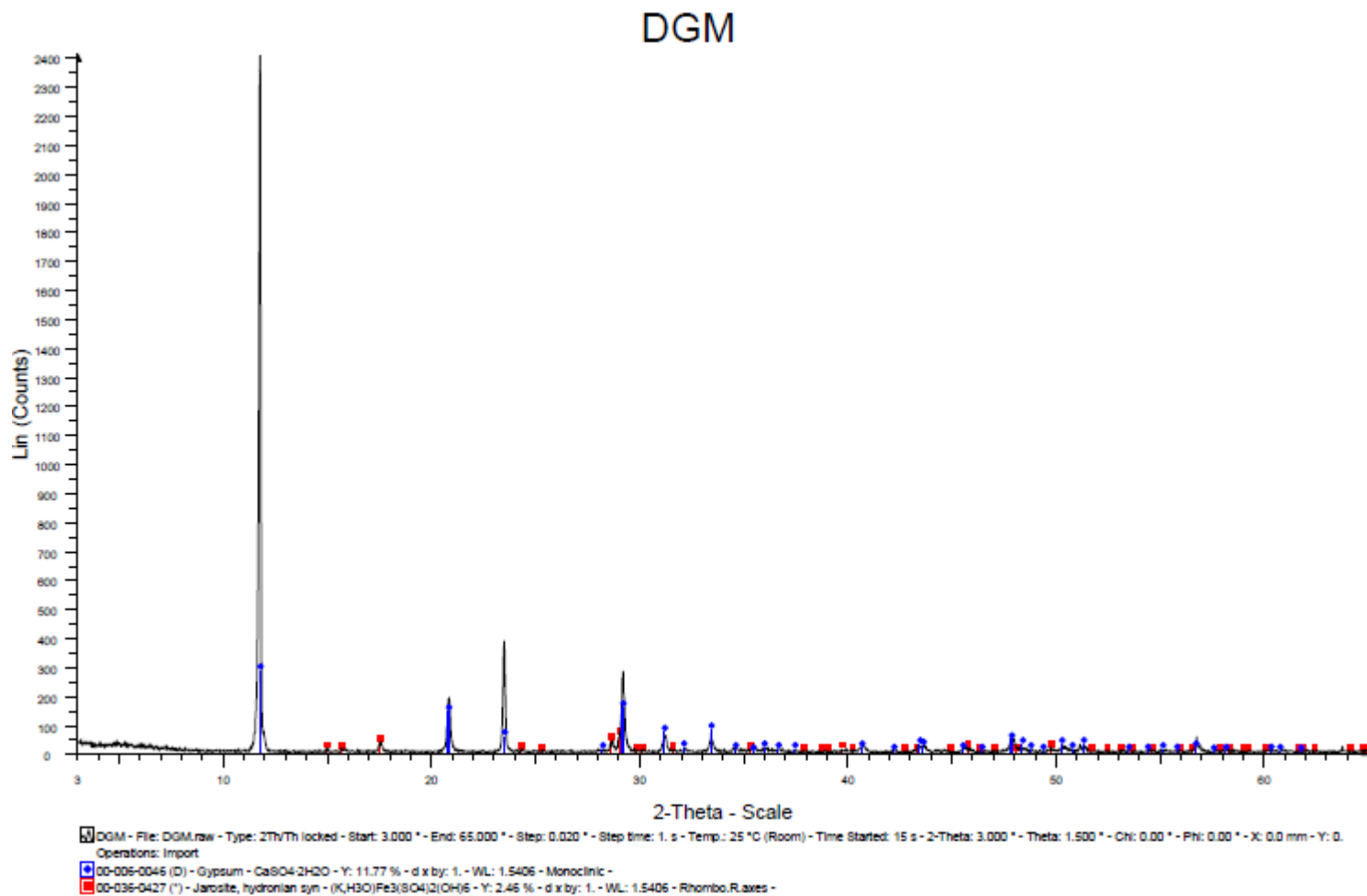


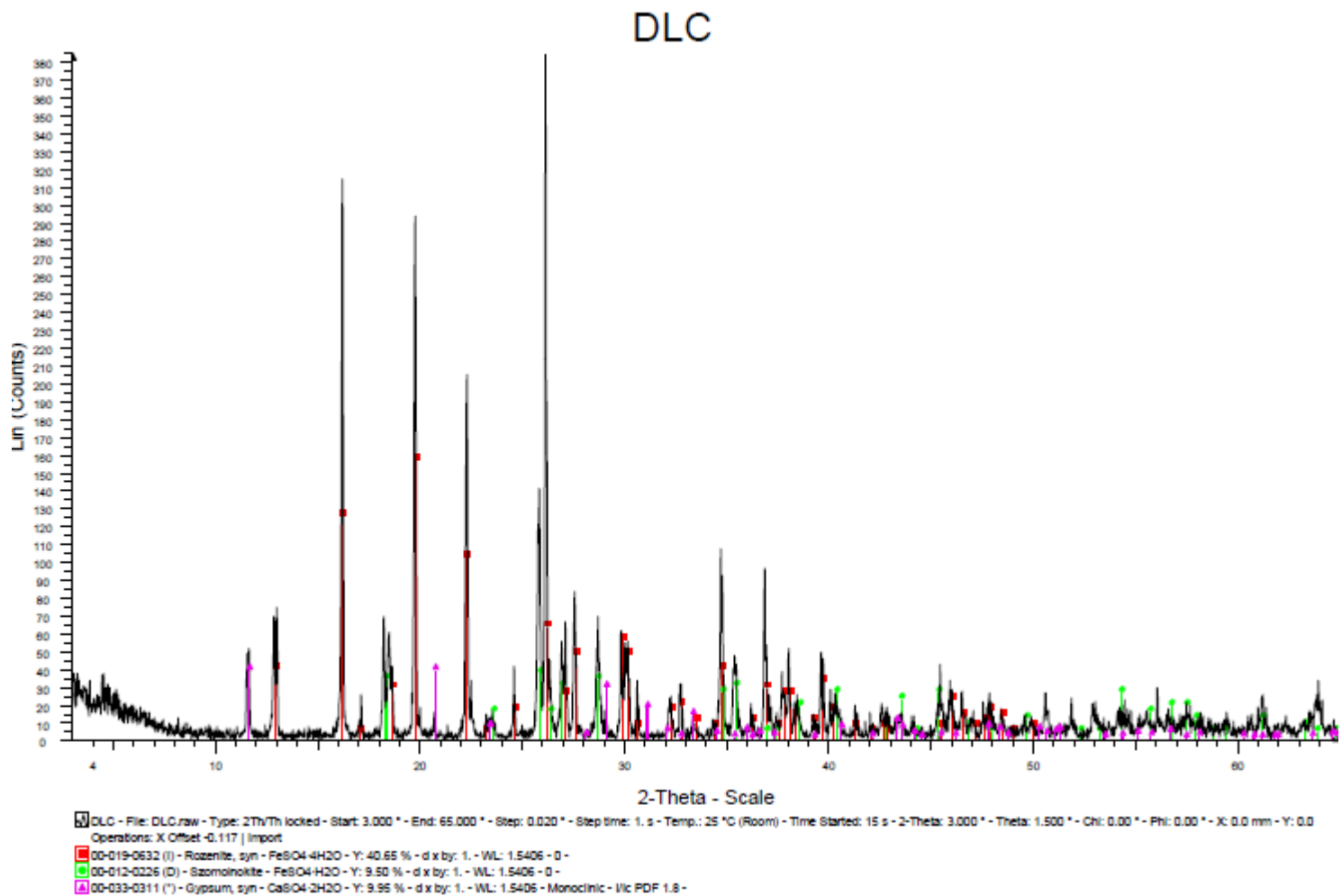
### CSL5

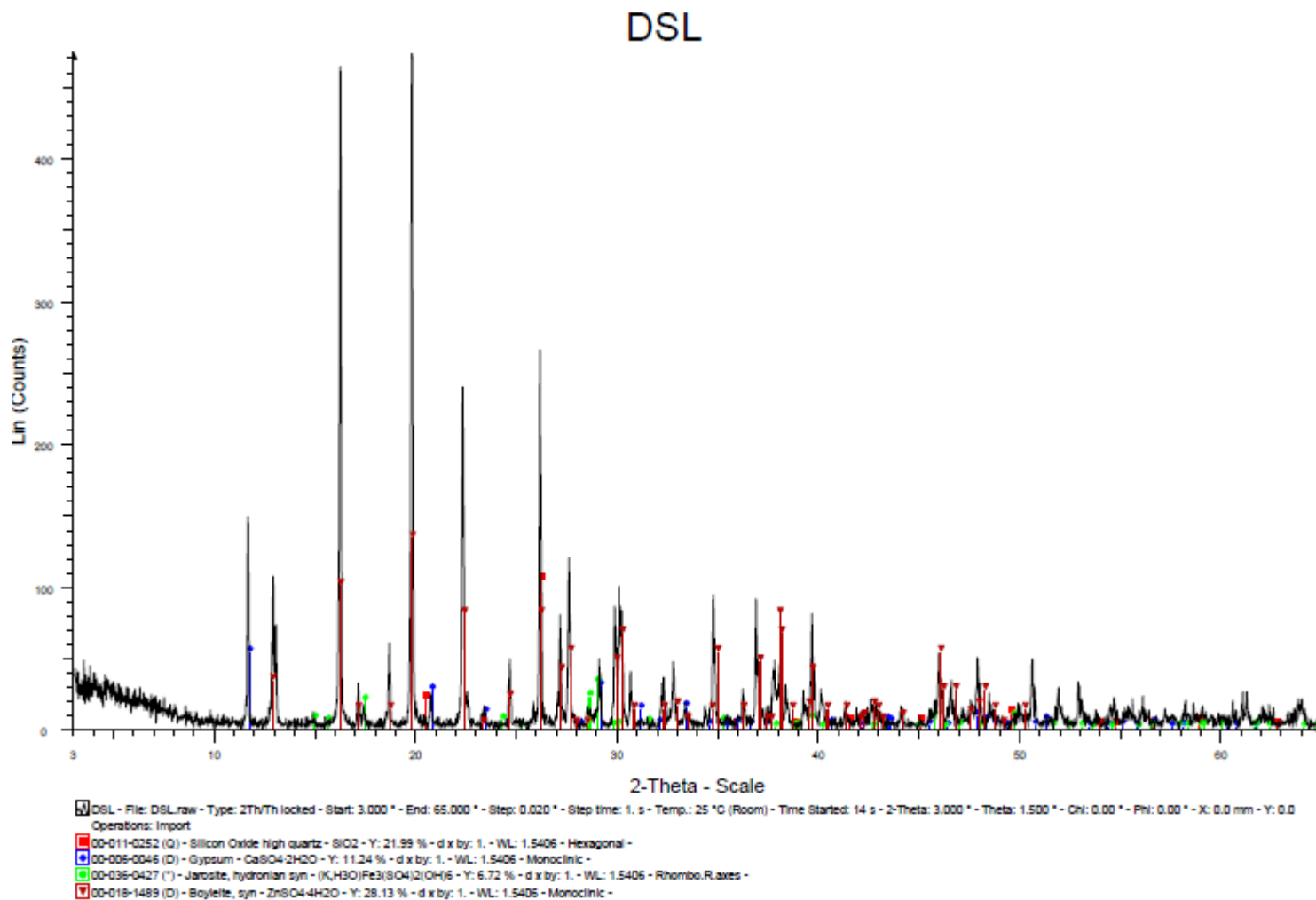


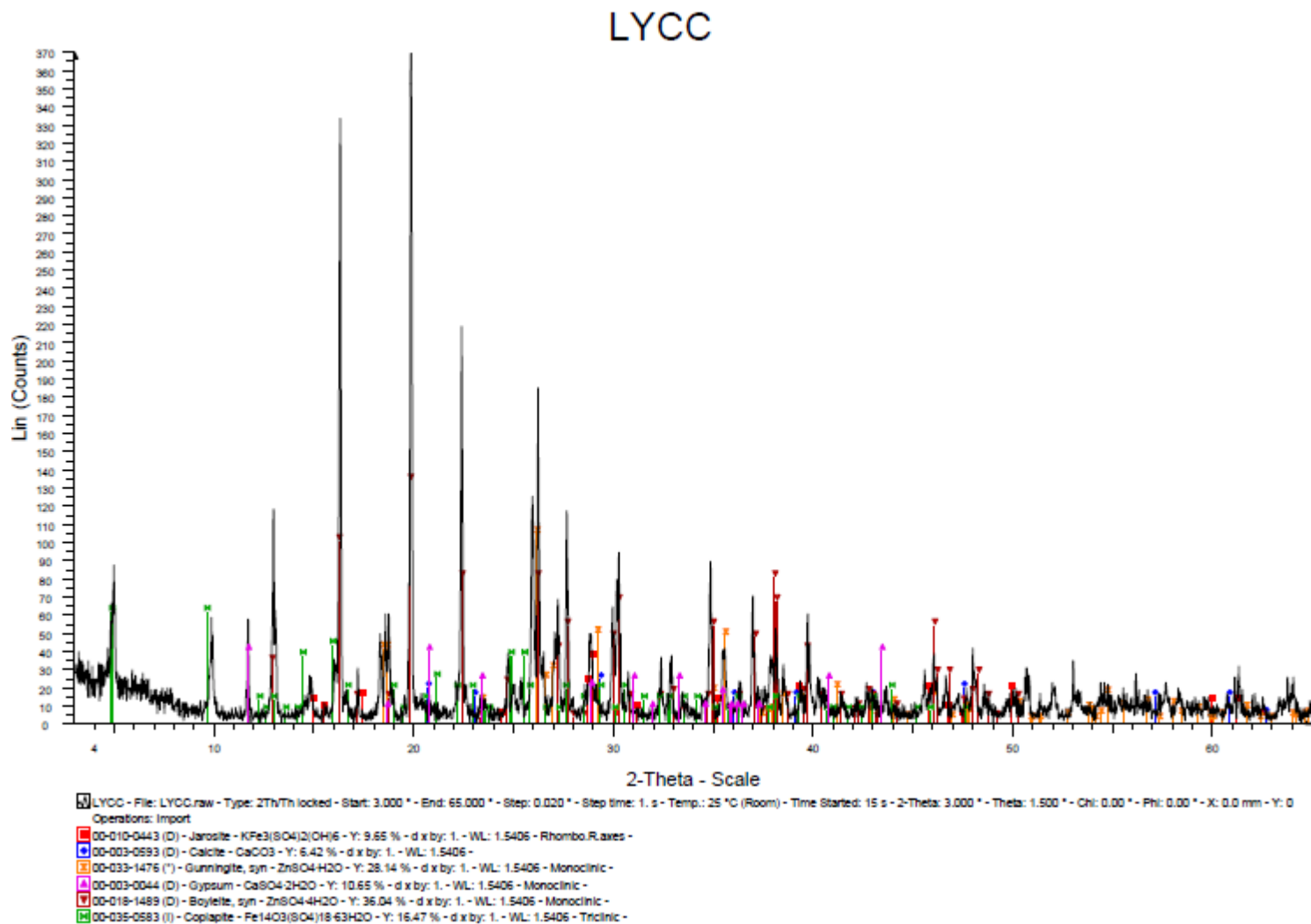
### DCC



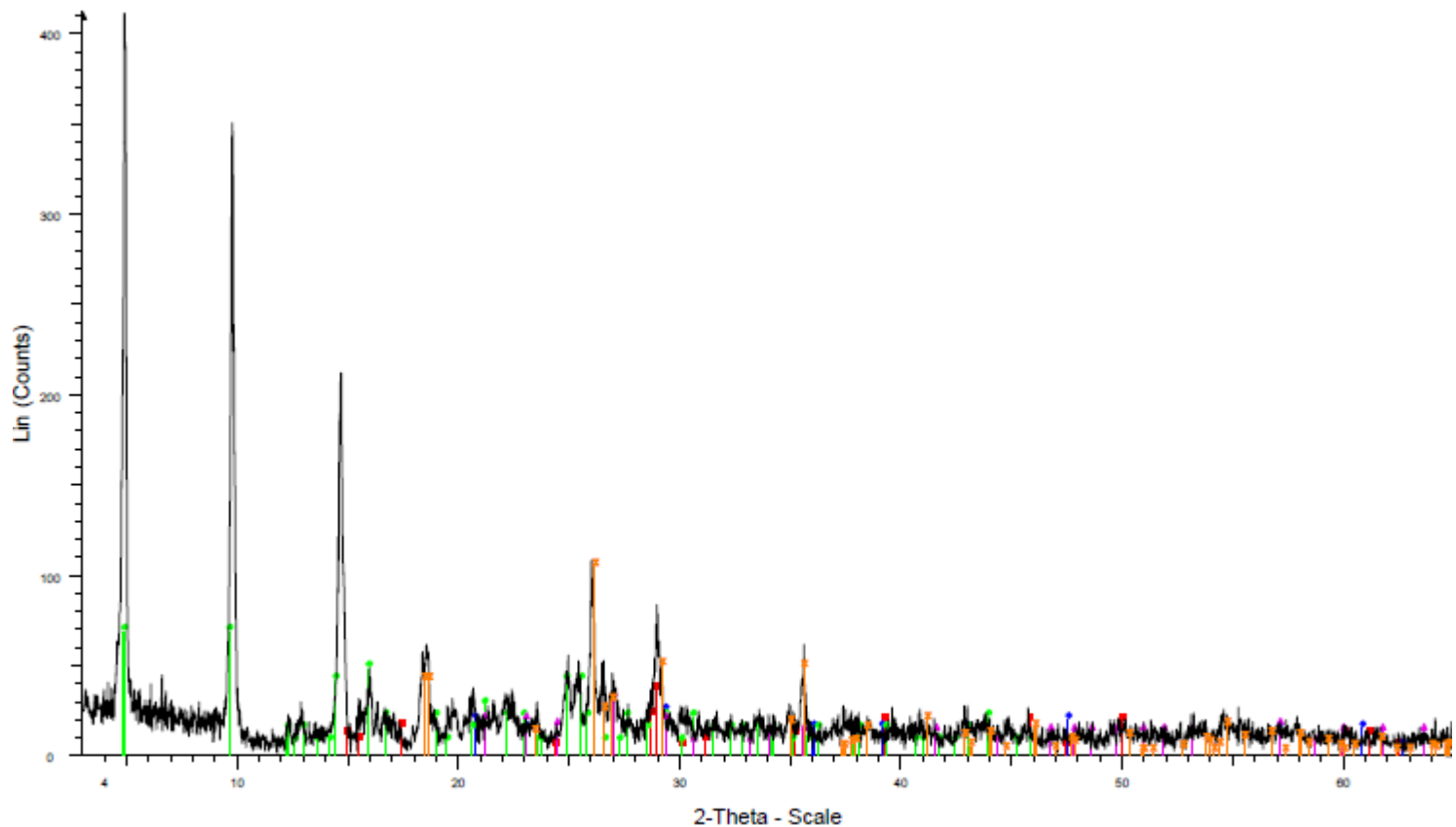








# LYCCI



LYCCI - File: LYCCI.raw - Type: 2Th/Th locked - Start: 3.000 ° - End: 65.000 ° - Step: 0.020 ° - Step time: 1. s - Temp.: 25 °C (Room) - Time Started: 15 s - 2-Theta: 3.000 ° - Theta: 1.500 ° - Chi: 0.00 ° - Phi: 0.00 ° - X: 0.0 mm - Y: Operations: Import

- 00-010-0443 (D) - Jarosite -  $\text{KFe}_3(\text{SO}_4)_2(\text{OH})_6$  - Y: 8.67 % - d x by: 1. - WL: 1.5406 - Rhombo.R.axes -
- 00-003-0593 (D) - Calcite -  $\text{CaCO}_3$  - Y: 5.77 % - d x by: 1. - WL: 1.5406 -
- 00-033-1476 (\*) - Gunningite, sym -  $\text{Zn}_8\text{O}_4\text{H}_2\text{O}$  - Y: 25.27 % - d x by: 1. - WL: 1.5406 - Monoclinic -
- 00-035-0583 (I) - Copiapite -  $\text{Fe}_{14}\text{O}_3(\text{SO}_4)_{18}\cdot 63\text{H}_2\text{O}$  - Y: 16.54 % - d x by: 1. - WL: 1.5406 - Triclinic -
- 00-003-0451 (D) - Abite -  $\text{NaAlSi}_3\text{O}_8$  - Y: 7.66 % - d x by: 1. - WL: 1.5406 - Triclinic -

Appendix II – Chemical analysis results.

Concentrations of Al, Ca, Mg, Fe, S, Na, K, Ti in %wt. All other elements in mg/kg.

| Sample    | pH   | Pb     | Zn     | Cd | As     | Cu   | Mn   | Al   | Ca     | Mg   | Fe     | S     | Na    | K     | Ti    | Pb_SBET | Zn_SBET  | Cd_SBET | Pb_TCLP | Zn_TCLP |  |
|-----------|------|--------|--------|----|--------|------|------|------|--------|------|--------|-------|-------|-------|-------|---------|----------|---------|---------|---------|--|
| CCL1      | 3.07 | >10000 | 6968   | 16 | 5285   | 677  | 248  | 0.25 | 5.58   | 0.04 | >15.00 | >5.00 | 0.05  | 0.18  | 0.01  | 82.5    | 108.90   | 3.50    |         |         |  |
| CCL2      | 2.94 |        |        |    |        |      |      |      |        |      |        |       |       |       |       |         |          |         |         |         |  |
| CCL3      | 2.8  | >10000 | 8286   | 18 | 6324   | 696  | 281  | 0.12 | 5.14   | 0.02 | >15.00 | >5.00 | 0.05  | 0.18  | <0.01 |         |          |         |         |         |  |
| CCL4      | 2.73 |        |        |    |        |      |      |      |        |      |        |       |       |       |       |         |          |         |         |         |  |
| CCL5      | 2.63 | >10000 | 7186   | 18 | 4998   | 679  | 282  | 0.21 | 5.78   | 0.03 | >15.00 | >5.00 | 0.05  | 0.22  | <0.01 |         |          |         |         |         |  |
| CSL1      | 6.32 | 711    | 242    | 4  | 1726   | 47.8 | 906  | 2.39 | 6.07   | 1.39 | 7.55   | 2.57  | 0.04  | 0.28  | 0.04  | 34.43   | 73.51    | 1.65    |         |         |  |
| CSL2      | 5.23 |        |        |    |        |      |      |      |        |      |        |       |       |       |       |         |          |         |         |         |  |
| CSL3      | 3.16 | >10000 | 448    | 11 | >10000 | 105  | 242  | 0.25 | 7.16   | 0.09 | >15.00 | >5.00 | 0.03  | 0.24  | <0.01 |         |          |         |         |         |  |
| CSL4      | 2.99 |        |        |    |        |      |      |      |        |      |        |       |       |       |       |         |          |         |         |         |  |
| CSL5      | 2.64 | 7002   | 350    | 11 | >10000 | 76.3 | 118  | 0.08 | 7.85   | 0.02 | >15.00 | >5.00 | 0.03  | 0.15  | <0.01 |         |          |         |         |         |  |
| CCC1A     | 6.96 | 948    | 456    | 3  | 183    | 53.9 | 1094 | 2.63 | 0.76   | 1.25 | 4.22   | 0.1   | 0.02  | 0.36  | 0.03  | 222.35  | 220.59   | 1.18    |         |         |  |
| CCC2A     | 7.76 | 248    | 184    | 1  | 127    | 17.5 | 447  | 0.98 | >15.00 | 2.79 | 1.47   | 0.09  | 0.02  | 0.16  | 0.02  |         |          |         |         |         |  |
| CCC3A     | 7.8  | 153    | 111    | 2  | 108    | 21.1 | 530  | 1.87 | 13.73  | 1.77 | 2.66   | 0.08  | 0.02  | 0.28  | 0.02  |         |          |         |         |         |  |
| CGM1      | 7.79 | 439    | 403    | 3  | 100    | 48.7 | 1117 | 2.99 | 2.85   | 1.62 | 4.16   | 0.06  | 0.02  | 0.39  | 0.04  | 175.39  | 275.73   | 1.46    |         |         |  |
| DCL-W     | 2.73 | 17     | >10000 | 28 | 9      | 172  | 1262 | 0.05 | 0.19   | 0.12 | >15.00 | >5.00 | <0.01 | <0.01 | <0.01 | 18.49   | 14332.08 | 19.87   |         |         |  |
| DCL-Y     | 2.99 |        |        |    |        |      |      |      |        |      |        |       |       |       |       |         |          |         |         |         |  |
| DSL       | 2.71 | 479    | 4589   | 21 | 683    | 294  | 2314 | 0.08 | 0.49   | 0.23 | >15.00 | >5.00 | 0.03  | <0.01 | <0.01 | 19.30   | 5420     | 12      |         |         |  |
| DGM       | 2.32 | 459    | 5299   | 16 | 308    | 409  | 521  | 0.14 | 12.31  | 0.06 | 12.29  | >5.00 | 0.14  | 0.04  | <0.01 | 42.00   | 6480     | 13.20   |         |         |  |
| DCC       | 2.5  | 245    | 9146   | 22 | 100    | 72.5 | 800  | 0.09 | 9.45   | 0.08 | >15.00 | >5.00 | 0.3   | 0.02  | <0.01 | 26.94   | 8583.33  | 18.15   |         |         |  |
| LYCCI     | 1.82 |        |        |    |        |      |      |      |        |      |        |       |       |       |       |         |          |         |         |         |  |
| LYCCO     | 2.03 |        |        |    |        |      |      |      |        |      |        |       |       |       |       |         |          |         |         |         |  |
| CRUST1 SL | 2.11 | 649    | 448    | 12 | 3327   | 50.8 | 345  | 0.71 | 0.28   | 0.25 | >15.00 | >5.00 | 0.09  | 0.15  | 0.02  | 20.19   | 498.11   | 2.92    |         |         |  |
| CRUST2 SL | 2.51 | 4140   | 2506   | 16 | 7889   | 91.2 | 5181 | 0.23 | 10.53  | 0.16 | >15.00 | >5.00 | 0.1   | 0.11  | <0.01 | 214.02  | 3219.38  | 9.77    |         |         |  |
| C1        | 8.67 |        |        |    |        |      |      |      |        |      |        |       |       |       |       | 96.90   | 92.00    | 0.90    | <dl     | <dl     |  |
| C2        | 6.22 | 8254   | 4708   | 12 | 2401   | 289  | 1025 | 2.73 | 2.33   | 1.15 | 11.55  | 3.02  | 0.03  | 0.36  | 0.04  | 52.79   | 3278.85  | 7.12    | 3.0     | 1240    |  |
| C3        | 4.16 | >10000 | 4929   | 12 | 4008   | 542  | 352  | 1.14 | 6.81   | 0.33 | >15.00 | >5.00 | 0.05  | 0.23  | 0.03  | 37.68   | 660.71   | 4.11    | 2.6     | 426     |  |
| C4        | 7.15 |        |        |    |        |      |      |      |        |      |        |       |       |       |       | 91.79   | 145.54   | 1.25    | 2.3     | <dl     |  |
| C5        | 6.92 | 1474   | 1554   | 5  | 833    | 101  | 1277 | 3    | 2.45   | 1.43 | 5.2    | 0.81  | 0.03  | 0.37  | 0.04  | 214.22  | 850.00   | 3.43    | 2.7     | 16.9    |  |
| GM1       | 8.68 | 801    | 910    | 4  | 180    | 69.6 | 1248 | 3.02 | 1.66   | 1.51 | 4.35   | 0.12  | 0.02  | 0.41  | 0.04  | 320.36  | 590.91   | 2.27    | 23      | 265     |  |
| GM2       | 8.63 |        |        |    |        |      |      |      |        |      |        |       |       |       |       | 523.46  | 895.19   | 3.08    | 38      | 680     |  |
| GM3       | 8.55 |        |        |    |        |      |      |      |        |      |        |       |       |       |       | 111.35  | 164.42   | 1.25    | 6.4     | 42.6    |  |
| GM4       | 8.16 | 1096   | 1257   | 4  | 213    | 80.9 | 1251 | 2.99 | 2.76   | 1.63 | 4.3    | 0.13  | 0.03  | 0.39  | 0.05  | 365.38  | 745.28   | 2.74    | 31      | 402     |  |
| GM5       | 8.71 | 518    | 470    | 3  | 123    | 51.9 | 1168 | 2.91 | 3.42   | 1.71 | 4.14   | 0.08  | 0.02  | 0.35  | 0.05  | 137.50  | 275.00   | 1.63    | 6.6     | 68      |  |
| SL1       | 7.06 |        |        |    |        |      |      |      |        |      |        |       |       |       |       | 104.91  | 193.52   | 2.87    | 4.4     | 36.6    |  |
| SL2       | 6.78 | 3929   | 641    | 6  | 6968   | 70.9 | 822  | 1.74 | 9.84   | 0.82 | 6.85   | >5.00 | 0.05  | 0.36  | 0.03  | 171.35  | 204.81   | 2.88    | 3.4     | 78      |  |
| SL3       | 1.97 |        |        |    |        |      |      |      |        |      |        |       |       |       |       | 28.68   | 287.74   | 2.64    | 2.8     | 216     |  |
| SL4       | 7.22 | 271    | 353    | 3  | 558    | 50   | 1385 | 2.89 | 1.84   | 1.47 | 4.54   | 0.7   | 0.02  | 0.39  | 0.04  | 84.81   | 105.77   | 1.44    | 5.8     | 25.6    |  |
| SL5       | 2.71 | 6437   | 463    | 7  | >10000 | 68   | 512  | 0.61 | 9.09   | 0.26 | 11.32  | >5.00 | 0.08  | 0.36  | 0.02  | 72.94   | 108.82   | 2.06    | 2.8     | 62      |  |
| CC1       | 8.03 |        |        |    |        |      |      |      |        |      |        |       |       |       |       | 161.70  | 135.85   | 1.51    | 2.8     | <dl     |  |
| CC2       | 7.26 | 909    | 777    | 5  | 1151   | 69.9 | 1141 | 2.74 | 1.79   | 1.4  | 6.53   | 0.71  | 0.03  | 0.37  | 0.04  | 192.64  | 275.47   | 2.26    | 2.2     | 3.2     |  |
| CC3       | 7.35 |        |        |    |        |      |      |      |        |      |        |       |       |       |       | 434.13  | 3932.69  | 14.33   | 2.2     | 372     |  |
| CC4       | 6.84 | 296    | 302    | 2  | 69     | 44   | 1128 | 2.68 | 2.96   | 1.48 | 3.76   | 0.05  | 0.02  | 0.35  | 0.04  | 125.58  | 200.00   | 1.25    | 2.2     | <dl     |  |
| CC5       | 7.86 | 609    | 284    | 3  | 108    | 52.4 | 1269 | 3.19 | 0.9    | 1.38 | 4.57   | 0.05  | 0.02  | 0.44  | 0.05  | 165.85  | 95.28    | 1.13    | <dl     | <dl     |  |

